Investigation of dimensional and structural properties of dye aggregates

Von der Fakultät für Naturwissenschaften
Department Chemie
der Universität Paderborn

zur Erlangung des Grades eines
Doktors der Naturwissenschaften
Dr. rer. nat.
genehmigte Dissertation

von
Richárd Péter Szopkó
aus Hajdúdorog (Ungarn)

Paderborn 2009

Die vorliegende Arbeit wurde in der Zeit von Februar 2005 bis April 2009 im Fachgebiet Physikalische Chemie am Department Chemie der Fakultät für Naturwissenschaften der Universität Paderborn unter Anleitung von Prof. Dr. Claudia Schmidt angefertigt.

Referent:	Prof. Dr. Claudia Schmidt
Korreferent:	PD. Dr. Hans Egold

Eingereicht am:	23.04.2009
Mündliche Prüfung am:	29.05.2009

First of all, I would like to address my thanks to my supervisor Prof. Dr. Claudia Schmidt, who gave me the possibility to work on this interesting topic. Thank you for your support and patience in completing my thesis!

By the same token, I wish to express my thanks to Prof. Dr. Ferenc Joó, who encouraged me to start my PhD work.

Further thanks to:
PD. Dr. H. Egold for being a valuable source of ideas and suggestions in the topic of NMR spectroscopy and moreover for agreeing to write the Korreferat.
Prof. Dr. K. Huber for providing the dyes.
Prof. Dr. U. Olsson for the opportunity to work in the Department of Physical Chemistry 1 at Lund University.
Prof. Dr. D. Topgaard, Dr. S. Lasic, Dr. M. Nilsson and I. Aslund for the technical support of the diffusion NMR measurements at Lund University.
B. Medronho from Coimbra and Lund University for the effective collaboration.
Dr. F. Kleinschmidt for the diffusion NMR measurements in Freiburg.
Dr. J. Sehnert for help with the quantum chemical calculations in Bayreuth.
M. Perez for help with NMR sample preparation.
My colleagues, Dr. T. Witte, Dr. A. Hoischen, Dr. S. Benning, Dr. M. Lauhof, Dr. H. Matthias, A. Lorenz, A. Redler, S. Lages, M. Bayer, Dr. S. Shafaei and G. Ar for a positive working atmosphere.
G. Jünnemann and S. Keuker-Baumann for the technical support and the every-day conversation in German.
I. Koralewicz for the fast and perfect all-around help.

Special thanks to Dr. L. Germán, O. Germán, Dr. B. Elsaesser, Dr. L. Majoros and B. Wolf for their personal and scientific advice and help.

Finally, I extend my honest thanks to my family for all they have shared and their continuous help!

Presentations and publications

R. Szopko, K. Huber, C. Schmidt: NMR investigation of the aggregation of dye molecules, Poster, 72nd Annual Meeting of the German Physical Society, Berlin, Germany, February 2008

R. Szopko, C. Schmidt: ^{1}H chemical shift analysis and diffusion study of dye aggregates, Poster, 7th Annual Surface and Colloid Symposium Nanostructures from self-assembly in solution, Lund, Sweden, November 2007

R. Szopko, C. Schmidt: Diffusion NMR study of dye aggregates, Poster, 21th Conference of the European Council of International Schools, Geneva, Switzerland, September 2007

R. Szopko, C. Schmidt: Aggregation of dye molecules: diffusion measured by pulsed field gradient NMR method, Talk, NMR meeting, Berlin, Germany, March 2007

R. Szopko: Structure determination of dye aggregates, Poster, GDCh Magnetic Resonance Division 28th Discussion Meeting, Poster, Tübingen, Germany, September 2006

R. Szopko: Structure determination of dyes, Talk, NMR meeting, Pottenstein, Germany, March 2006

B. Medronho, S. Shafaei, R. Szopko, M. G. Miguel, U. Olsson, C. Schmidt: Shear-induced transitions between a planar phase and multi-lamellar vesicles: Continuous versus discontinuous transformation, *Langmuir* **2008**, *24*, 6480-6486

B. Medronho, S. Shafaei, R. Szopko, M. G. Miguel, U. Olsson, C. Schmidt: Shear-induced structural transformations of the lyotropic lamellar phase: Continuous or discontinuous transitions?, Poster, 21th Conference of the European Council of International Schools, Geneva, Switzerland, September 2007

CHAPTER 1 INTRODUCTION

Many small molecules form aggregates in solution. This phenomenon of aggregation plays an important role in technology and biology. The self assembly of molecules or particles is often an unwanted effect, for example in the case of dyestuffs[1], where it leads to several problems during the dyeing process like clogging of filters or uneven dye distribution on the fiber. Another example of aggregation is found for small amyloid polypeptides.[2,3] Their aggregation leads to the formation of the plaques that have been related to diseases. Therefore, a control of aggregation is in demand and a better physicochemical understanding of aggregation processes and of the properties of the aggregates is required.

In the formation of organic dye aggregates two different kinds of forces are important: dispersion forces due to the interaction between the π system of the molecules and forces resulting from the hydrophobic effect[4], which becomes relevant when hydrophobic substances are added into a hydrophilic medium, like water. When molecules in aqueous solution form aggregates the single molecules release their individual ordered solvation shells and the entropy of the system increases. In this case the attraction between the dyestuff molecules is less relevant, but the interaction of the water molecules which results in a highly organized water structure and the elimination of the water-dyestuff contact through aggregate building drives the aggregation. Between the surfaces of flat aromatic rings van der Waals interaction and H-bonds can stabilize the aggregates[5] and the molecules tend to arrange themselves like a stack of coins.

The aromatic interactions are ubiquitous in nature. They are believed to provide stability to J- and H-aggregates or to the duplex DNA, they have been proposed to contribute to the unique properties of proteins[6], they may play a role in the aggregation of amyloid in Alzheimer's disease[7] and they are common motifs in biomolecular recognition. Extensive work has focused on these interactions to determine their importance[8-12]. π-π interactions are caused by intermolecular overlapping of p-orbitals in π-conjugated systems, so they become stronger as the

number of π-electrons increases. The change of the electron cloud around the molecule, due to the stacking of the ring, affects the behavior of the system, thus NMR chemical shift analysis and optical spectroscopy can provide information about the aggregates.

The phenomenon of the aggregation process of dyestuff has been observed in 1936 by Scheibe[13] and Jelley[14] who investigated cyanine dyestuff by optical spectroscopy and described the aggregation of the molecules. These aggregate structures are an intermediate stage of the dyestuff from the dissociated stage to the crystals. The aggregate formation can be followed by studying the absorption properties of solutions with different concentrations in the UV/VIS range. During the aggregation process the intensity of the main absorption band increases or disappears while several new absorption bands appear in the spectra either at lower or higher wavelengths and an intense change in the color of the solution can be observed. These aggregates are usually referred to as J- or, occasionally, Scheibe-aggregates. If the aggregate absorption band is blue shifted (towards higher absorption energy) with respect to that of the monomer the aggregates are called H-aggregates (hypsochromic shift). Many spectroscopic investigations on the dye aggregates have been conducted since their first discovery[15-27].

In several dye systems a concentration-dependent variation in the NMR chemical shifts of aromatic protons[28-34] was observed as a result of the stacking of aromatic rings. If there are molecules in the aggregates that contain protons held in position directly over an aromatic ring a characteristic upfield chemical shift value is observed by NMR spectroscopy.

The chemical shift of a proton can be calculated by quantum chemical methods and together with the measured NMR spectra structural information can be acquired.[35-39] Furthermore, the shape and the dimension of molecules and aggregates are reflected in their diffusion properties. The fact that molecular self diffusion can be measured by NMR methods was realized in the early days of NMR spectroscopy.[40,41] The most practical pulse sequence for measuring diffusion coefficients by NMR spectroscopy was introduced by Stejskal and Tanner.[42-44]

Nowadays diffusion NMR spectroscopy is used in many different fields[45-50], such as medical[51] and material science.[52-54]

The dyes "Rot 2G" (RD) and "Gelb GA" (YD) used in this study, which are anionic direct dyes are employed as colorants in the production of tinted cellulose. A mixture of those dyes is used to produce orange-hued paper. However, in the presence of alkaline-earth ions, such as Mg^{2+}, aggregates are formed, which interfere with this dyeing process. Time-resolved static light scattering observed within 15 – 20 minutes after mixing the two dye solutions, has shown the formation of short aggregates with a contour length of 250 – 300 nm in the presence of Na_2SO_4, whereas substituting Na^+ ions with Mg^{2+} ions leads to a nearly tenfold increase of the contour length.[55,56] A RD/YD molar ratio 1/1.16 for the aggregates was found.[57]

In this doctoral thesis, the pure YD was used (no salt added) as a model molecule in order to demonstrate the capabilities of methods for studying dimensional and structural properties of the aggregates. NMR relaxometry[58-62] and diffusion NMR (using the pulsed field gradient technique),[28,45-47,63-65] as well as other methods, such as polarizing light microscopy and UV/VIS spectroscopy were applied to investigate the aggregates. The NMR chemical shift analysis together with the quantum-chemical computatios[66,67] was carried out to study the structure of aggregates.

CHAPTER 2 THEORETICAL ASPECTS

2.1 OPTICAL PROPERTIES OF J- AND H-AGGREGATES

The optical properties of aggregates can be described by Davydov´s exciton[68] model by using a quasi-classical vector-model which considers the electrostatic interaction of the transition dipole moments[69]. The excited state resonance interaction is approximated by considering the electrostatic interaction of transition dipole moments. If there is an electrostatic repulsion between the transition dipole moments, the energy of the dimer will be higher compared to the energy of the monomer.

The absorption of the electromagnetic irradiation is connected to the transition dipole vector μ.[70]

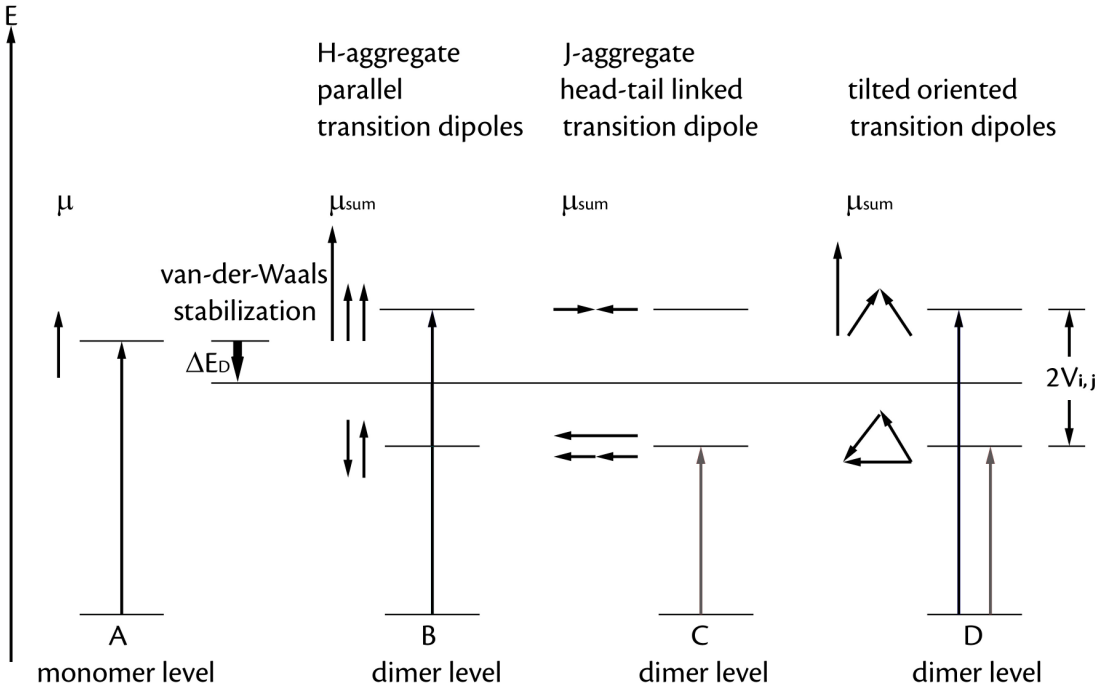

FIGURE 2.1: Vector model - energy diagram for the alignment of the transition dipoles in dimers and the monomer[70] (Figure from ref. 70).

In the easiest case the dimers are coupled at their chromophores whereby the transition dipoles can interact. The excited state is split into two separate levels.

Depending on the relative directions of the transition dipoles of the aggregate there can be different borderline-cases. The total transition state moment arises from the sum of the vectors in the single molecules. If we are stacking the chromophores then both parallel and antiparallel dipole directions are possible (Fig. 2.1B). If this direction is antiparallel then the transition dipole is 0, i.e. the transition is electrically forbidden[71].

However, if the transition dipoles are parallel then a light absorption can occur which is shifted hypsocrome in comparison to the monomer since the dipoles of the excited state are higher due to the electrostatic repulsion. This is called an H-aggregation (H like hypsochrome), because the absorption peak of the aggregate appears at lower wavelengths compared to the monomer absorption.

If the chromophores are linked head to tail behind each other and their transition dipoles point into the same direction then the sum of the transition moments can differ from zero only if the transition dipoles are parallel (Fig. 2.1C). In this case, the energy of the exited state is lower than that of the monomer and we can observe a bathochromically shifted J-band (called J after the discoverer, Jelly) in the absorption spectra. Such aggregates are called J-aggregates. If the chromophores (and the transitions dipoles) of the dimer are tilted then both the attractive and repulsive combination of the dipoles result in a non-zero transition moment, where the vectors of the transition dipoles for the two transitions are vertical to each other (Fig. 2.1D). These aggregates show two different absorptions where one has a bathochromic and the other one has a hypsochromic shift in comparison to the absorption band of the monomer.

For aggregate stacking an important property is the shearing angle $\alpha \leq 90°$, which is the acute angle between the axis of the transition dipoles and the line connecting the centers of neighboring molecules (Fig. 2.2).

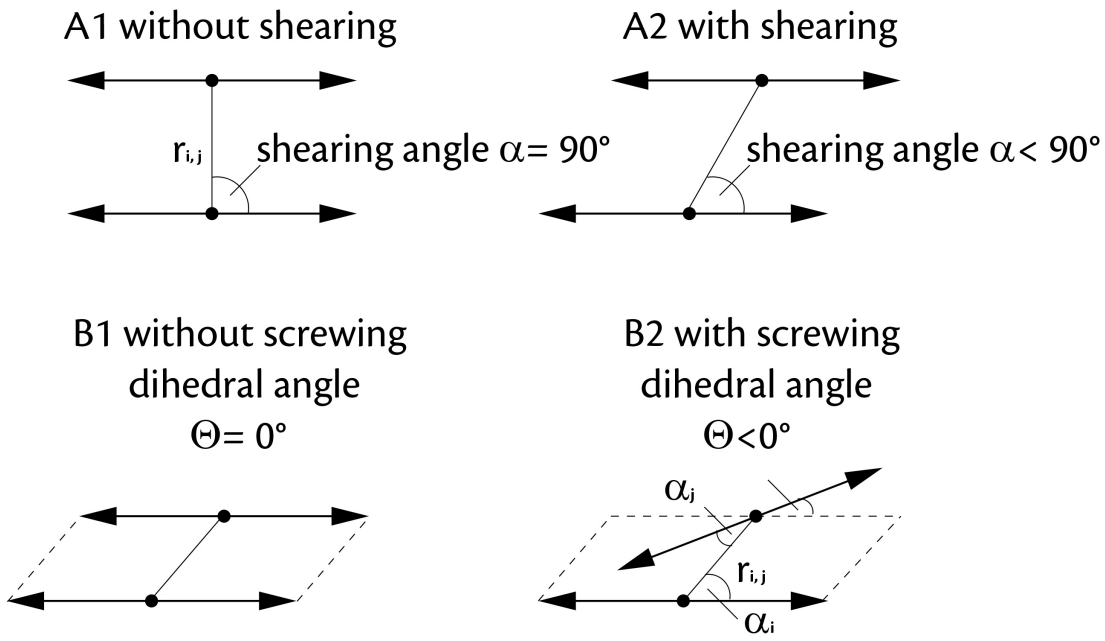

FIGURE 2.2: Representation of the terms shearing (A) and screwing (B) for the orientation of the transition dipoles of the dimer[70] (Figure from ref. 70).

If the aggregate is even helically twisted then this torsion can be described by a dihedral angle Θ as shown in Fig. 2.2. According to the point dipole approximation the interaction energy $V_{i,j}$ of the neighboring transition dipoles depends on the value of the transition moment of the monomer, the intermolecular distance $r_{i,j}$ and the geometry of the angles in the aggregate α_i, α_j and Θ (Fig. 2.2 B2). The excition-splitting (or Davydov-Splitting) of an aggregate of N molecules can be described as follows:

$$2V_{i,j} = 4\left|\left(\frac{N-1}{N}\right)\left(\frac{\left|\vec{M}\right|^2}{r_{i,j}^3}\right)(\cos\Theta\sin\alpha_i\sin\alpha_j - 2\cos\alpha_i\cos\alpha_j)\right| \qquad [2.1]$$

In a dimer stacked in a parallel way without screwing ($\alpha_i = \alpha_j$, Θ = 0°) at a shearing angle of α = arc cos $1/\sqrt{3}$ = 54.7° the excition splitting is zero. α > 54.7° corresponds to an H-aggregate and for α < 54.7° to a J-aggregate. In both cases there is only one allowed transition, which can be described by the in-phase interaction of the

transition dipoles. If the molecules in the aggregate are twisted a dihedral angle $\Theta \neq 0°$ occurs and the intensity of the formerly forbidden transition dipole increases and an additional absorption is allowed. One exemption is the case when $\alpha = \Theta = 90°$, where the transition dipoles are vertical to each other and therefore the dipole-dipole interaction becomes zero. The general case ($\alpha_i \neq \alpha_j$) considers an additional tilted orientation of the dipoles.

In an aggregate of N linked chromophores an exciton band with N excited states can be observed. Significantly, in a classical H- or J-aggregate only the highest and the deepest excited state of the aggregate can be obtained via electrically allowed transitions.[71]

Several examples about the investigation of the optical properties of J- and H-aggregates are available in the literature.[16,27,72,73,26,74-77]

2.2 NMR SPECTROSCOPY

Nuclear magnetic resonance spectroscopy exploits the magnetic properties of the nuclei[78-81] and it can provide physical, chemical, electronic and structural information about molecules in the solid or liquid phase[82-86].

2.2.1 ONE-DIMENSIONAL NMR TECHNIQUES

Nuclei with non zero spin ($I \neq 0$), when immersed in a static magnetic field, adopt $2I+1$ spin orientations, each with different energy. The difference between the energy levels depends on the magnetic moment of the nuclei and the strength of the magnetic field. Transitions of the nuclei between the energy levels can be induced by a radio frequency (rf) pulse (if the frequency of the electromagnetic radiation fulfills the resonance condition $\Delta E = h\upsilon$). This is the principle of NMR.[79,87,81,80]

One-dimensional (1D) NMR experiments contain two stages: preparation and detection. The preparation phase is the excitation by using one rf pulse or several pulses, while during the detection phase the resulting signal is recorded.

Chemical shift

A general feature of NMR spectroscopy is the dependence of the observed resonance frequencies on the local environments of the individual nuclei. The differences in frequency are referred to as chemical shift; they offer the possibility to distinguish between nuclei in different chemical environments.[78]

The effect of the small magnetic field, which is caused by the motion of the electrons, is called nuclear shielding. The strength of the shield depends on the molecular environment in that the nucleus is embedded. Therefore the changes in molecular environment lead to changes in the peak position. For example in case of aromatic stacking a change of the ^{1}H NMR chemical shift can occur due to the shielding of the aromatic protons by neighboring molecules.[66,67]

Chemical exchange

Chemical exchange[60,61] means that a nucleus moves from one environment to another. For example this can occur in case of isomers or aggregating systems.

Exchange processes are classified by their rate relative to the NMR timescale. There is slow exchange, which is defined by a situation where characteristic individual sites can be observed in the spectra by their individual signals, and fast exchange, which yields a spectrum time-averaged over the different sites.[47]

Between these extremes a rich variety of chemical exchange line shapes can be observed, as illustrated for azapropazone in Fig 2.3.[60] Based on the conjugation between the nitrogen ion pairs and the aromatic π system a partial double bond is formed which is a significant barrier to the rotation of the dimethylamino group. The barrier height is comparable to thermal energies at accessible temperatures, so

that the phenomenon of chemical exchange between the two methyl sites can be seen in the NMR spectra. At low temperature, two separate methyl peaks are seen, but with increasing temperature the rate of rotation about the bond increases. The lines broaden and then coalesce.

In case of an aggregation, there can be fast or slow exchange between the monomer and the aggregates, thus there can appear just one average signal in the ^{1}H NMR spectrum or individual peaks of both the monomers and the aggregates.

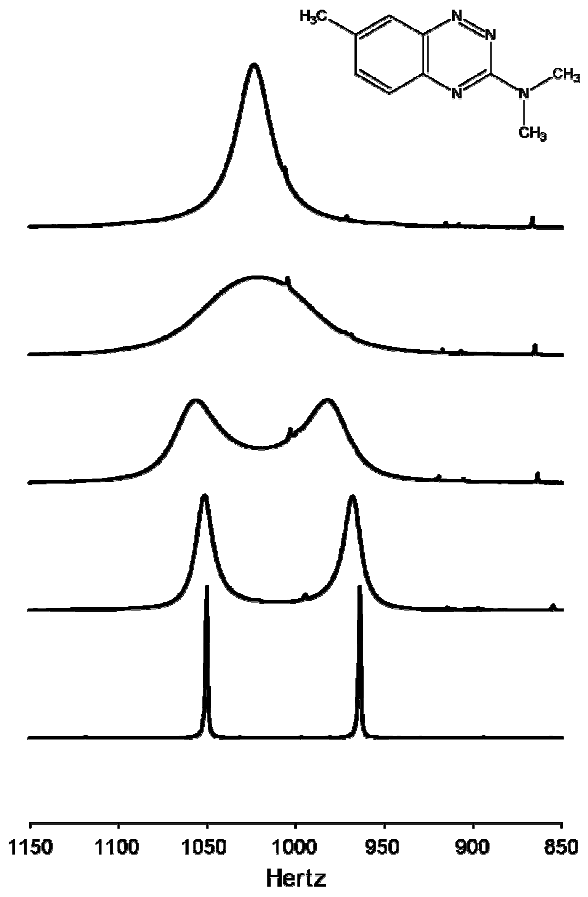

FIGURE 2.3: Proton NMR spectra at 300 MHz of the N-methyl signals in a derivative of azapropazone (structure shown in the figure) as a function of temperature. The lowest spectrum is at 223 K, and then at 243, 253, 263, and 273 K[60] (Figure from ref. 60).

2.2.2 TWO-DIMENSIONAL NMR TECHNIQUES

Two-dimensional (2D) NMR spectra provide more information about a molecule than one-dimensional NMR spectra and are especially useful in determining the structure of a molecule, particularly for molecules that yield spectra too complicated to be interpreted using one-dimensional NMR or when more detailed investigations are required.[88]

A two-dimensional NMR method involves a series of one-dimensional experiments. Each experiment consists of a sequence of radio frequency pulses with delay periods in between them. It is the timing, frequencies, and intensities of these pulses that distinguish different NMR experiments from one another. During some of the delays, the nuclear spins are allowed to freely process for a determined length of time known as the evolution time. The frequencies of the nuclei are detected after the final pulse by recording the resonance signals. By incrementing the evolution time in successive experiments, a two-dimensional data set is generated from a series of one-dimensional experiments.

In this thesis the following 2D NMR techniques were used:[79,81]

COSY (Correlation Spectroscopy)

COSY shows homonuclear correlation due to J couplings between protons. Two- and three-bond correlations yield COSY signals.

HMQC (Heteronuclear Multiple Quantum Coherence)

The HMQC experiment provides correlations between protons and their attached heteronuclei through the heteronuclear J coupling. This is the most common two-dimensional experiment because of its high sensitivity.

HMBC (Heteronuclear Multiple Bond Correlation)

The HMBC experiment detects long range coupling between proton and carbon (two or three bonds away) with great sensitivity.

2.2.3 DIFFUSION AND RELAXATION

Self-diffusion is the random translational motion of species (molecules/ions/aggregates) driven by internal kinetic energy.[54] Translational diffusion is the most fundamental form of transport and is responsible for all chemical reactions, since the reacting species must collide before they can react. Diffusion is also closely related to molecular size. According to Einstein the diffusion coefficient D depends on the friction factor f:

$$D = \frac{k_B T}{f} \qquad [2.2]$$

where k_B is the Boltzmann constant and the T is temperature. For the simple case of a spherical particle with an effective hydrodynamic radius R_h in a solution of viscosity η the friction factor is given by the Stokes relationship:

$$f = 6\pi\eta R_h \qquad [2.3]$$

In NMR spectroscopy there are two main ways to study self-diffusion coefficients, which are also known as tracer diffusion or intradiffusion coefficients: analysis of relaxation data and pulsed-field gradient (PFG) NMR. However, the two methods report on motions with very different time scales and thus, even though a translational diffusion coefficient can be derived in both cases. The two estimates will agree only under certain circumstances (in case of medium size and not very mobile species) since the relaxation method is in fact sensitive to rotational diffusion, which is proportional to the relaxation time, thus the molecular size, whereas the PFG method measures translational diffusion form the signal attenuation.[80]

Relaxation and Linewidth

Any excited magnetic moment relaxes back to equilibrium, which is called relaxation[79,80]. In other words, relaxation times describe how fast spins “forget" the direction in which they are oriented. There are two types of relaxation for isotropic systems in the absence of chemical exchange: longitudinal or spin-lattice (T_1) and transverse or spin-spin (T_2) relaxation. Different physical processes are responsible for the relaxation of the components of the nuclear spin magnetization vector M parallel (longitudinal) and perpendicular (transverse) to the external magnetic field, B_0 (which is conventionally oriented along the *z* axis).

In principle in liquids T_2 can be obtained by measuring the signal width at half-height:

$$\Delta\upsilon = \frac{1}{\pi T_2} \qquad [2.4]$$

However, the line width for non-viscous liquids is most often dominated by field inhomogeneity. The experimental relaxation rate, extracted from the line width, is called $1/T_2^*$

$$\frac{1}{T_2^*} = \frac{1}{T_2} + \frac{1}{T_{2(\text{inhom})}} \qquad [2.5]$$

In modern NMR spectroscopy $T_{2(\text{inhom})}/\pi$ is on the order of 1 Hz.

The transverse relaxation rate (T_2^{-1}) values are approximately proportional to the overall rotational correlation time[80] of the big molecules, such as proteins or aggregates and thus depend on molecular mass and shape of the molecules, solvent viscosity and temperature. In case of small molecules this is not true base on the high mobility of the molecules.

The correlation time for rotational diffusion can be measured experimentally or calculated by using a variety of hydrodynamic theories. In the absence of more accurate information, the simplest theoretical approach for approximately spherical molecules calculates the isotropic rotational correlation time from Stokes law:

$$\tau_c = \frac{4\pi\eta R_h^3}{3k_B T} \qquad [2.6]$$

where η is the viscosity of the solvent, R_h is the effective hydrodynamic radius of the molecule, k_B is the Boltzmann constant and T is the temperature.[80]

Diffusion NMR – PFG pulse sequences

Pulsed-field gradient NMR spectroscopy has become a convenient method for measuring diffusion in solution.[86,89,90,45-48,50,91,49] The diffusion coefficient of a molecule is a function of its effective molecular weight, size, and shape, so the measured diffusion data can be used to study molecular dimensions. Gradient NMR spectroscopy is a powerful tool not only for studying diffusion and dimensions of the species but it also provides structure information about cavities in cells or zeolites in the range of 0.1–100 mm when the diffusion is restricted on the NMR timescale.[86]

The basis for diffusion measurements is that magnetic field gradients can be used to label the spatial position of nuclear spins through their Larmor frequency,

$$\omega_0 = \gamma B_0 \qquad [2.7]$$

given in radians per second. γ is the gyromagnetic ratio, given in rad/Ts and B_0 is the strength of the static magnetic field. If B_0 is spatially homogeneous throughout the sample, ω_0 is the same over the whole sample but using an additional space

dependent B_0 field (gradient pulse) the effective Larmor frequency will depend on the position of the nuclei.

$$\omega_{eff}(r) = \omega_0 + \gamma Gr \qquad [2.8]$$

r is the coordinate vector of the nuclei. G is the gradient of the magnetic field, according to equation [2.9], where i, j, and k are the unit vectors in the x, y, and z directions, respectively, of the laboratory frame of reference. The gradient can be applied along three directions.

$$G = \nabla B_0 = \frac{\partial B_z}{\partial x} i + \frac{\partial B_z}{\partial y} j + \frac{\partial B_z}{\partial z} k \qquad [2.9]$$

If a gradient of known magnitude is applied over a defined time period, the Larmor precession yields an additional phase shift that is dependent on the spatial position of the spin, the direction of the gradient, and the duration and strength of the gradient.

If the gradient is applied along the z axis (parallel to B_0) the phase shift for a single spin is described by equation [2.10]

$$\phi(\delta) = \gamma B_0 \delta + \gamma \int_0^{\delta} G(t) z(t) dt \qquad [2.10]$$

δ is the duration of the gradient and t is the integration variable and z(t) the time dependent z position of the nucleus.

In order to measure diffusion the Hahn spin echo[41,40] pulse sequence was modified by Stejskal and Tanner.[43,42] The pulsed-field gradient spin echo (PFG-SE) sequence contains a 90° pulse as an excitation pulse and a 180° pulse, which flips the

magnetization of the spin. Thus exactly the same gradient pulses (length, strength and direction of the pulses) can be applied (Fig. 2.4)

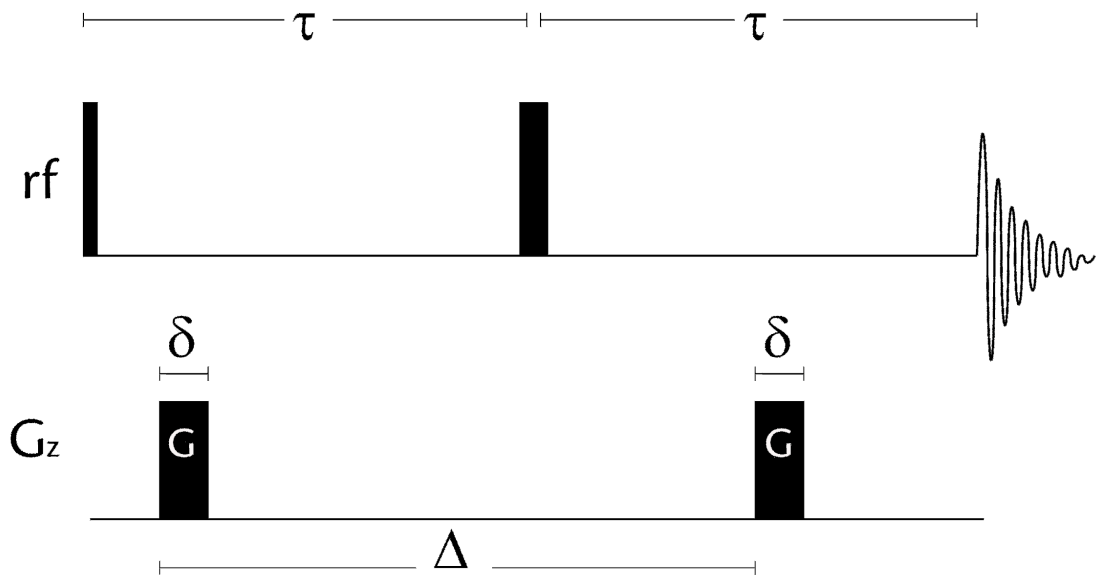

FIGURE 2.4: Schematic representation of the Stejskal and Tanner pulse sequence. In each delay, τ, a gradient pulse of duration δ and magnitude G is inserted.

After the 90° pulse the magnetization of the system flips from the z plane to the x-y plane. The first gradient pulse with duration δ and magnitude G is applied and the spins experience a phase shift, according to [2.10]. Due to the inversion of the phase shifts acquired from the first gradient by the 180° pulse, the second gradient pulse will refocus the magnetization of all the spins dephased by the first gradient. The spins that did not change their z-position are fully refocused, but those spins that moved during the evolution interval Δ are not fully refocused. Since the phases are averaged over all spins in the sample the echo is not phase shifted but attenuated.

In addition to the echo attenuation due to diffusion there is also a decrease of the echo amplitude due to relaxation. The echo amplitude is given by equation [2.11].

$$S(2\tau) = S_0 \underbrace{\exp\left(-\frac{2\tau}{T_2}\right)}_{\text{relaxation}} \underbrace{f(\delta, G, \Delta, D)}_{\text{diffusion}} \qquad [2.11]$$

If τ is kept constant during all the experiments, the relaxation-induced signal attenuation is constant and can be separated from diffusion-induced attenuation.

The relationship between the diffusion and the observed signal attenuation is described by equation [2.11]. A step-wise time-dependent integration of the Bloch equation for the given pulse sequence results

$$\ln S = -\gamma^2 G^2 \delta^2 D\left(\Delta - \frac{\delta}{3}\right) \qquad [2.12]$$

The attenuation of the signal depends on the gyromagnetic ratio (γ) of the observed nuclei and the parameters of the diffusion measurement, such as gradient pulse length (δ), gradient strength (G) and diffusion time (Δ).

For small molecules the spin echo sequence can be applied because T_2 relaxation is slow and sufficient signal is obtained even for long diffusion time (Δ). In case of medium size molecules the T_1 relaxation time has a minimum and it increases for very small and very big molecules. Contrarily the T_2 relaxation time is high for small molecules and decreases for increasing molecular size. Thus the T_2 relaxation time of big molecules is much shorter than their T_1 relaxation time ($T_1 >> T_2$). Because of the limitation of the T_2 relaxation time the spin echo experiment cannot be applied for large molecules.

The stimulated-echo (STE) pulse sequence with pulsed-field gradients, which is presented in Fig. 2.5, is applied for measuring diffusion of macromolecules or aggregates. In this pulse sequence the magnetization is “stored” along the z axis during the τ_2 period and therefore subjected only to the lower longitudinal T_1 relaxation.

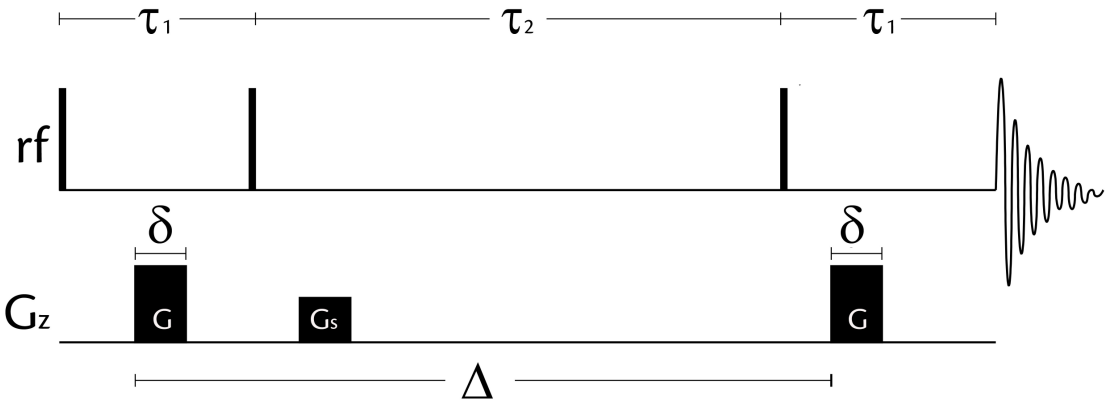

FIGURE 2.5: The stimulated-echo (STE) pulse sequence with pulsed-field gradients. During the τ_2 period, magnetization is stored along the z axis and therefore subjected only to longitudinal T_1 relaxation. G_s indicates a spoil gradient, which eliminates the remaining x-y components.

Temperature gradient and convection – DSTE sequence

A typical problem affecting diffusion measurements is the convection within a sample, especially at elevated temperature.[92] Convection currents are generated by small temperature gradients in the sample and cause additional signal decay. This artifact can corrupt the diffusion measurements. Some improvement can be achieved, for instance by sample rotation,[93] special sample cells or use of transverse gradients, but the perfect elimination of this problem is difficult. Jerschow and Müller developed a pulse sequence[94] which suppresses the convection effects in stimulated echo diffusion experiments to first order, provided that the convection current has a constant laminar flow profile during the diffusion interval of the pulse sequence. This condition is fulfilled in many systems of practical relevance. However, this method is not effective for turbulent convection. Convection compensation sequences are based on the pulse scheme shown in Fig. 2.6 in which only the gradient pulses are shown.

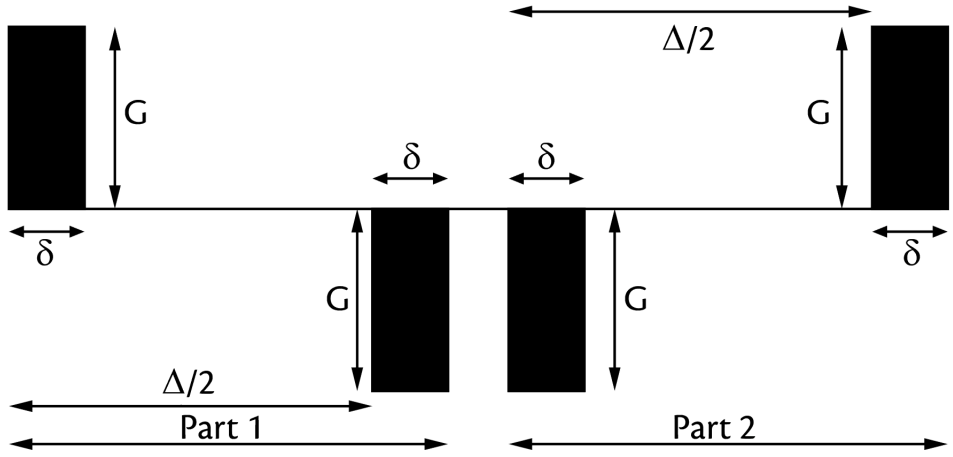

FIGURE 2.6: Basis of convection compensation sequence.

As can be seen in Fig. 2.6 part 1 and part 2 of the pulse sequence only differ in the signs of the gradients. If there is laminar convection present, the effect during the first part is expressed by:

$$\exp\left(\mathrm{i}v\gamma G\delta\frac{\Delta}{2}\right) \qquad [2.13]$$

while during the second part this is

$$\exp\left(-\mathrm{i}v\gamma G\delta\frac{\Delta}{2}\right) \qquad [2.14]$$

which results in a total effect of:

$$\exp\left(\mathrm{i}v\gamma G\delta\frac{\Delta}{2}\right)\exp\left(-\mathrm{i}v\gamma G\delta\frac{\Delta}{2}\right)=1 \qquad [2.15]$$

where v is the flow velocity, G is gradient strength and Δ is the diffusion time.

By choosing both values of Δ in equation [2.15] equal the effect of laminar convection is completely removed. The physical reason for this is that in the case of laminar convection the displacement of a molecule during the second part of the sequence is exactly the same as during the first part, and thus the value of the

phase difference obtained is also the same. However, because the gradient is oppositely signed, the phase difference is also oppositely signed. Therefore the total phase difference is zero. In case of turbulent convection the displacement in the first and second parts are not equivalent so the phase differences do not have the same value.

2.3 COMPUTER SIMULATION

Recent years have witnessed an increase in the number of people using computational chemistry to understand a problem more completely.[35,37,95,96,66,97,98] There has been an enormous progress in the field of computational investigations of chemical and biochemical systems over the last decade. There are some properties of a molecule that can be obtained computationally more easily than by experimental means. Additional insights into molecular bonding can be obtained from the results of computations that cannot be obtained from any experimental method. Molecular modeling and simulation methods can address fundamental questions that cannot easily be answered experimentally. Thus, many experimental chemists are now using computational modeling also to gain additional understanding of the compounds being examined in the laboratory.

NMR spectroscopy is a valuable technique for harvesting molecular information. The structure of the molecule and the NMR spectra is in strong relation, thus the spectrum is very sensitive to a change of the molecular structure.[39]

Before an NMR spectrum can be calculated, a good model of the true molecular structure must be obtained by a computational procedure, known as structure optimization, in which the energy minimum is searched for by variation of the atomic coordinates.

Density functional theory[38] (DFT) is a quantum mechanical theory used in physics and chemistry to investigate the electronic structure (principally the ground state) of many-body systems, in particular atoms, molecules and the condensed phases, where the electron density is expressed as a linear combination of basis functions similar in mathematical form to Hartree-Fock (HF) orbitals. A determinant is then formed from these functions, called Kohn-Sham orbitals, which is then used to compute the energy. The major problem with DFT is that the exact functionals for exchange and correlation are not known except for the free electron gas. However, approximations exist which permit the calculation of certain physical quantities quite accurately. One of the most popular functional is the BLYP (from the name

Becke for the exchange part and Lee, Yang and Parr for the correlation part). Even more widely used is B3LYP, which is a hybrid functional in which the exchange energy, in this case from Becke's exchange functional, is combined with the exact energy from Hartree-Fock theory. Along with the component exchange and correlation functionals, three parameters define the hybrid functional, specifying how much of the exact exchange is mixed in. The adjustable parameters in hybrid functionals are generally fitted to a 'training set' of molecules. Hence in the current DFT approach it is not possible to estimate the error of the calculations without comparing them to other methods or experiments.

After having obtained an accurate structure, the spectra can be calculated, such as NMR or UV spectra. NMR chemical shifts can be computed from the shielding tensor of atoms[37,95,98] in simple model systems incorporating functional groups that exert through-space effects. Once the shielding tensors have been computed, the chemical shifts can be determined by subtracting the isotropic shielding values for the molecule of interest from the TMS values. Computing shielding tensors is difficult because of gauge problems (dependence on the coordinate system's origin). It is extremely important that the shielding tensors be computed for equilibrium geometries with the same method and basis that were used to complete the geometry optimization.

One of the most popular techniques is called GIAO. This originally stood for gauge invariant atomic orbitals. More recent versions have included ways to relax this condition without loss of accuracy and subsequently the same acronym was renamed gauge including atomic orbitals. The GIAO method is based on perturbation theory. It is a means for computing shielding tensors from HF or DFT wave functions.

It is also possible to calculate the electronic excited states of a molecule. These calculations are an important tool for the analysis of UV spectroscopy.

CHAPTER 3 EXPERIMENTAL

3.1 MATERIALS

The azodyes "Rot 2G" (RD) and "Gelb GA" (YD) (Fig.3.1) are anionic direct dyes that were provided by Ciba Spezialitätenchemie AG. The dyes in form of their salts, $RDNa_4$ and $YDNH(C_2H_4\text{-}OH)_3$ are employed as colorants in the production of tinted cellulose.

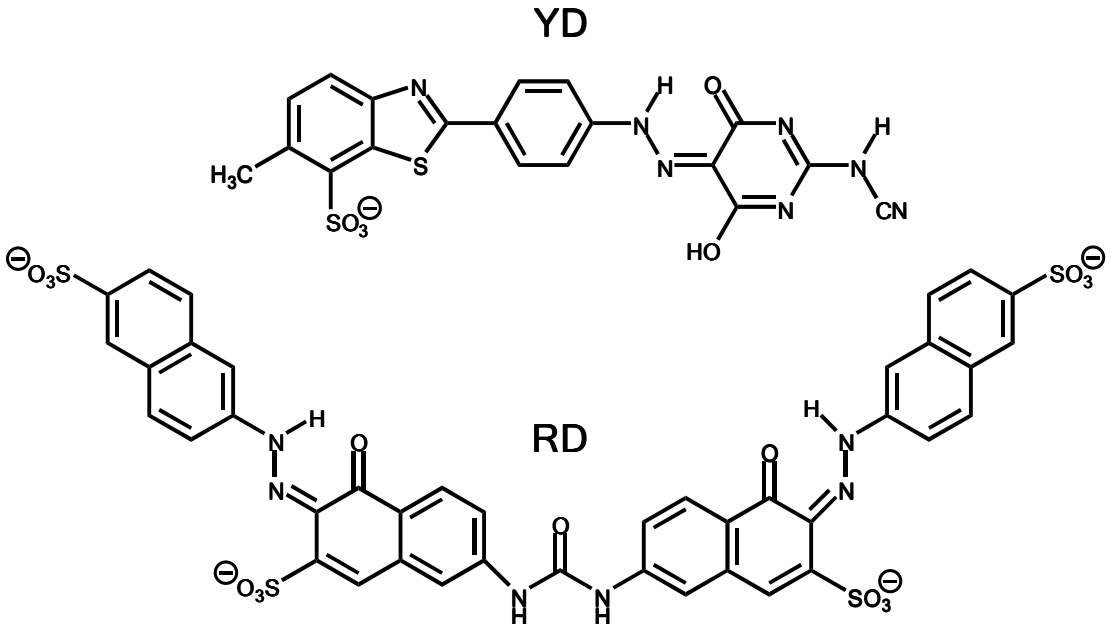

FIGURE 3.1: Chemical structures of the azodyes used: anion of the yellow dyestuff (YD) and anion of the red dyestuff (RD).

For the investigations, the two dyes were used in their sodium salt form (the molar mass of the anions are M_{YD}= 505 g/mol and M_{RD}= 1061 g/mol). In case of YD an ion exchange was necessary. The purification of the dyestuffs was achieved by dialysis of aqueous solutions of the raw material to produce the pure sodium salt of the dyes which was used for further investigations.

3.1.1 SAMPLE PURIFICATION

The dialysis was carried out with dialysis hoses (type: 50303, Reichelt). The diameter and length of the hoses were 12 and 25 cm, respectively. For each dyestuff, two hoses were filled with a 250 ml of concentrated solution (4 g/L) of dyestuff. Each hose was sealed with clamps at both ends and placed in a 10 L vessel. The vessel was completely filled with the dialysis medium. Dialysis was performed at first against an aqueous solution (1.2 g/L) of NaCl for 2 days, and the dialyzing medium was changed twice a day.

At the beginning of the fourth day, the NaCl solution was replaced by distilled water as the dialyzing medium, and the dialysis was continued for 3 days against distilled water which was again changed twice a day. The endpoint of the dialyzing process was indicated by subjecting the dialyzing medium to a precipitation test for Cl^- ions with an Ag^+ solution. In all cases, the test was negative after 3 days meaning that there were no Cl^- ions in the dye solution.

After the dialysis, the water content in the hoses had increased by about 50 % because of water penetrating the membrane. To recover the dyestuff, their aqueous solutions were first concentrated by rotation evaporation of about 90 % of the water at 30 °C under reduced pressure. The remaining water was then removed by freeze-drying of the concentrated dyestuff solutions.

3.1.2 SAMPLE PREPARATION

Light microscopy

Three different samples in aqueous solution were prepared. 66 mg dye (YD, RD, or 1:1 w/w% MIXTURE) and 4 mg $MgSO_4.7H_2O$ (Magnesium sulfate, Merk, p.a., > 99,5 %) were dissolved in 1 mL H_2O in each case. Moreover three further samples were prepared in DMSO (Dimethyl sulfoxide-d6, Deutero GmbH, 99.8%). After mixing the components, one droplet of the solution was placed on a glass slide and then covered by another one.

The concentrations of the dye solutions used are listed in Table 3.1 and Table 3.2.

TABLE 3.1

Dye samples in DMSO solution for light microscopy measurements.

The dyes were dissolved in 1 mL DMSO

Dye	Dye-amount (mg)	c_{Dye} (mM)
YD	66	130
RD	66	62
1:1 w/w MIX	66	96

TABLE 3.2

Dye samples in aqueous solution for light microscopy measurements.

The dyes were dissolved in 1 mL magnesium sulfate solution ([$MgSO_4$]=33 mM) in D_2O

Dye	Dye-amount (mg)	c_{Dye} (mM)
YD	66	130
RD	66	62
1:1 w/w MIX	66	96

UV measurements

A small amount of the dyes was weighted using an analytical balance and the desired amount of solvent was added with a micropipette. In order to prepare the 0.07 mM samples the 0.7 mM sample was diluted. Due to the limited amount of the dyes, the preparation of a dye stock solution was not possible. The measurements were performed at room temperature immediately after the preparation. Because of the high absorbance in the visual range of YD a special thin sample holder was created from two agglutinated glass slides (Menzel Glaeser 76 x 26 mm) which were separated by a 25 µm foil. A foil frame was glued to the first glass slide and a small drop pf the solution was added to the center of the slide and then covered by the second slide. Finally the slides were glued together, thus it was not refillable. The glass sides have no absorption in the UV range so the measurements are not affected by the glass. The reference sample holder was not chanced during the measurements contrary to the sample holder with the dye solutions. Thus the background correction can be imprecise.

TABLE 3.3

Dye samples for UV measurements

Solvent	YD (mg)	c_{YD} (mM)
1 ml DMSO	0.074	0.07
1 ml D_2O	0.074	0.07
1 ml D_2O	0.74	0.7
1 ml D_2O	1.33	2.5
1 ml D_2O	2.65	5

^{1}H, ^{13}C, COSY, HMQC and HMBC NMR spectroscopy

5 mg of the sample (YD or RD) was put in a plastic sample holder and 0.5 ml of DMSO was added. The sample holder was shaken manually for about a minute and then the solution was injected in a 5 mm NMR tube. A ^{1}H NMR spectrum was

recorded immediately after the sample preparation (time zero). The chemical shift values are given in ppm relative to TMS (based on the known chemical shift of the solvent peak). The measurements were carried out at room temperature. Before and after each 2D measurement a 1D ^{1}H spectrum was recorded to confirm the stability of the sample.

TABLE 3.4

Dye samples for the ^{1}H, ^{13}C, COSY, HMQC and HMBC measurements

Dyes	Dye amount (mg)	c_{YD} (mM)
YD + 0.5 ml DMSO	5	20
RD + 0.5 ml DMSO	5	10

^{1}H Diffusion NMR and temperature dependent ^{1}H NMR spectroscopy

An amount of the sample determined by the desired analytical concentration was put in a plastic tube and 0.5 ml of D_2O, containing 0.18 mM DSS (2,2-dimethyl-2-silapentane-5-sulfonic acid) as internal standard, was added. The sample holder was shaken manually for about a minute and then the solution was injected in a 5 mm NMR tube. The ^{1}H NMR spectrum of time zero was recorded immediately and the change of the spectra was monitored afterwards as a function of time. The solutions were stable for weeks, since the corresponding ^{1}H NMR spectrum was unchanged. Before and after each 2D measurement a ^{1}H spectrum was recorded to confirm the stability of the sample. The viscosity data of D_2O were taken from the literature.[99]

TABLE 3.5

Dye samples for the ^{1}H diffusion NMR and temperature dependent ^{1}H NMR measurements

Solvent	YD (mg)	c_{YD} (mM)
0.5 ml DMSO	5	20
0.5 ml D_2O	0.36	0.7
0.5 ml D_2O	0.66	2.5
0.5 ml D_2O	1.36	5
0.5 ml D_2O	2.73	10
0.5 ml D_2O	4.18	15
0.5 ml D_2O	5.31	20
0.5 ml D_2O	6.58	25
0.5 ml D_2O	8.10	30

3.2 *TECHNIQUES*

3.2.1 POLARIZING MICROSCOPY

The microscopy experiments were performed in transmission mode under crossed polarizers using a Leitz ORTHOLUX 2 POL microscope. A lens (L5) with fivefold magnification was used. The pictures were recorded with a JVC TK-C1381 color video camera. The samples were measured at room temperature.

3.2.2 UV SPECTROSCOPY

The UV absorption spectra were recorded with a Lambda 19 Spectrometer from Perkin Elmer. The wavelength interval of the measurement was from 350 nm to 600 nm, the resolution was 0.1 nm and the scanning speed was 240 nm/min. Distillated water or DMSO was used as reference depending on the solvent of the sample. Before every measurement background correction was carried out to reduce artifacts.

3.2.3 NMR SPECTROSCOPY

One- and two dimensional (1D, 2D) NMR experiments in DMSO, such as ^{1}H, ^{13}C, COSY, HMQC, HMBC, were performed on a BRUKER ARX 500 NMR spectrometer operating at 500 and 125 MHz for ^{1}H and ^{13}C, respectively, using Bruker standard pulse sequences. The NMR chemical shift values are given in ppm relative to TMS.

The diffusion measurements and the ^{1}H NMR measurements for temperature dependent ^{1}H chemical shift and linewidth analysis were performed on a Bruker DMX-200 spectrometer (Lund University, Sweden) operating at 200.11 MHz for ^{1}H. The spectrometer was equipped with a Bruker diffusion probe, capable of

generating field gradients up to 9 T/m. The temperatures of the measurements were varied between 10 and 70 °C. The spectra were taken forty minutes after changing the set temperature.
Up to 30 °C the standard Bruker pulsed-gradient stimulated echo sequence was used and at higher temperature the double stimulated echo sequence with square shaped gradients. The pulse programs are shown in the appendix. The gradient pulse duration was 0.5 ms. The diffusion times and gradient strengths were optimized for each experiment. The diffusion times were 20 ms, 40 ms and 100 ms. The gradient strength was varied between 0 and 9 T/m in steps 0.5 T/m. The measured data were analyzed by the Bruker software package (Topspin) and a Matlab script (The original script from Lund University).

DSS as internal standard was used in aqueous solution. The ppm chemical shift values were measured with respect to the internal standard peak, but reported relative to TMS. The recorded NMR spectra with or without the internal standard were identical, except for the presence of the internal standard signal.

In all NMR experiments the optimal number of scans (16-256) was used to reach a good signal to noise ratio depending on the dye concentration.

3.2.4 COMPUTER SIMULATION

The program package NWCHEM was used to find the starting structure of the monomer and the dimer. The Gaussian03 computational chemistry software was used to determine the structure of YD and to simulate the NMR and UV spectra. The simulations were performed on the RZ cluster at RWTH Aachen and on the Arminius cluster of the University of Paderborn using 4-16 processors. GaussView and MOLDEN programs were used to visualize the input and output structures of the molecules.

CHAPTER 4 RESULTS AND DISCUSSION

4.1 OPTICAL PROPERTIES OF DYES

Precipitation was observed by visual inspections with the naked eye in case of dye mixtures and yellow dye at high ($\geq$ 62 mM) concentrations in aqueous solution in the presence of positively charged ions. The motivation for microscopic experiments was to investigate the size and the shape of the aggregates at higher concentration where they are big enough to be detected by microscopy (the size of the particles is in the µm range). Thus, yellow (YD) and red (RD) dyes, as well as their 1:1 mixture (MD) were investigated by light microscopy in aqueous solution with Mg^{2+} added. UV/Vis spectroscopy provided further information of the aromatic stacking (Chapter 2.1) about the pure YD based on the color change by increasing the dye concentration.

4.1.1 POLARIZING MICROSCOPY

Light microscopy was used to obtain information regarding the size and shape of the aggregates. This method, however, is applicable only in the µm diameter range, which means, in our case, that it can be applied when the concentration of the dye and the Mg^{2+} is relatively high (over 62 mM, dye concentration). During these experiments, only aqueous solutions of the dyes were examined (since no aggregates are formed in DMSO).

Fig. 4.1 shows the polarizing microscopy picture of RD. No aggregates are visible under these conditions ([dye]= 62 mM; [$MgSO_4$]= 33 mM at room temperature). Hence the dye is in perfect solution or any aggregates are below the detectable size. Under similar circumstances ([dye]= 130 mM, [$MgSO_4$]= 33 mM at room temperature) YD forms aggregates, which are in the observable size range as shown in Fig. 4.2. The aqueous dye solution contains clearly visible aggregates of various

shapes and sizes. Treating the 1:1 mixture of the two dyes in a similar way, the resulting system is composed of huge aggregates as shown in Fig. 4.3.

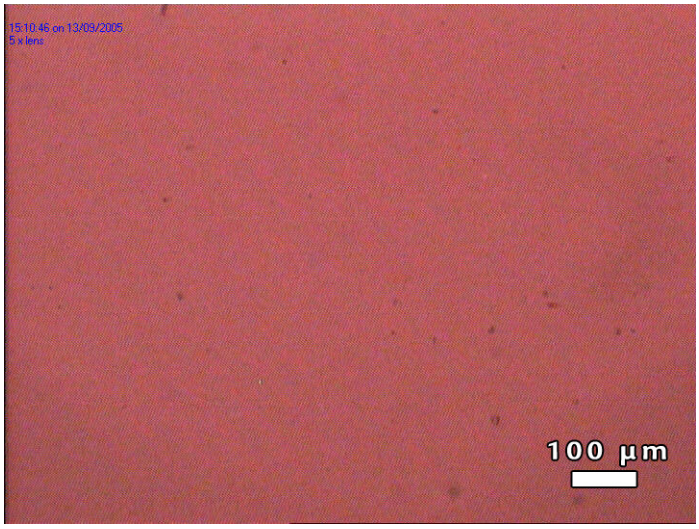

FIGURE 4.1: Light microscope picture of RD in aqueous solution [dye]= 62 mM, [$MgSO_4$]= 33 mM at room temperature. The picture was taken two hours after sample preparation. No aggregates can be observed.

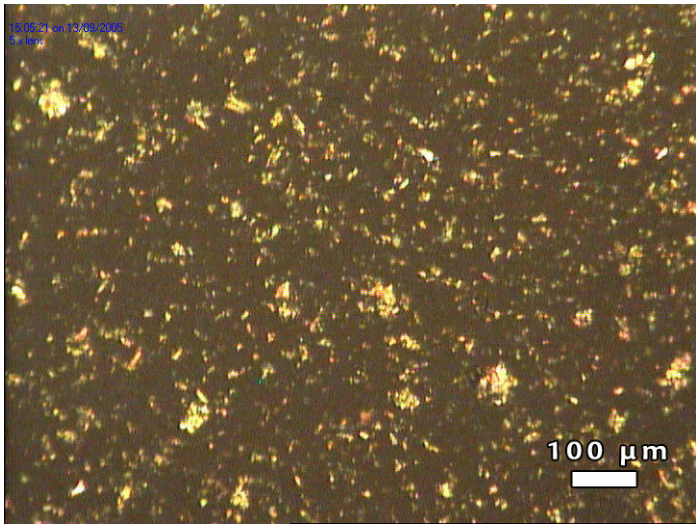

FIGURE 4.2: Light microscope picture of YD in aqueous solution [dye]= 130 mM, [$MgSO_4$]= 33mM at room temperature. The picture was taken two hours after sample preparation. The size of the aggregates is up to hundred micrometers.

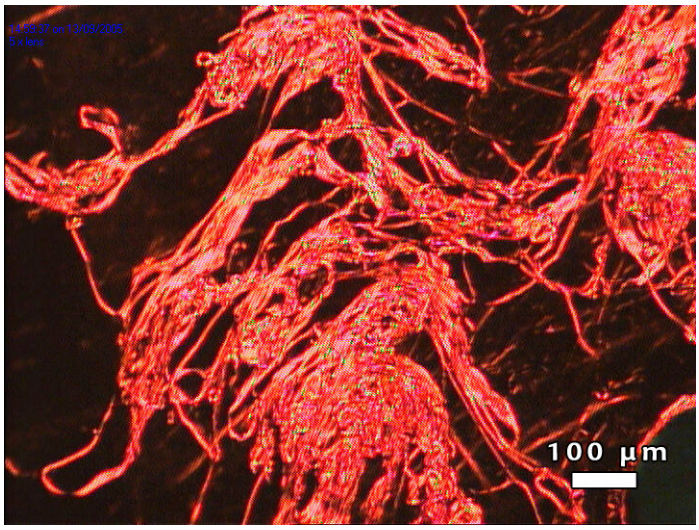

FIGURE 4.3: Light microscope picture of 1:1 w/w mixture of YD:RD in aqueous solution [dye]= 96 mM, [$MgSO_4$]= 33 mM at room temperature. The picture was taken two hours after sample preparation. Huge aggregates can be observed.

It is obvious that, although optical microscopy is a powerful technique, it has its limitation, being unable to detect aggregates smaller than about one µm. Since this method can only be used at higher concentrations and with positively charged metal ions (such as Mg^{2+}) added, other techniques are necessary to investigate small aggregates.

In case on YD and the mixture of YD and RD aggregation was observed in aqueous solution. Because of the simple NMR spectrum of YD and the limited amounts of dye available most of the following studies will focus on YD. The results of the diffusion NMR measurements of the dye mixture are presented in the Appendix.

4.1.2 UV/VIS SPECTROSCOPY

In Fig. 4.4A the UV/Vis absorption spectra of YD in water/DMSO at different concentrations at room temperature are shown. Increasing concentration shifts the maximum absorbance to lower wavelengths (blue shift). In case of the 0.07 mM solution in D_2O the absorption between 500 and 600 nm is higher compared to the other samples. Due to the home made sample holders used in the UV measurement there may be additional absorption of the glass slides.

Plotting the maximum absorbance as a function of [YD] yields by Fig. 4.4B where the aforementioned shift can be seen clearly. The absorbance at 0 concentration is a hypothetical value referring to the solution in DMSO, where no aggregation occurred. Within this concentration range (0-5 mM) the measured hypsochromic shift in wavelengths is 16 nm, which is similar to what was observed in the case of other dyes.[30,100-102,55]

The results of these optical measurements provide us a hint of parallel transition dipoles. In case of aromatic rings the molecular dipole moment, which is in the molecular plane, is parallel to the transition dipoles.[69,71] Thus based on the exciton model (Chapter 2.1), the shearing angle α is in the 54.7-90° range. In case of blue shift there is a vertical stacking of the dye molecules in the aggregate, which is called an H aggregate.

Fig. 4.5 shows the molar extinction coefficient as a function of wavelength for the four different aqueous solutions of YD. The molar extinction coefficient is reduced substantially at concentrations higher than 0.07 mM. In case of big aggregates the light is also scattered and the intensity of the detected light is lower.

A

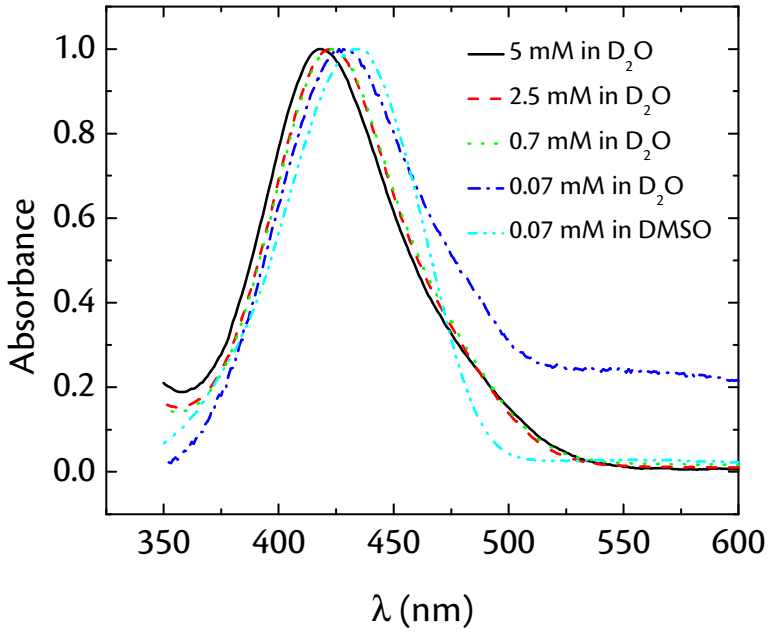

B

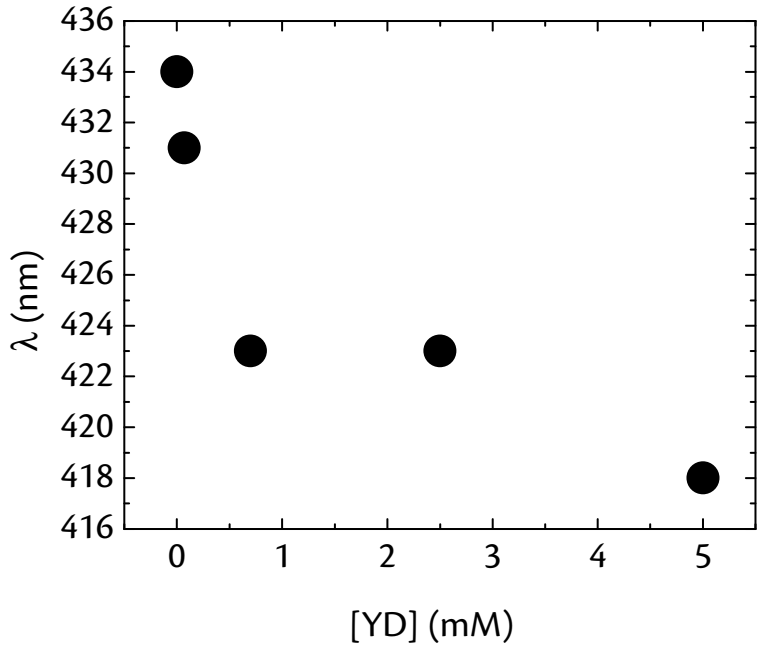

FIGURE 4.4: UV/Vis absorption spectra of YD in water/DMSO at different concentrations as a function of wavelength at room temperature (A) and wavelength of maximum absorbance as a function of YD concentration (B). The 0 concentration refers to the absorbance in DMSO.

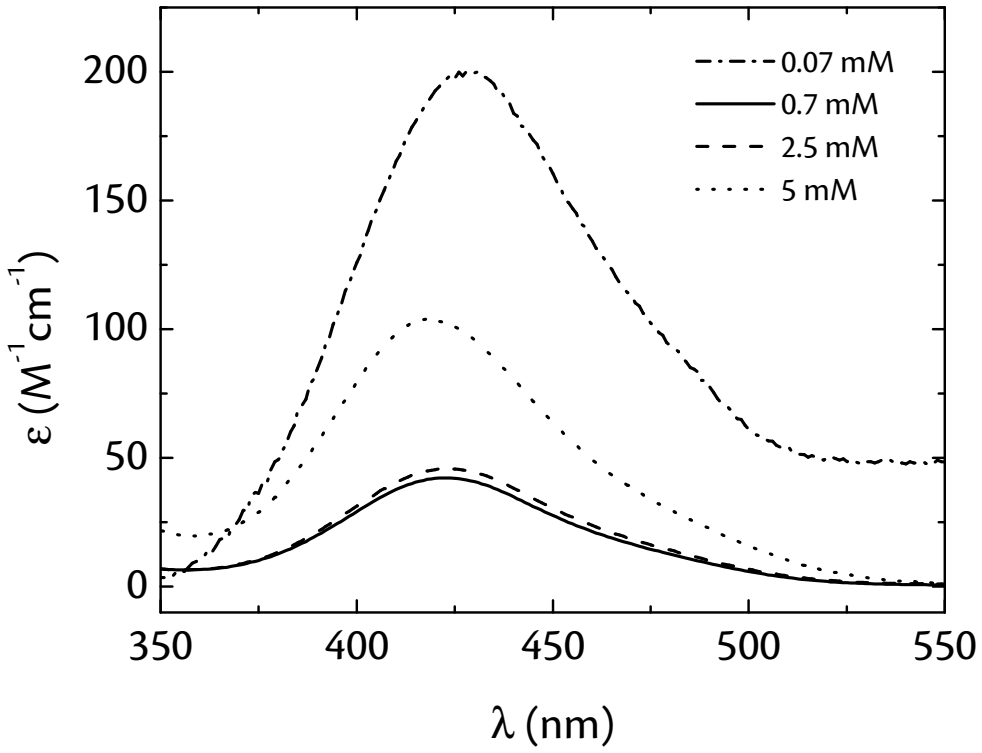

FIGURE 4.5: Molar extinction coefficients, of YD in water at different concentrations at room temperature as a function of wavelength.

The UV/VIS spectra prove the formation of aggregates in dilute solutions even without any salt added, where no visible precipitation occurred. Using further optical studies[102] could provide more details about the aggregating system, but in this work the results of the optical techniques was used primarily to confirm the NMR experiments discussed in the following.

4.2 *NUCLEAR MAGNETIC RESONANCE*

The main technique used in this thesis was NMR spectroscopy, which is a powerful tool that provides essential information regarding the dimensional and structural properties of the dyes in the molecular level. The chemical structure of the molecules was reconfirmed by using high resolution liquid NMR methods, such as ^{1}H, ^{13}C, COSY, HMQC and HMBC. The peak assignment of the NMR spectra is also required for interpreting the changes of chemical shifts with concentration and temperature in order to get information about the structure of the aggregates. The dimension of the species was estimated from the ^{1}H NMR linewidth and from the pulsed field gradient diffusion NMR data.

4.2.1 PEAK ASSIGNMENT

In the initial step of the NMR measurements an organic solution (DMSO) of YD (Fig. 4.6) was examined by one- and two-dimensional NMR techniques to assign the peaks of the spectra. Peak assignment is of importance for the detailed study of the aggregation process in aqueous solution.

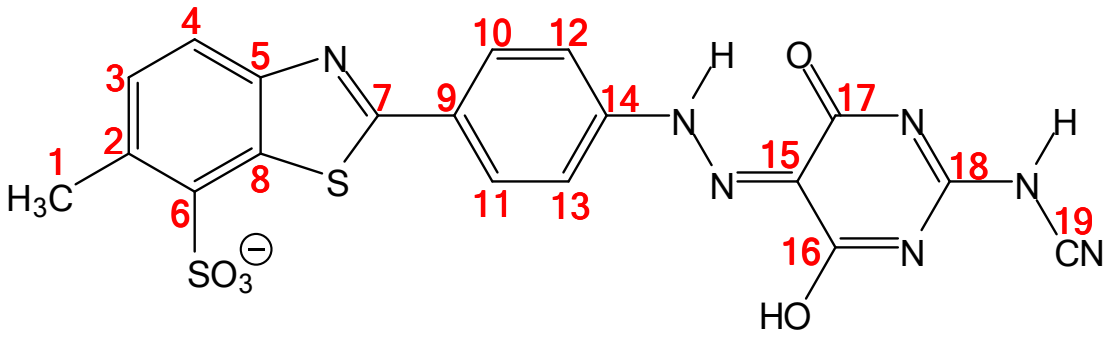

FIGURE 4.6: Chemical structure of YD with numbered atoms. The numbers refer to the carbon atoms and the directly attached hydrogen atoms.

The samples were prepared with deuterated DMSO as solvent to prevent aggregation. The following NMR methods were used: ^{1}H-NMR, ^{13}C-NMR, COSY, HMQC and HMBC. The results of these experiments are detailed below.

^{1}H-NMR

The measurements were preceded by a simple and fast estimation of ^{1}H and ^{13}C chemical shifts using the ChemOffice Ultra 10.0 software to predict the peak positions in the NMR spectra. The software carries out an estimation procedure based on empirical methods. The simplest empirical calculation called group additivity method is applied, so these can be performed very quickly on small desktop computers. As a drawback, however, the estimation is of limited value for atoms with unique or undocumented chemical environments.

The ^{1}H-NMR spectrum in DMSO is shown in Fig. 4.7. In accordance with literature,[99] the solvent peak appears at 2.50 ppm. Since DMSO always contains small amounts of water, a second solvent peak (HDO) is visible at 3.4 ppm. According to the literature data aliphatic hydrogen peaks are expected to appear at lower ppm (2-3) values. This, together with the fact that YD contains a single aliphatic group, the methyl peak can be readily identified (2.7 ppm). The molecule has six aromatic hydrogen atoms. Since 10 and 11 as well as 12 and 13 have similar chemical environments, only four peaks are visible in the spectrum. The two peaks showing double intensity are assigned to the hydrogen pairs 10-11, and 12-13. All aromatic peaks appear as doublets due to scalar couplings. Identification of the peaks referring to 10-11, 12-13, 3 and 4 is impossible based solely on the ^{1}H NMR spectra.

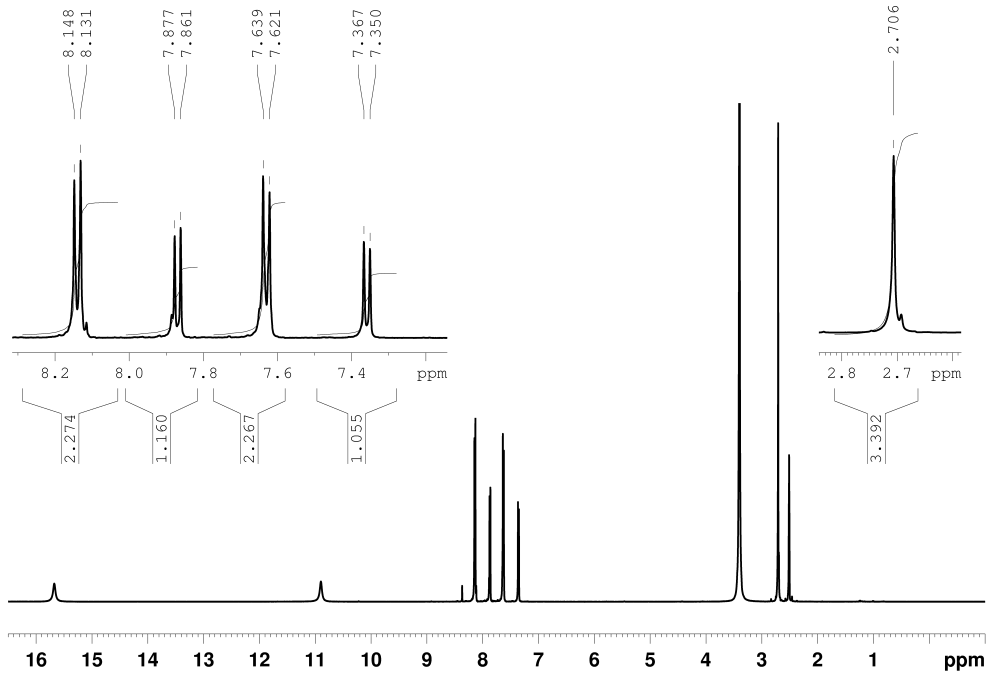

FIGURE 4.7: Measured ^{1}H NMR spectrum of YD ([YD]=130 mM) at room temperature in DMSO solution. The expansions show the aromatic regime and the methyl peak.

OH and NH protons appear as broad peaks in ^{1}H NMR spectra as a result of the chemical exchange between the hydrogen atoms of these groups and the solvent molecules, making them easily recognizable. This broadening can be so excessive that it leads to the disappearance of these peaks into the baseline. In the spectrum of YD two such broad peaks can be observed, both with smaller maximum height due to the line broadening by chemical exchange. These peaks at 10.9 and 15.7 are assigned to OH and NH groups.

COSY

Correlated spectroscopy was used for determining signals which arise from protons in YD that are coupled to each other through bonds. Two, three as well as four bond correlations yield COSY signals, which is shown in Fig.4.8.

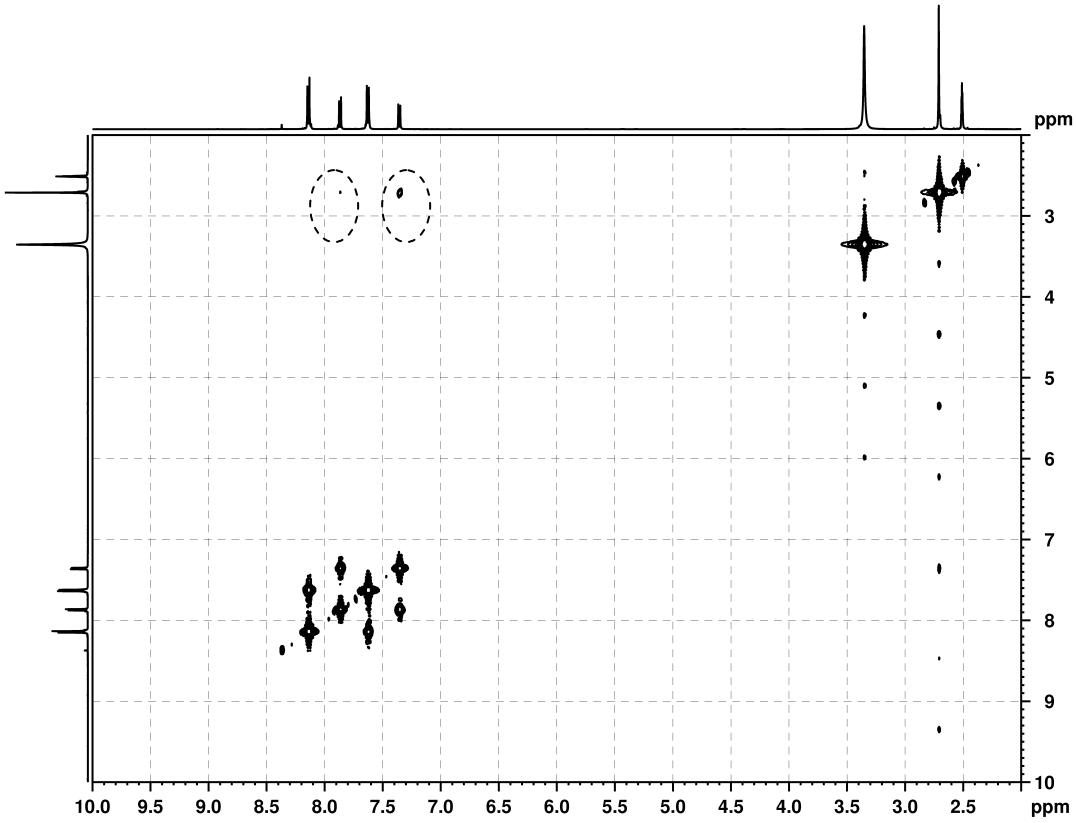

FIGURE 4.8: Measured COSY spectrum of YD in DMSO-d6 at room temperature.

This spectrum was used to identify the peaks of the hydrogen atoms 3 and 4. The ^{1}H peak arising at 2.7 ppm from the methyl hydrogen atoms was already assigned to hydrogen 1; therefore it was chosen as a starting point. The COSY spectrum shows two cross peaks for hydrogen 1 which are encircled in Fig. 4.8: one with the peak at 7.30 ppm (not very strong but visible) and another even weaker one with the peak at 7.85 ppm. Since there are only two H-atoms (3 and 4) in the aromatic ring that contains the methyl group, the cross peaks can be assigned to these atoms. The stronger correlation peak belongs to those atoms, which are closer to each other, thus the peak at 7.3 ppm is assigned hydrogen 3.

In Fig. 4.9 an enlargement of the aromatic region is shown. The peaks assigned to hydrogen 3 and 4 show the expected cross peaks with each other. The remaining two doublets at 7.65 ppm and 8.15 ppm, which are correlated only with each other, had been assigned to hydrogen 10-11 and 12-13 already. The COSY results confirm

that the hydrogen atom pairs 10-11 and 12-13 are on the same ring but it is impossible to identify which peak belongs to 10-11 and which one to 12-13.

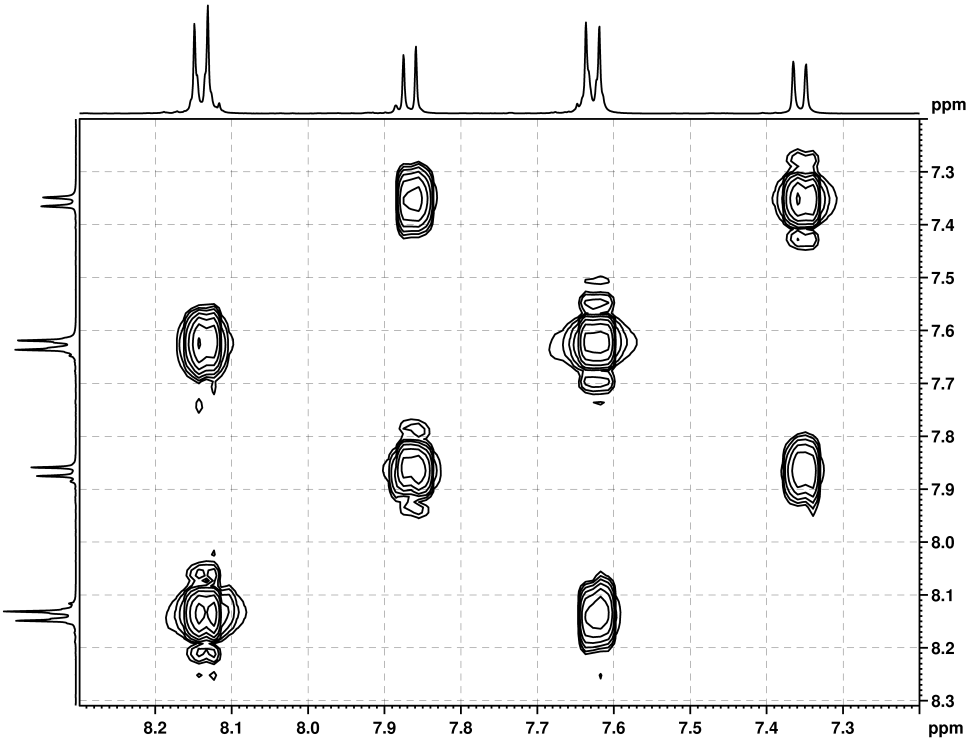

FIGURE 4.9: Aromatic hydrogen region of the measured COSY spectrum of YD in DMSO.

Thus, the only new information from the COSY experiment is the assignment of peaks 3 and 4 – everything else was known from the 1D spectrum.

^{13}C-NMR

The ^{13}C spectrum of YD in DMSO-d6 is shown in Fig. 4.10. According to the literature data[99] the broad solvent peak appears at 40 ppm. YD molecule contains only one aliphatic group, namely the methyl group, which appears at 20.74 ppm in the ^{13}C spectrum.

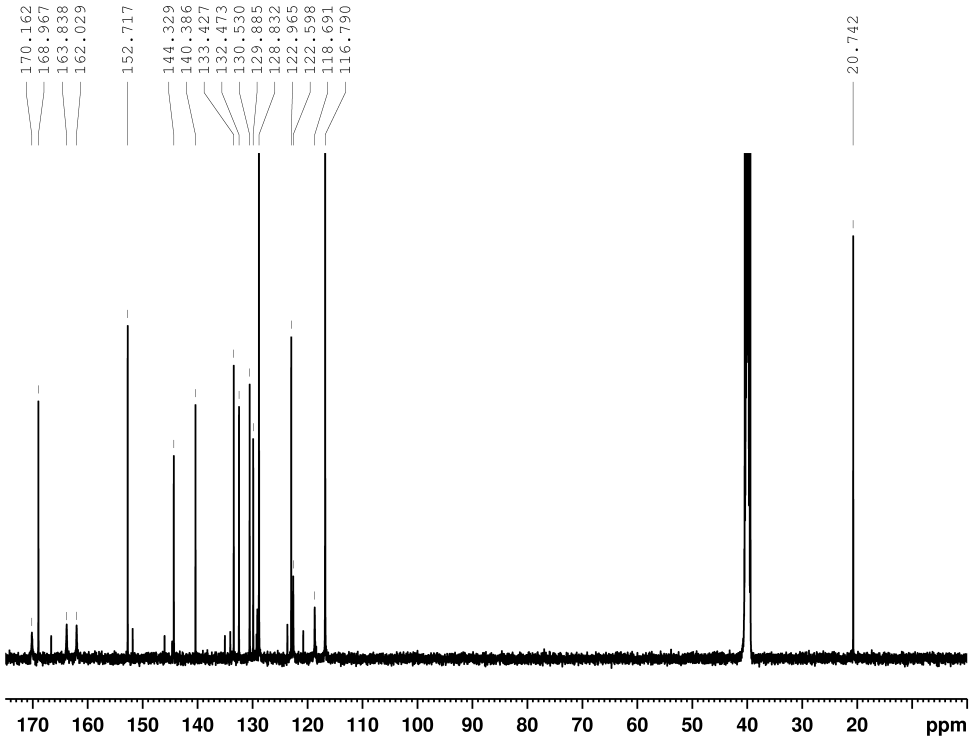

FIGURE 4.10: Measured ^{13}C NMR spectra of YD in DMSO.

The peaks of the aromatic carbon atoms appear between 110-180 ppm, resulting in a somewhat crowded spectrum. Fig. 4.11 presents this range in higher resolution. The peaks of the quaternary carbon atoms have long relaxation times (T_1) because there is no strong dipolar coupling that could provide a relaxation mechanism. These peaks appear with low intensity and are broad (170.16, 163.84, 162.03, 122.60, 118.69 ppm). In order to gain further information, 2D methods were applied.

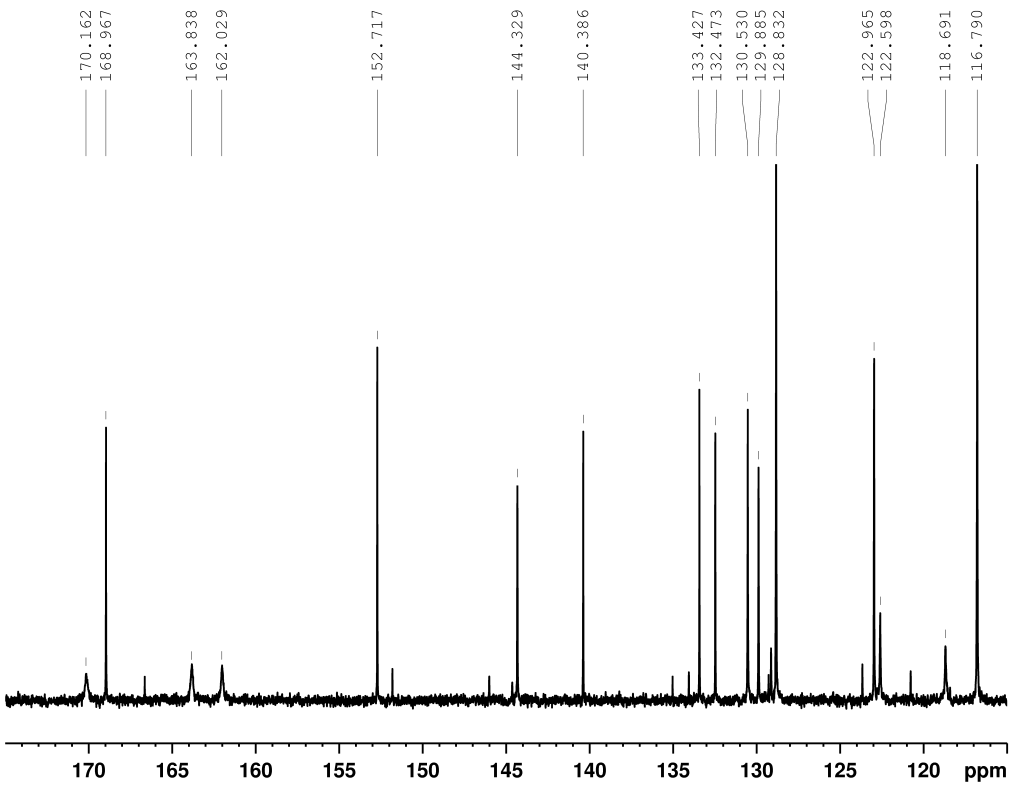

FIGURE 4.11: 110-180 ppm range of the measured ^{13}C NMR spectrum of YD in DMSO. The unlabelled peaks with very low intensity result from impurities.

HMQC

The HMQC spectra of YD show the one-bond correlations between ^{13}C atoms and ^{1}H atoms (Fig. 4.12). Based on the previously assigned hydrogen atoms, the carbon atoms can be assigned, which are directly bonded.

In the aliphatic range, the methyl carbon appears at 20.74 ppm. Furthermore the solvent peak is recognizable at 40.05 ppm.

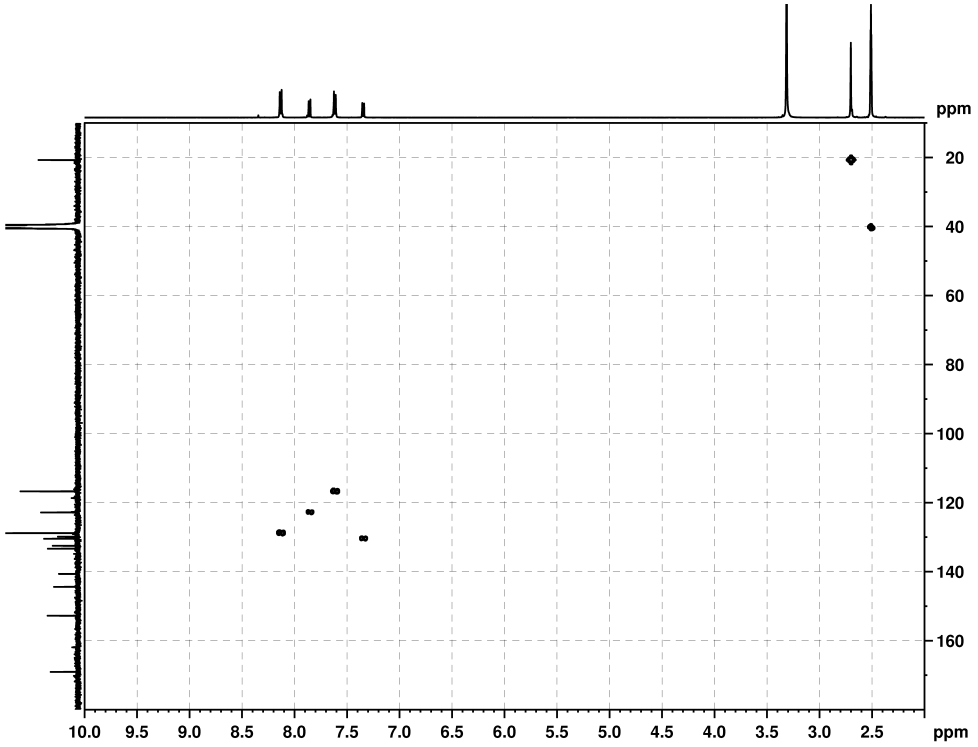

FIGURE 4.12: HMQC spectrum of YD in DMSO at room temperature.

An enlargement of the aromatic region of the spectrum is shown in Fig. 4.13.

By using the estimated data (Table 4.1) and the previous assignments of hydrogen atoms 3 (7.30 ppm), 4 (7.85 ppm), 10-11 (8.15 ppm) and 12-13 (7.65 ppm) the directly attached carbon atoms are assigned: 3 (130.53 ppm), 4 (122.97 ppm) and 10-11 or 12-13 (128.83 ppm and 116.79 ppm)

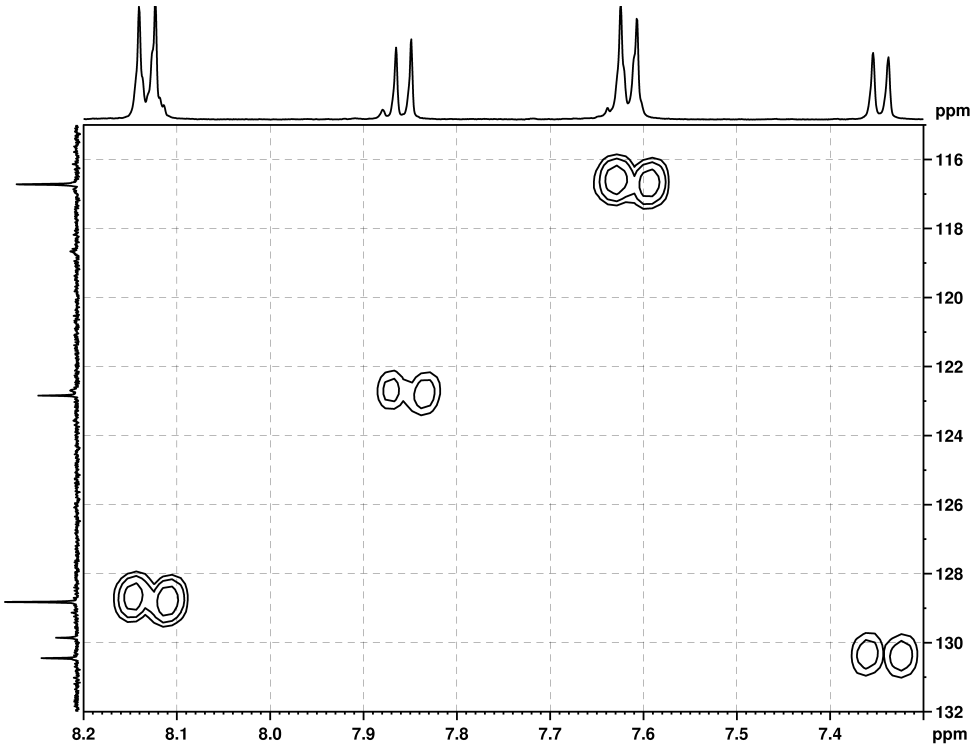

FIGURE 4.13: Aromatic region of the HMQC spectrum of YD.

HMBC

Although HMBC is a heteronuclear long range technique yielding single cross peaks for $^{2}J_{CH}$, $^{3}J_{CH}$ and $^{4}J_{CH}$ couplings, occasionally $^{1}J_{CH}$ couplings are also visible in the spectra as two symmetric peaks positioned on a line parallel to the ^{1}H frequency axis and centered at the crossing point of the ^{13}C and ^{1}H frequency. In this case we can see the carbons and the directly attached protons.

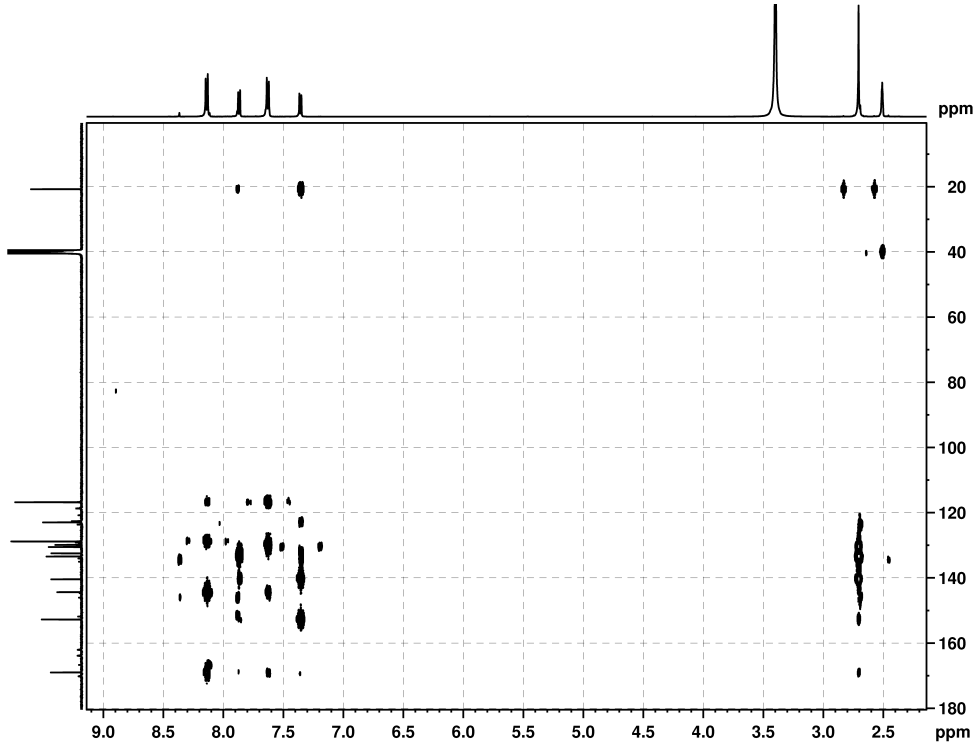

FIGURE 4.14: HMBC spectrum of YD in DMSO at room temperature.

The HMBC spectrum shown in Fig. 4.14 confirms the findings of the ^{1}H-NMR and COSY techniques, since the carbon of the methyl group correlates with hydrogen atoms 3 and 4. Certainly, the correlation with 3 is stronger than with 4 due to the shorter distance. The one-bond correlation between the methyl carbon and hydrogen atoms can also be observed. Examination of the correlation of methyl hydrogen atoms and aromatic carbons usually provides valuable information, but in this case the peaks overlap and therefore no additional information can be obtained. Correlations between the aromatic carbon and hydrogen atoms appear in the crowded part of the spectrum. A higher resolution plot of that region is shown in Fig. 4.15.

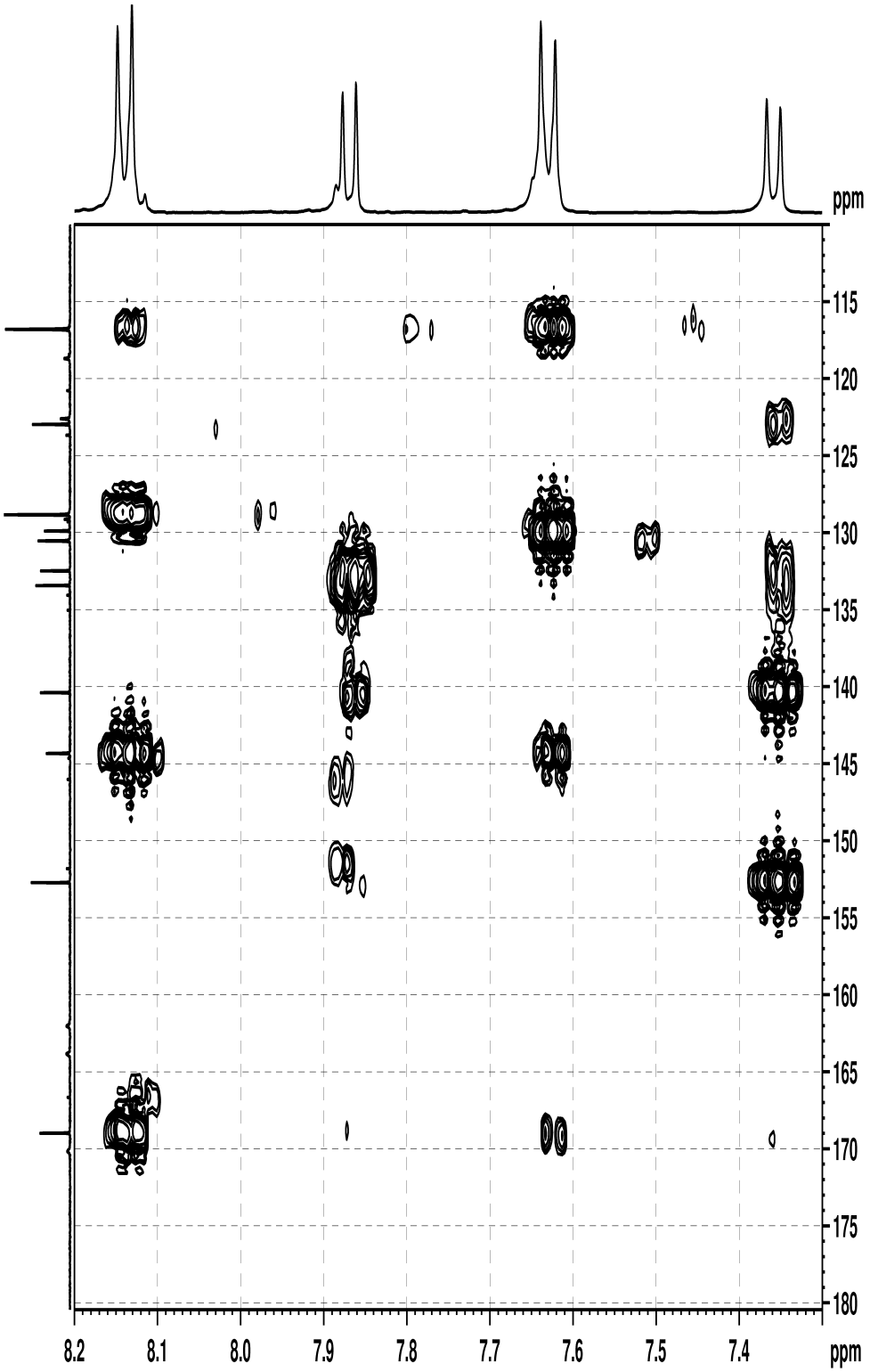

FIGURE 4.15: Aromatic region of the HMBC spectrum of YD at room temperature.

The first challenge of the spectrum assignment is the selection of a suitable point of reference. In this instance, carbon 7 was the best possible choice because of its expected strong correlation with hydrogen atoms 10-11 and a weaker one with hydrogen atoms 12-13. Moreover, a very weak correlation with hydrogen 4 and almost no correlation with hydrogen 3 are expected.

The positions of the hydrogen atoms are known from the COSY and ^{1}H spectra. The only carbon peak in the HMBC spectrum showing correlations with all of the hydrogen atoms designated 10-11, 12-13, 3 and 4 is the one at 168.97 ppm. Therefore it can be assigned to carbon 7 (168.97 ppm). By using the HMQC data carbons 10-11, 12-13, 3, and 4 were already assigned. (carbons 10-11 at 128.83 ppm and hydrogen atoms 10-11 at 8.15 ppm; carbons 12-13 at 116.79 ppm and hydrogen atoms 12-13 at 7.65 ppm; carbon 3 at 130.53 ppm and hydrogen 3 at 7.30 ppm; carbon 4 at 122.97 ppm and hydrogen 4 at 7.85 ppm).

The next step is the identification of carbons 9 and 14. As expected, the strong correlations with hydrogen pairs 10-11 and 12-13 were the only ones detectable, while the available estimation data suggest that 14 appears in the higher ppm region of the spectrum (carbon 9 at ~129 ppm; carbon 14 at ~144 ppm).

Considering the first ring which contains the methyl group, carbons 3 and 4 are already assigned. Besides these, there are four (2, 5, 6, 8) other carbon atoms that should display a correlation with hydrogen atoms 3 and 4. Three of these four peaks appear at chemical shifts values close to each other, namely at 132.47, 133.43 and 140.39 ppm, which refer to carbons 8, 2 and 6 as these atoms all have their estimated values between 131 and 134 ppm. Moreover the peak with appears at 152.72 ppm, based on the estimation, is assigned to 5. As a consequence of similar chemical environments of 2, 6 and 8, however, the available information is not sufficient to assign the peaks to the distinctive carbons.

The last phase of the spectrum assignment takes the last ring of the molecule containing exclusively quaternary carbon atoms into consideration. The single hydrogen in the OH group is not informative due to the exchange with the solvent. Thus, no correlation in the HMBC spectrum can be seen, which obstructs the selection of a reference point.

Quaternary carbons, because of their extremely long relaxation times, appear with low intensity. Using the estimated data the quaternary peaks can be assigned as follows: carbon 19 at 118.69 ppm; carbon 16 at 170.16 ppm; carbon 18 at 162.03 ppm; carbon 15 at 122.60 ppm; carbon 17 at 163.84.

The summary of the peak assignment based on the different methods is listed in Tables 4.1 and 4.2.

TABLE 4.1

^{1}H NMR chemical shifts of YD

Designation of H atoms	Chemical shift (ppm)	
	measured	estimated
1	2.70	2.64
3	7.30	7.61
4	7.85	7.89
10, 11	8.15	7.76
12, 13	7.65	6.69
NH	15.70	13.24
OH	10.90	12.57

TABLE 4.2

^{13}C NMR chemical shifts of YD (unclear assignments are highlighted in italic).

Designation of C atoms	Chemical shift (ppm) measured	estimated
1	20.74	21.6
2, 6 or 8	133.43	133.0
3	130.53	127.6
4	122.97	126.5
5	152.72	152.4
6, 2 or 8	140.39	133.4
7	168.97	166.5
8, 2 or 6	132.47	131.8
9	129.88	121.0
10, 11	128.83	129.6
12, 13	116.79	116.8
14	144.33	143.0
15	122.60	*154.0*
16	170.16	*163.0*
17	163.84	*193.0*
18	162.03	*163.0*
19	118.69	*118.0*

The concentration and the temperature dependence of the chemical shifts of the ^{1}H NMR peaks were investigated for dye concentrations between 0.7 and 130 mM at various temperatures from 10° C to 70° C. No change of chemical shift is observed, meaning that there are no aggregates in this organic solvent. The recorded spectra belong to the monomeric state of the dye.

4.2.2 ^{1}H Chemical shift Analysis

In order to investigate the aggregates the organic solvent DMSO was substituted by deuterated water, D_2O. This change in conditions leads to the formation of aggregates as demonstrated by optical techniques before. Using the peak assignments in DMSO the aggregation process observed in aqueous solution can be more thoroughly understood.

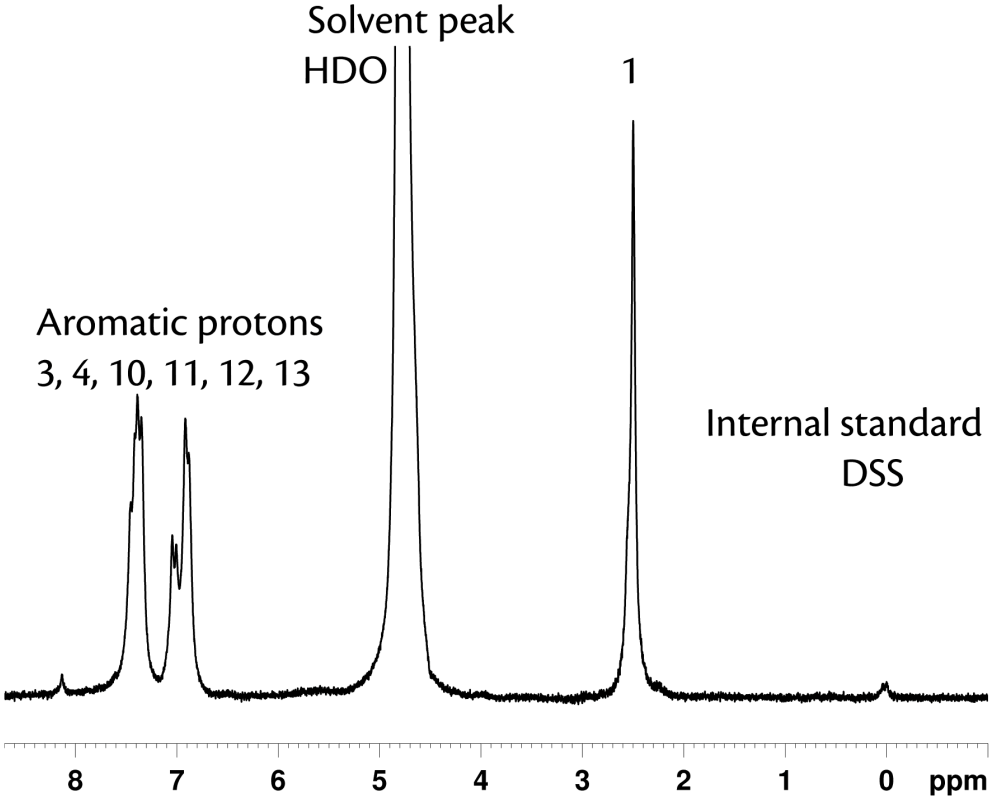

Figure 4.16: ^{1}H NMR spectrum of YD in 30 mM concentration D_2O solution at 25°C (recorded by 200 MHz spectrometer).

The ^{1}H NMR spectrum of YD in aqueous solution (Fig. 4.16) displays line broadening because of the short transverse relaxation time (T_2) of bigger molecules produces broader lines[80]. Three distinct groups of peaks appear in the spectrum. The unresolved four doublets from 6.7 to 7.7 ppm correspond to six aromatic hydrogen atoms; the large peak at 5.8 ppm is the solvent peak, while the remaining one at 2.46 ppm arises from the methyl group.

The previously used concentration, which was used for the microscopy measurements, is too high to be able to provide additional information about the aggregation process by using NMR. At high concentration of the dye the spectrum is unresolved (due to the broad lines from the big aggregates) and the peaks have low intensity (due to precipitation). Therefore a dilute solution of YD (0.7 mM concentration) was investigated, which is in the concentration range used for the UV/VIS measurements.

A comparison of the line widths of the spectra measured in DMSO as solvent and in the most dilute aqueous solution measured in NMR displays considerable agreement. (Fig. 4.17)

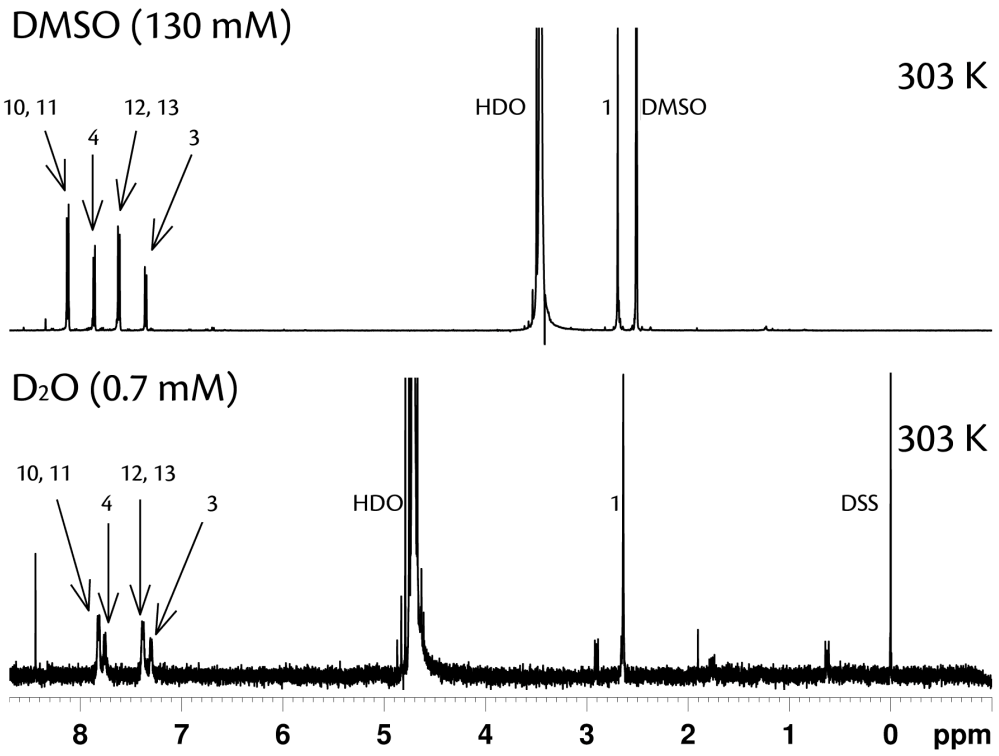

FIGURE 4.17: ^{1}H NMR spectra of YD in DMSO and dilute D_2O solution at room temperature.

At the high concentration of 30 mM the resulting spectrum demonstrates significantly broader and shifted peaks. Therefore a series of measurements (0.7 –

30 mM) was carried out to verify the suspected dependence on the dye concentration [YD].

The aromatic regions of several selected spectra measured in D_2O at different dye concentrations are presented in Fig. 4.18. For comparison the spectrum in DMSO solution, where no aggregation occurs, is shown on top. The concentration of the dye in D_2O was increased between 0.7 mM and 15 mM.

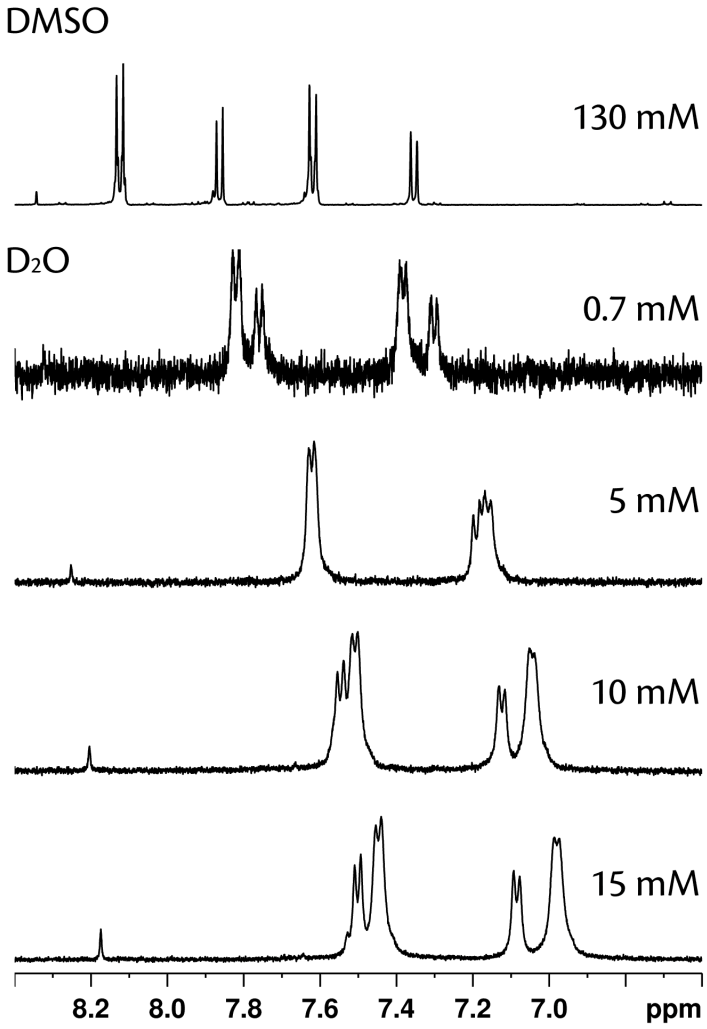

FIGURE 4.18: Aromatic regions of ^1H NMR spectra of YD in DMSO and D_2O solution.

As can be seen in Fig. 4.18 increasing the dye concentration leads to an upfield shift of all peaks. Fig. 4.19 shows this effect in more detail and the related chemical shift values are presented in Table 4.3. The change in chemical shifts is larger at low

concentrations; while it levels off at higher dye concentrations. The chemical shift value of the methyl group displays a smaller variation.

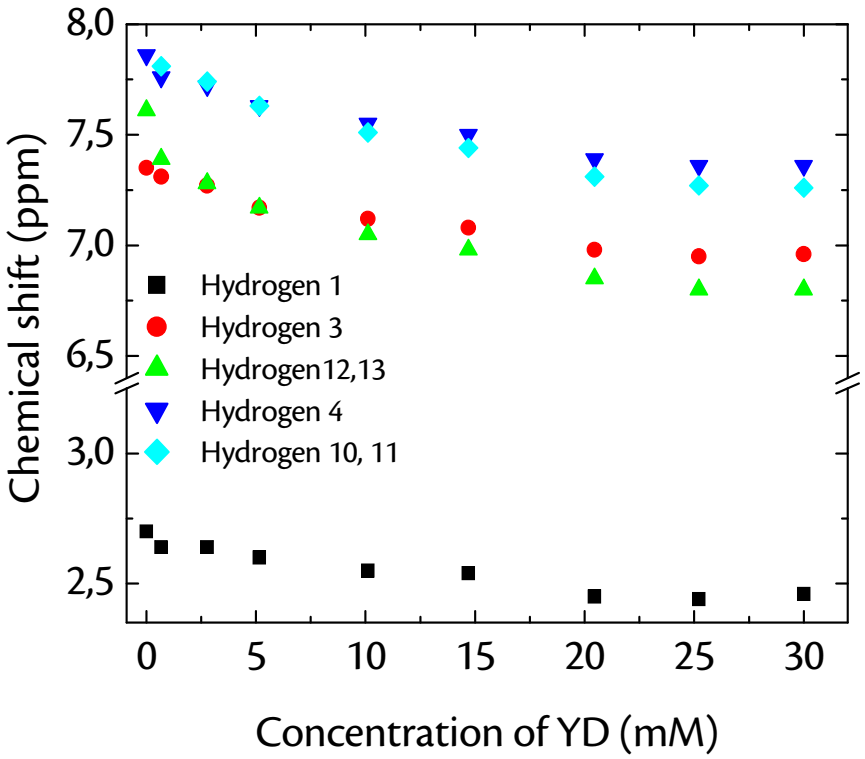

FIGURE 4.19: Proton NMR chemical shifts as a function of [YD] in aqueous solution at room temperature.

TABLE 4.3

Concentration dependence of ^{1}H NMR chemical shift of YD at room temperature

[YD] (mM)	^{1}H NMR chemical shifts (ppm)				
	1	3	12, 13	4	10, 11
0.0	2.7	7.35	7.61	7.86	8.13
0.7	2.64	7.31	7.39	7.76	7.81
2.5	2.64	7.27	7.28	7.72	7.74
5.0	2.6	7.17	7.17	7.63	7.63
10.0	2.55	7.12	7.05	7.55	7.51
15.0	2.54	7.08	6.98	7.5	7.44
20.0	2.45	6.98	6.85	7.39	7.31
25.0	2.44	6.95	6.8	7.36	7.27
30.0	2.46	6.96	6.8	7.36	7.26

The concentration dependence of ^1H chemical shift values indicates a stacking of the aromatic rings and formation of aggregates. With the increase of the concentration the peaks are subjected to an upfield shift, which is more pronounced for atoms located in the central regions of the molecule, namely hydrogen pairs 10-11 and 12-13. This shift occurs as a result of the shielding property of π-electrons, since the molecules are stacked upon each other. The methyl group, which is located in the outer part of the molecule, is less affected by π-shielding. These results correspond with the UV/VIS data very well, where a shear angle of 54.7-90° was found.

Another aspect of the aggregation process worth examining is its temperature dependence. The most dilute solution was investigated at three different temperatures, and the results were compared with those of the DMSO solution. Fig. 4.20 shows the temperature dependent spectra in both D_2O and DMSO.

Substantial changes are observed in the spectra at the lowest measured dye concentration in aqueous solution as the temperature increases, while almost no temperature dependence is found with DMSO as solvent. The small high field shift is within experimental error. No internal standard was used in case of DMSO solutions and the solvent peak was used as reference, which can be shifted by changing the temperature. These observations suggest that DMSO solutions contain individual molecules, but in D_2O there is already some aggregation even at lower concentrations. With increasing temperature the aggregates dissolve or become smaller, which leads to the observed changes of the chemical shifts.

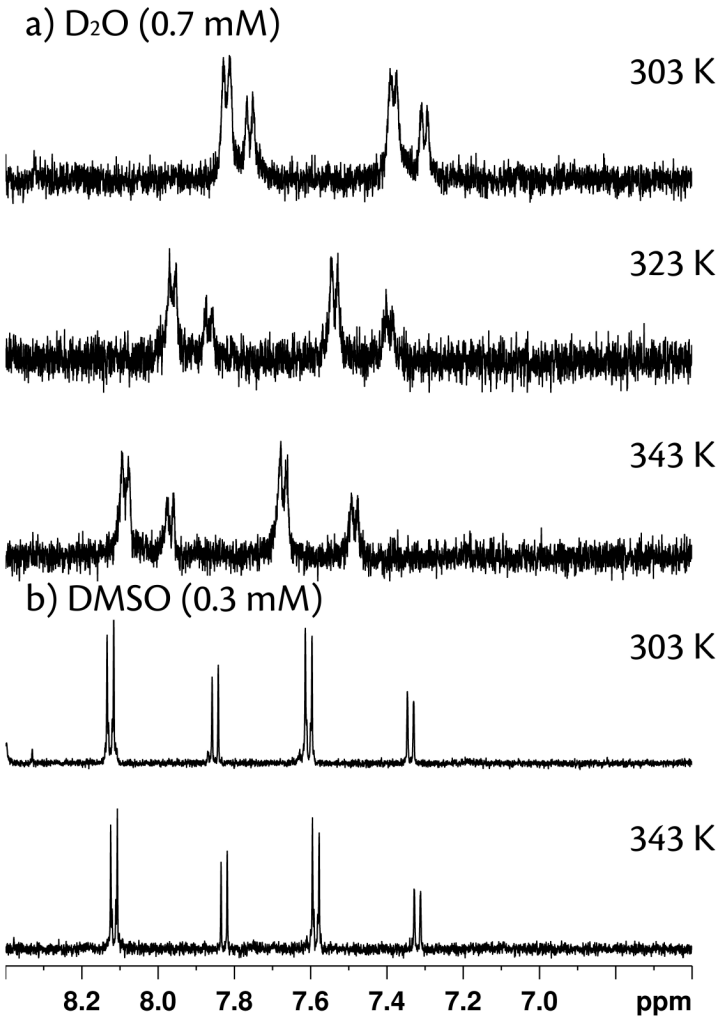

FIGURE 4.20: Aromatic regions of ^{1}H NMR spectra demonstrating the temperature dependence of chemical shifts in YD solutions at the measured lowest concentration in organic and inorganic solvents.

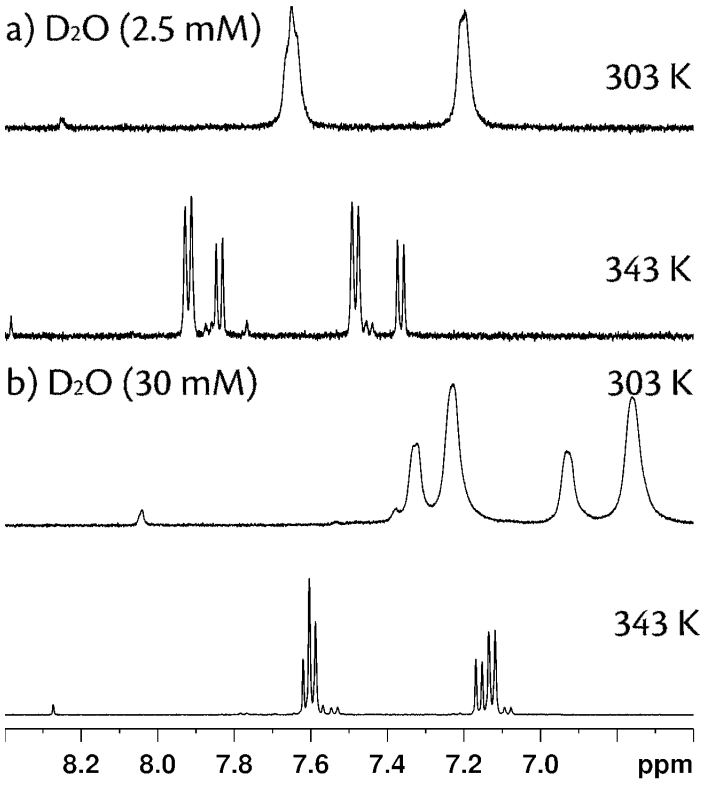

FIGURE 4.21: Aromatic regions of ^{1}H NMR spectra demonstrating the concentration dependence of chemical shifts of YD in aqueous solution.

Fig. 4.21 shows the temperature dependence for the aromatic regions of ^{1}H NMR spectra in aqueous solutions with different YD concentrations of 2.5 mM (a) and 30 mM (b). For each concentration spectra recorded at room temperature and at 70° C, which was the upper temperature limit of the instrument, are shown. In case of the more dilute solution elevating the temperature results in a spectrum substantially down-field shifted, suggesting that there is less aggregation at higher temperature. Under identical conditions the more concentrated solution shows a similar phenomenon, but to a much less degree. Theoretically, given the possibility of elevating the temperature above the inherent limit of the system, a spectrum most similar to the one describing the monomer state might be obtained (aside from solvent effects).

4.2.3 SIGNAL INTENSITIES

In case of YD aggregates there are no additional peaks of the aggregates in the ^{1}H NMR spectra (Fig. 4.16) in comparison with the monomer state spectra in DMSO, indicating that there is a fast chemical exchange between the aggregates and the individual dye molecules. The observed spectra are time-averaged spectra over the aggregates and the monomers. Fast exchange was confirmed by diffusion NMR measurements (Chapter 4.2.3.). The signals in the high resolution liquid NMR spectrum arise from both dissolved molecules and aggregates. Based on the formation of dye aggregates the maximum signal intensity can be decreased, when the aggregates are too big and/or rigid to be detected by classical liquid NMR methods and their signals are not contributing to the measured NMR spectrum. Even aggregates in solution, which have not precipitated may not be observed.

A quantitative analysis of dissolved species was performed by measuring the signal intensity of the methyl peak at various concentrations and temperatures. The results are presented in Fig. 4.22.

At low temperatures the measured peak intensities are always lower than at high temperatures. For each concentration the intensity increases with increasing temperature and a constant plateau is reached. The plateau values are reached at lower temperature for the lower concentrations. This indicates that signal intensity is lost at low temperature due to big aggregates, which cannot be detected by the solution state NMR method used here. For example in case of 30 mM sample at 10°C the maximum signal intensity is about 40 and at 70°C it is about 72, thus the loss of signal can be around (72-40)/72= 44 %.

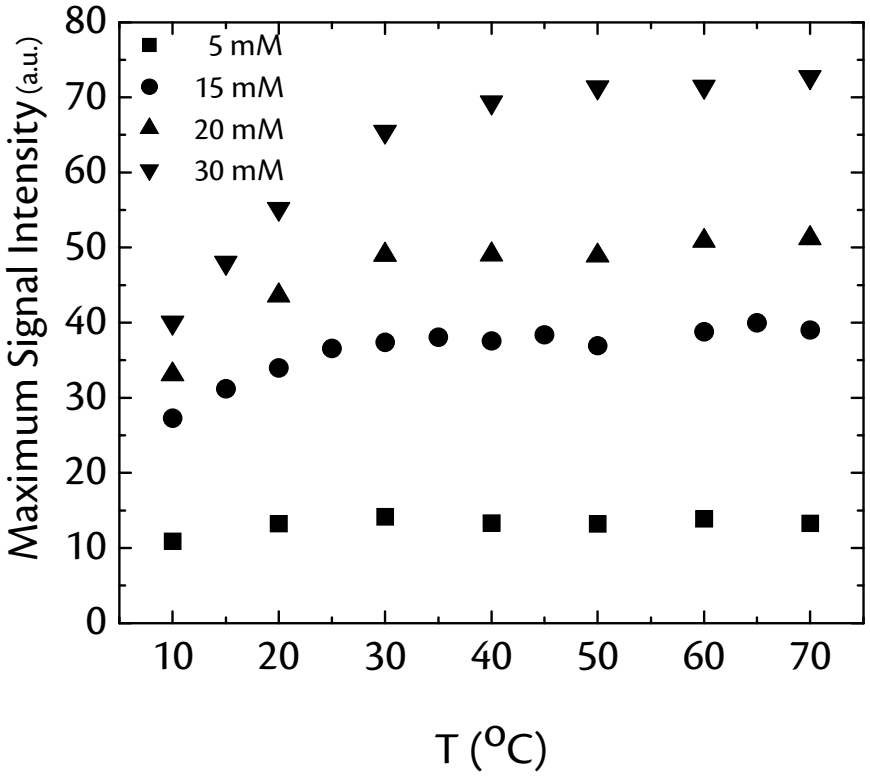

FIGURE 4.22: Maximum signal intensity of the methyl proton as a function of temperature in D_2O solutions of different concentrations.

4.2.4 CHEMICAL EXCHANGE AND LINE WIDTH

The line width of the peaks, which is defined as the full-with at half height of a resonance line, depends on the T_2 relaxation time of the molecules. There are two other effects for additional broadening, namely chemical exchange between the individual dye molecules and the aggregates and the broadening due to the magnetic field inhomogeneity.

Under the experimental conditions with the 500 MHz spectrometer these two additional effects are negligibly small due to the fast chemical exchange and the high resolution of the NMR instrument. For the measurements of the 200 MHz spectrometer those effects were taken account.

The very small and the very big molecules have extremely long T_1 relaxation time, but the T_2 relaxation time, which is relevant for the line width[80] and remains low for big molecules results in broad peaks in the spectra. Even midsize molecules, such as the NMR detectable YD aggregates, have short T_2 relaxation time which produces broad peaks.

Similar to the signal intensity analysis the methyl peak line width was analyzed for each case. The overlapping signals of aromatic protons cannot be measured with high accuracy so only the methyl peak was analyzed. The linewidth of the methyl signal as a function of temperature in aqueous solution at various dye concentrations is shown in Fig. 4.23. The same data are presented in Fig. 4.24 showing linewidth versus dye concentration at various temperatures.

At higher concentrations and at lower temperatures the lines get broader as a result of bigger aggregates which have shorter relaxation times and produce broader peaks in the NMR spectra. The discontinuity of the 20 mM sample can be a measurement error, such as shimming.

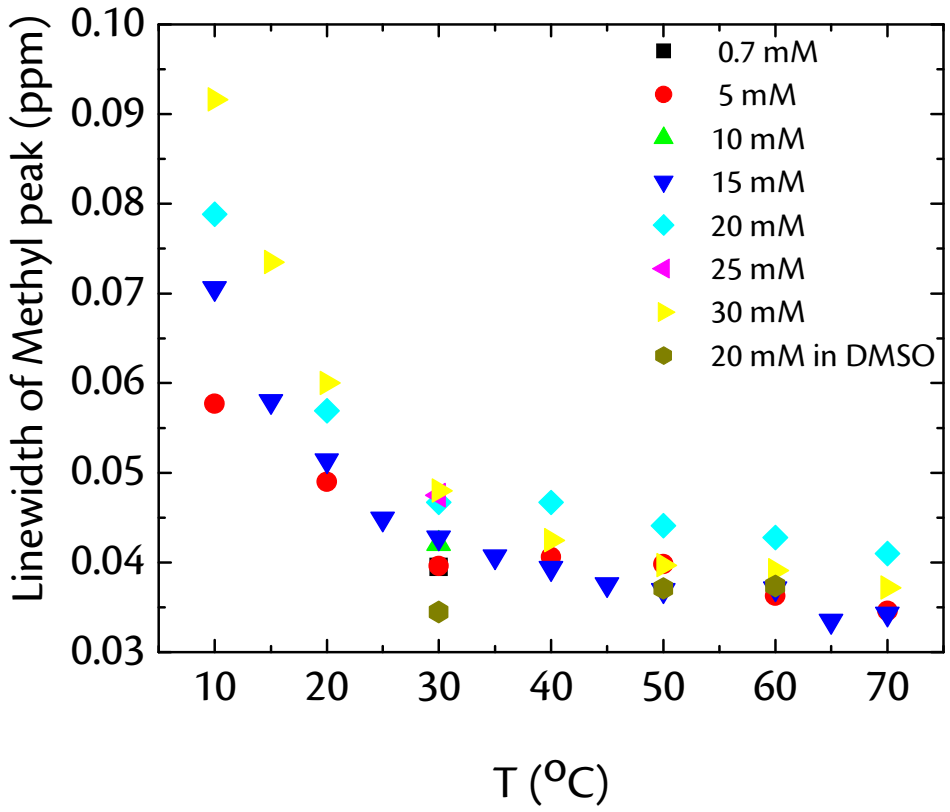

FIGURE 4.23: Linewidth of the methyl protons as a function of temperature in aqueous solutions at different dye concentrations in DMSO at a concentration of 20 mM.

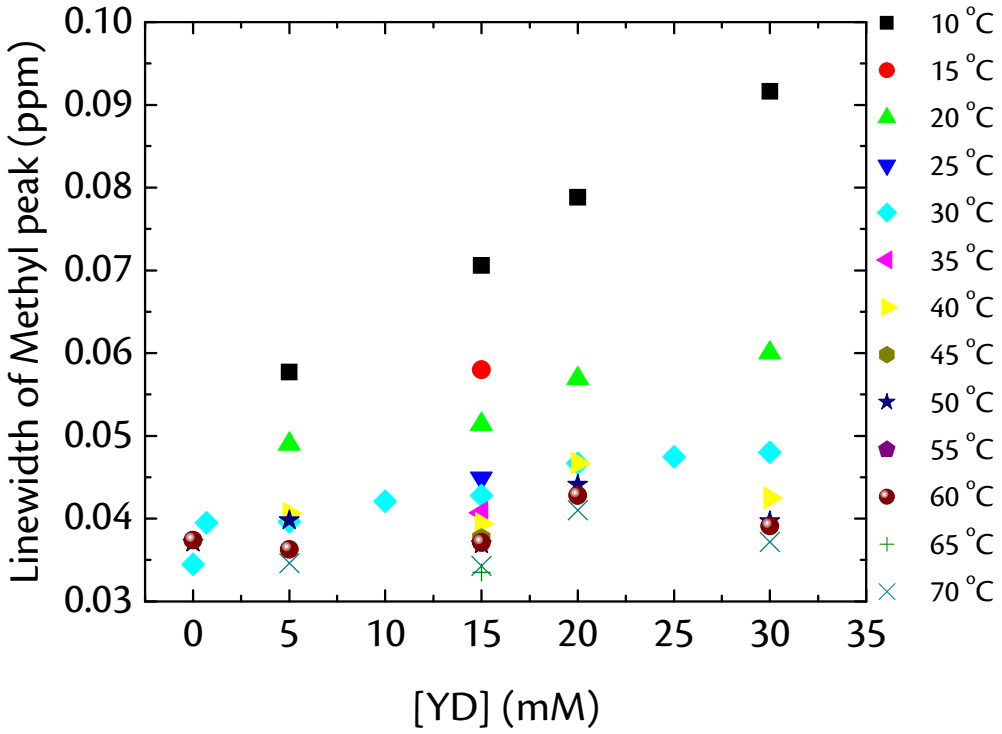

FIGURE 4.24: Linewidth of the methyl peaks as a function of YD concentration at different temperature in aqueous solution.

Based on equation [2.4] the measured line widths are converted to T_2 relaxation times, which are shown in Fig. 4.25.

$1/T_2$ is approximately proportional to the overall rotational correlation time (τ_c), which depends on the mass and shape of the molecule. τ_c is approximately the average time for the molecule to rotate by one radian.

In order to obtain τ_c from the measured line widths a calculated relationship from the literature was used.[80] This relationship is shown in Fig. 4.26.

The principal uncertainties in the calculation are due to the following factors: anisotropic rotational diffusion of nonspherical molecules, differential contribution from internal motions, cross correlation effect, ^1H dipolar interaction with nearby protons, chemical shift anisotropy. In light of these uncertainties, the result, presented in Fig. 4.26 should be regarded as an approximate guideline.[80] For

example ^{1}H measured linewidths in ubiquitin are 6-9 Hz. This value is consistent with 5 Hz in Fig. 4.26.

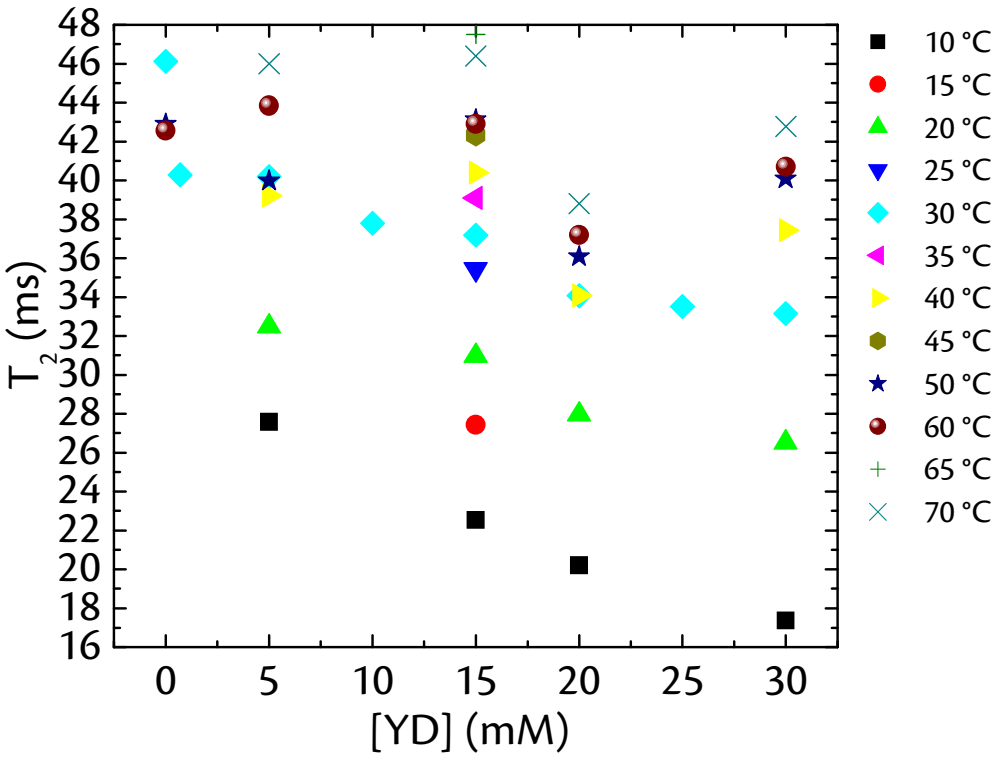

FIGURE 4.25: Relaxation times as a function of YD concentration at different temperature.

According to Fig. 4.26 the correlation times were estimated from the linewidths, the resulting values shown in Fig. 4.27.

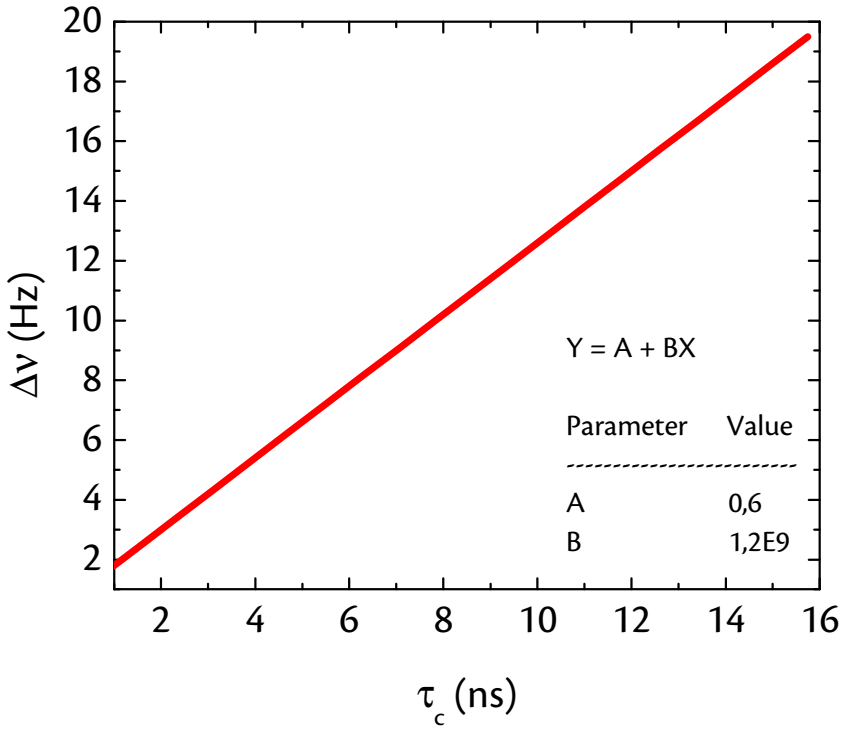

FIGURE 4.26: Resonance linewidths of ^{1}H spins are shown as a function of rotational correlation time. Adapted from the literature[80] where the linewidth was calculated as a function of the rotational correlation time τ_c for various types of nuclei. The line shows the data for the case of ^{1}H spins. The line is represented by $\Delta\upsilon=0.6+1.2E9\ \tau_c$.

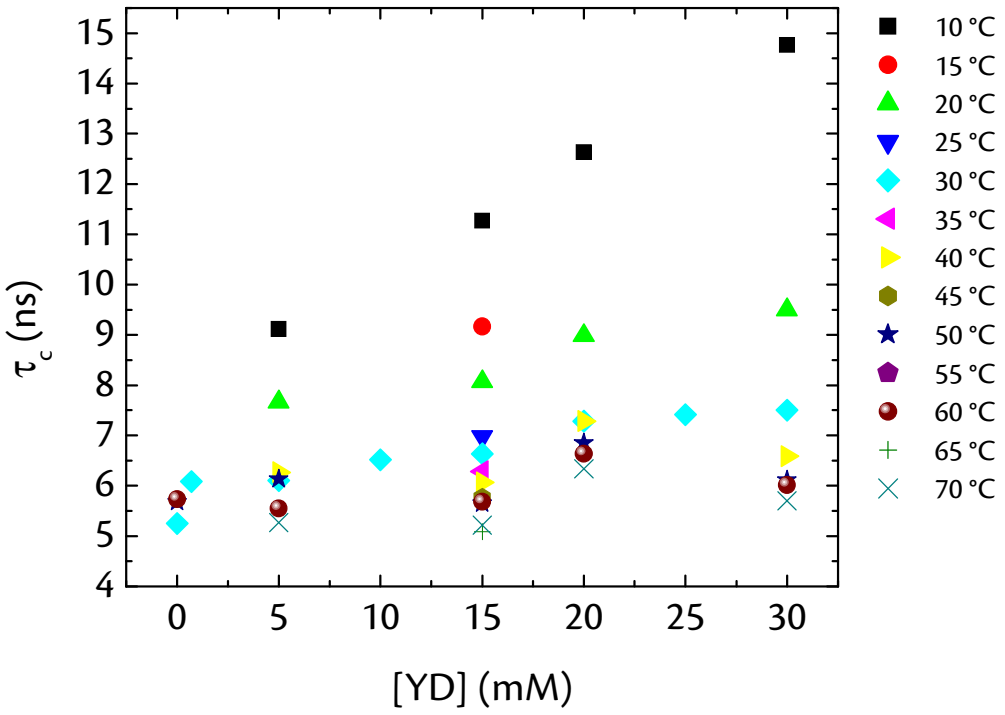

FIGURE 4.27: Estimated rotational correlation times are shown as a function of YD concentration at various temperatures.

The correlation time varies with molecular size, solvent viscosity and temperature. The simplest theoretical approach for approximately spherical globular particles calculates the isotropic rotational correlation time from Stokes law. Using equation [2.6] and the values of the estimated τ_c, R_h was calculated. The results are shown in Fig. 4.28.

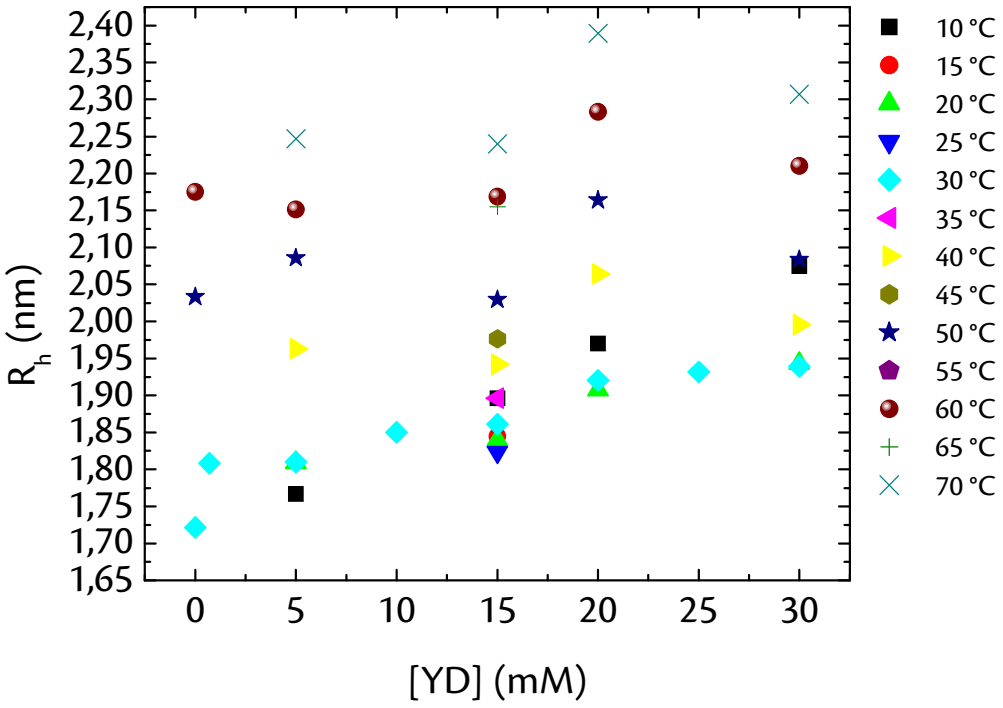

FIGURE 4.28: Estimated hydrodynamic radii are shown as a function of YD concentration at various temperatures.

The measured linewidth used in the previous analysis can be much bigger than the homogeneous linewidth especially in case of sharp peaks (small molecules). Shimming of the 200 MHz magnet used for the diffusion NMR experiments was not perfect and the magnet field inhomogeneity cannot be neglected. To decrease this problem a correction of the linewidth was carried out.

The correction of the linewidth was calculated from the methyl peak of YD in DMSO. Based on computer simulations one half of the molecular length is 0.7 nm. It was taken as R_h of the monomer. The rotational correlation time was calculated according to equation [2.6] and the homogeneous linewidth corresponding to τ_c was obtained form Fig. 4.26. Then all of the measured linewidth values were corrected by the difference of the measured and the calculated value of the methyl peak width in DMSO. The measured linewidth of the methyl protons was 6.9 Hz

and the calculated one was 1.345 Hz. Thus the broadening of the peak due to the magnetic field inhomogeneity and other effects, which was discussed before, is 5.555 Hz.

All of the corrected linewidths are shown in Fig. 4.29.

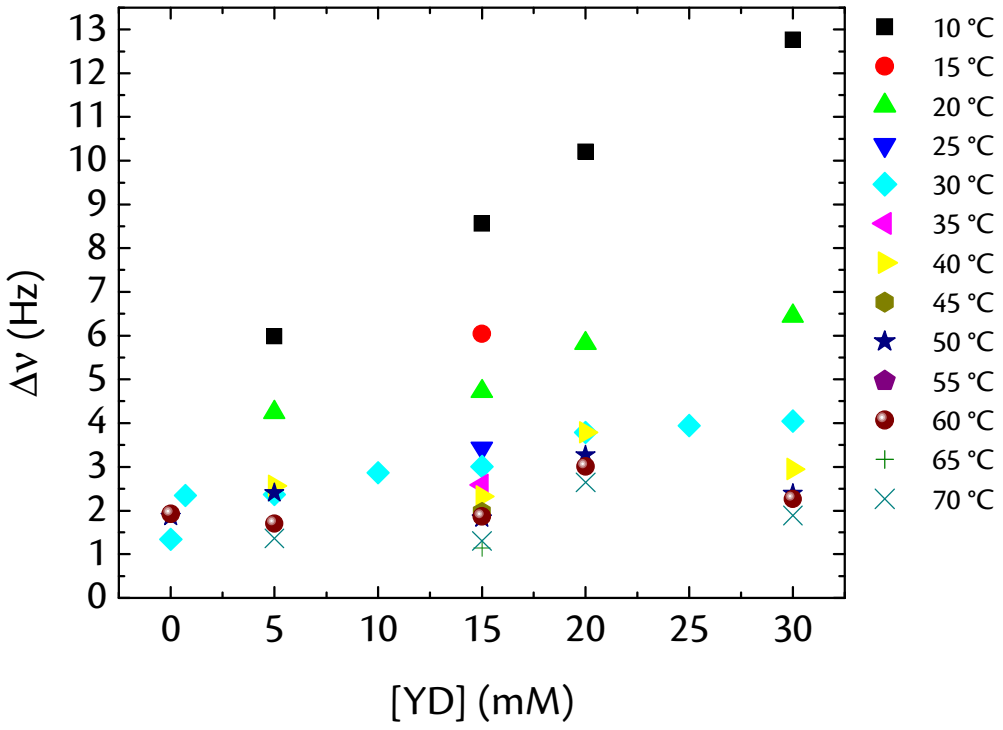

FIGURE 4.29: Estimated proton resonance homogeneous linewidths are shown as a function of YD concentration at various temperatures.

From the estimated homogeneous linewidth the rotational correlation time (Fig. 4.30) was calculated, which then was used for the R_h determination (Fig. 4.31).

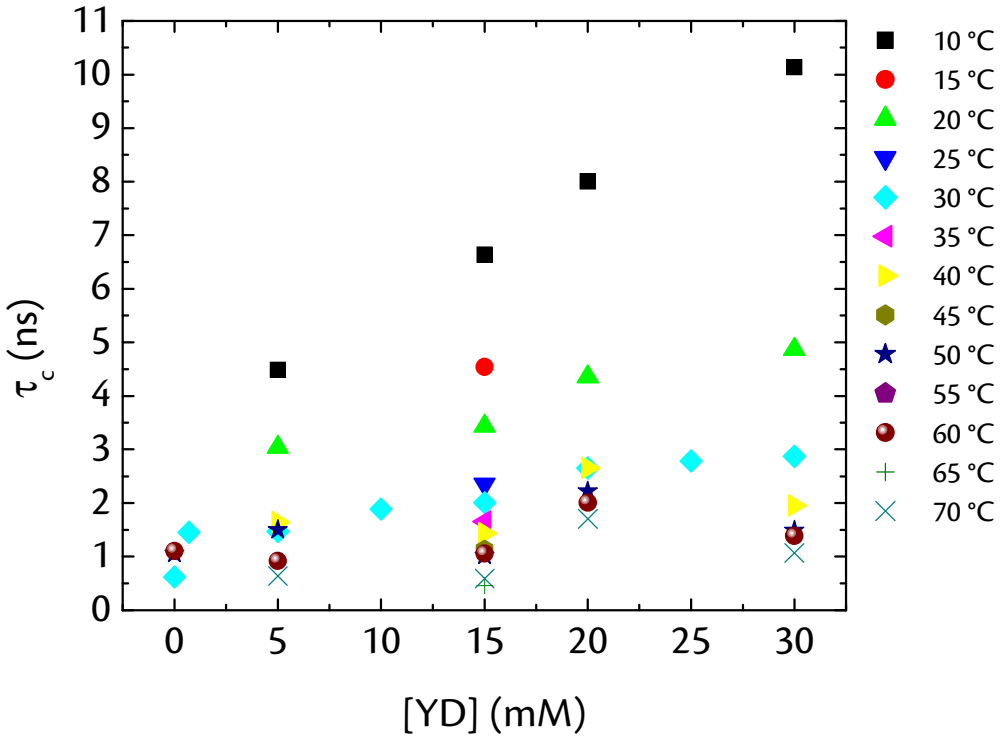

FIGURE 4.30: Corrected rotational correlation times are shown as a function of YD concentration at various temperature.

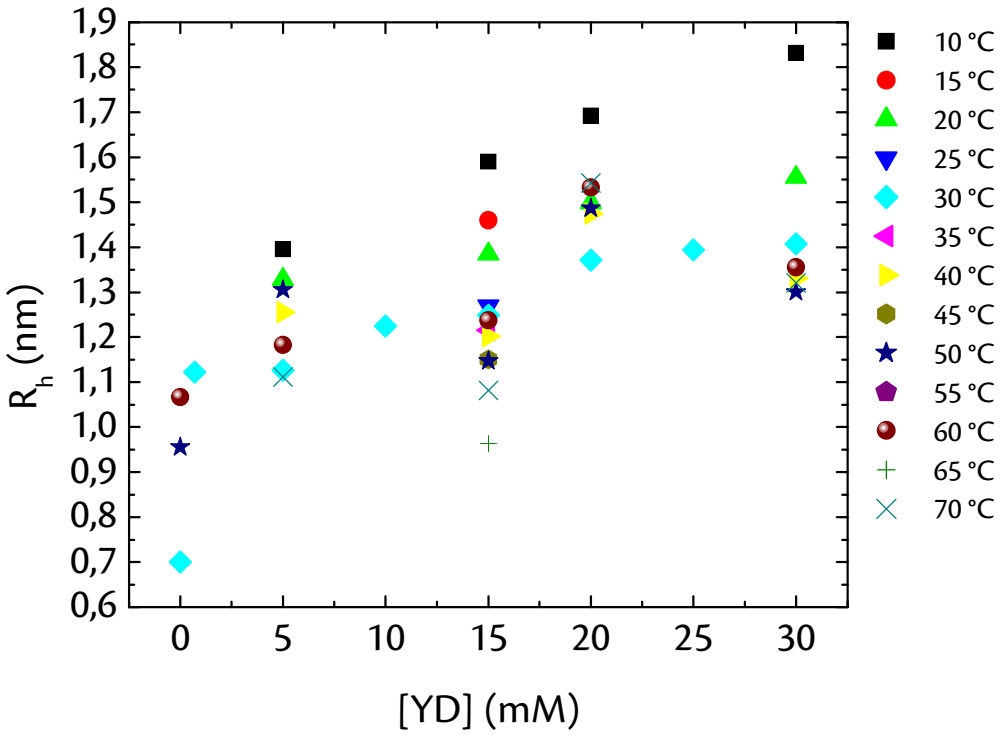

FIGURE 4.31: Corrected estimated hydrodynamic radii are shown as a function of YD concentration at various temperatures.

The radius of the particles increases with increasing concentration and decreasing temperature up to 1.9 nm. There is some scattering of the data due to the estimation error and the accuracy of the magnet shimming.

4.2.5 NMR DIFFUSOMETRY

NMR diffusometry was used to determine the diffusion coefficients of the dye molecules/aggregates at various concentrations (0.7–30 mM) and temperatures (10–70 °C). The same samples were used for the high resolution and the diffusion NMR measurements.

Determination of the diffusion coefficient

The data analysis of the PGSTE diffusion experiments is presented in the following. Fig. 4.31a shows an example of the diffusion NMR spectra of YD. The strength of the pulsed-field gradient along the z axis was varied between 0 and 650 G/cm. At the highest gradient almost no signal was detected.
The protons of the water disappear at lower gradient strength than the aromatic- and the methyl protons of the dye. In this sample the dye forms aggregates and the observed diffusion of the dye molecules is much slower than that of the solvent molecules.

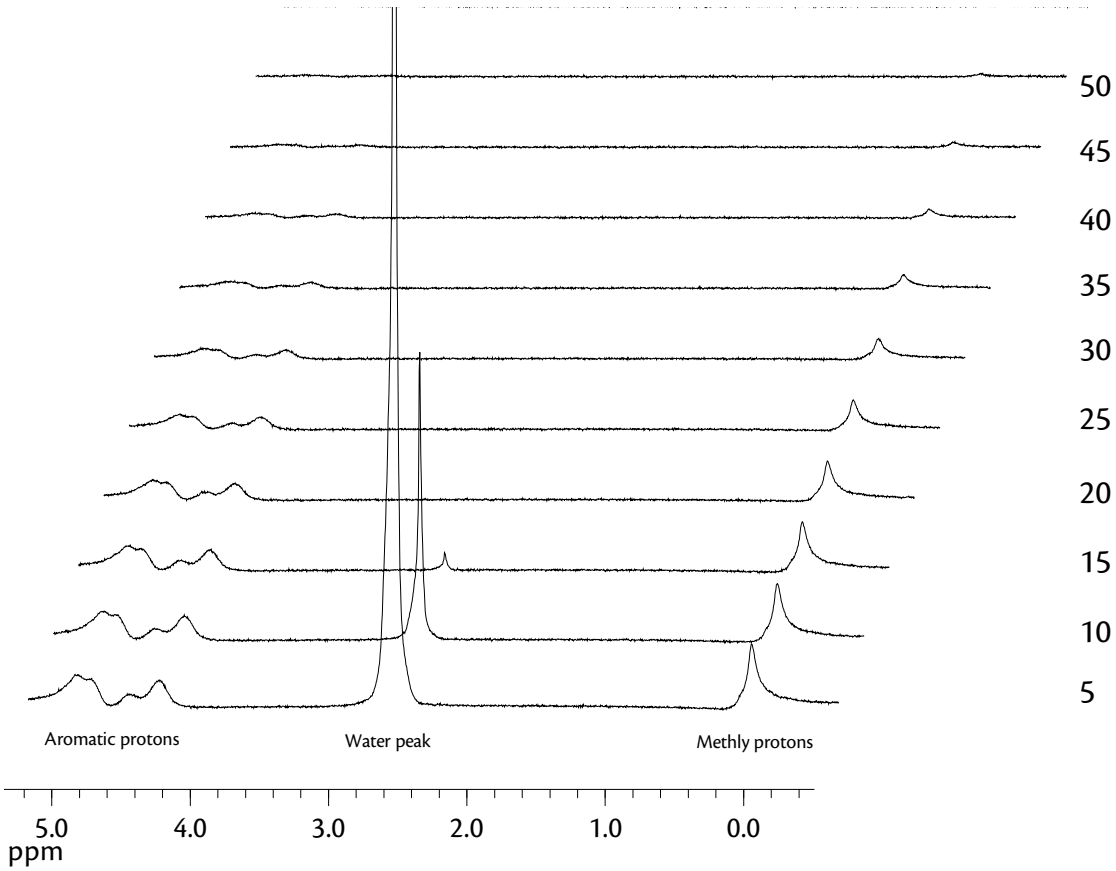

FIGURE 4.31a: ^{1}H PGSTE diffusion experiment of YD. ([YD]= 30 mM, T= 10 °C, Δ= 100 ms, δ= 500 μs, g_{max}= 650 G/cm, $n_{spectrum}$=64, ns= 128) 64 spectra were recorded, but only every fifth one is shown (starting with number 5 at the bottom and ending with number 50 at the top) and the last 3 spectra were mainly noise and they were neglected. The signal attenuation of methyl- and aromatic protons is very similar while the water proton intensity decreases faster.

The integral of each peak versus the gradient strength is shown in Fig. 4.32. The normalization was necessary to get a better comparison.

The intensity of the overlapping aromatic protons was measured together. The integration was performed using the same ppm intervals at each case. For comparison the attenuation of the methyl peak was also analyzed.

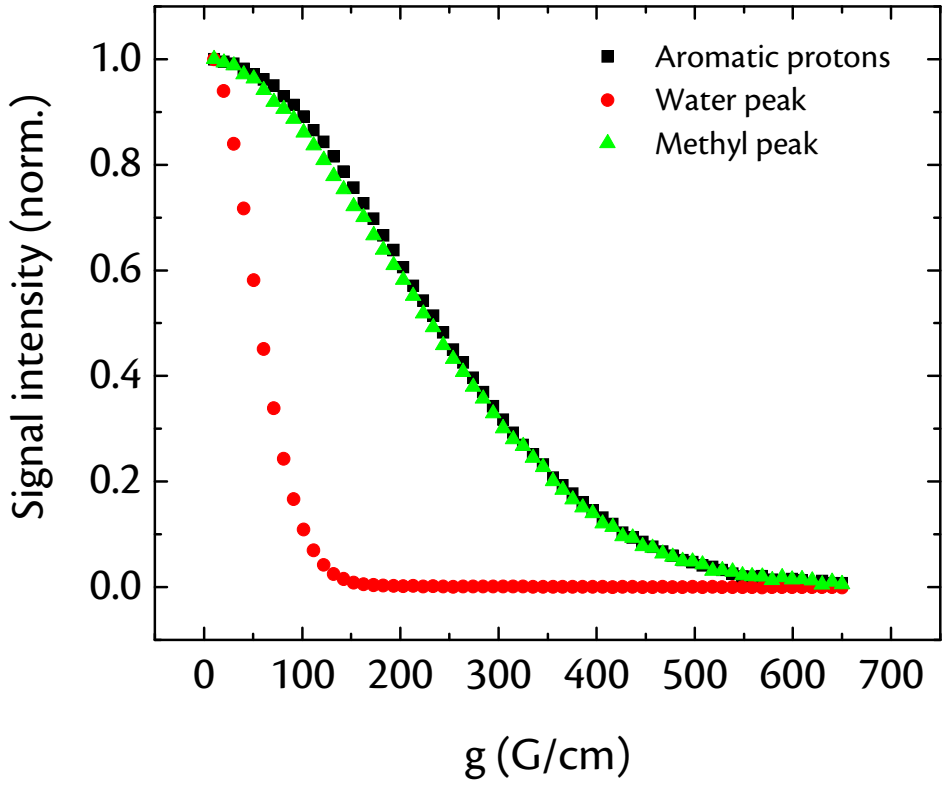

FIGURE 4.32: Normalized signal intensity from the diffusion experiment shown in Fig. 4.31 as a function of gradient strength.

Plotting the logarithm of the signal intensity versus kg^2 (with $k=\Delta\delta^2\gamma^2$) results in straight lines, which is shown in Fig. 4.33. The linearity of the attenuation of the signal shows that there is only one diffusing component based on the before mentioned fast chemical exchange. The slope of each line is related to the diffusion coefficients of the component. The diffusion coefficient values of the methyl signal and the aromatic proton signal are in a good agreement. The calculated measurement error is around 2 %.

The linear form of the resonance signal decays are presented in Fig. 4.33.

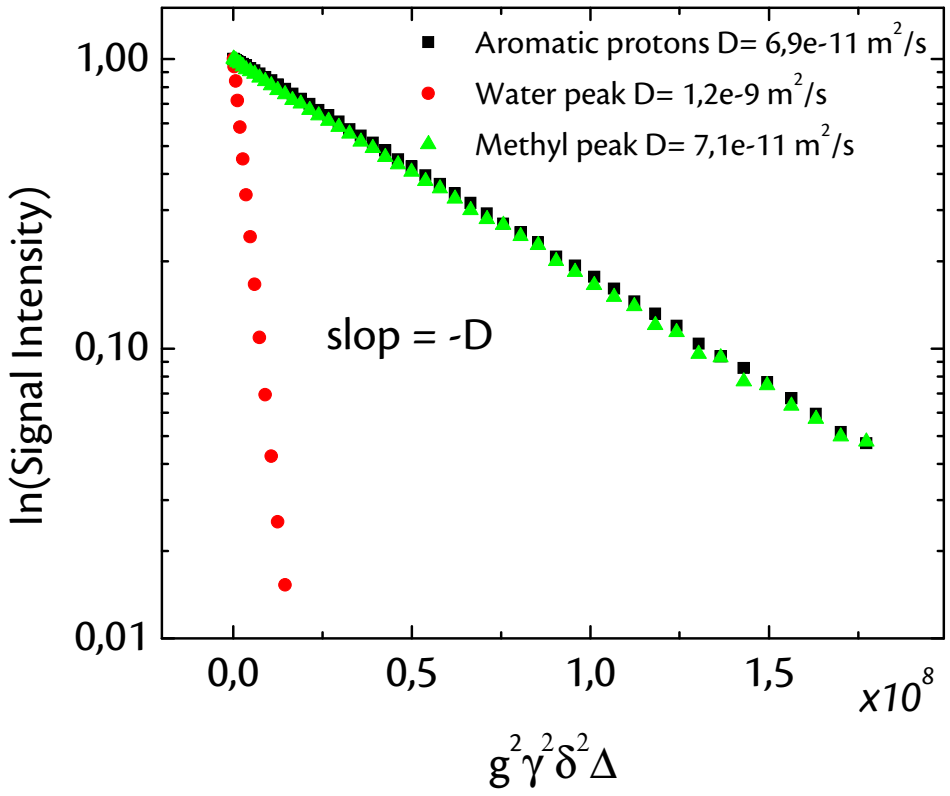

FIGURE 4.33: Normalized signal intensity from the diffusion experiment shown in Fig. 4.31 as a function of kg^2.

The Stokes-Einstein equation: from D to R_h

The Stokes-Einstein equation shows the relationship between the diffusion coefficient and the structural properties of the diffusing particles, such as the hydrodynamic radius (R_h) (equation [2.2] and [2.3]). Based on this equation the measured diffusion coefficients were converted to the hydrodynamic radius. The calculated dimensions of the above mentioned sample are collected in Table 4.4

TABLE 4.4

Estimated molecular dimension of YD

Derived from Aromatic protons		Derived from Methyl protons		Derived from Water protons	
D (m^2/s)	R_h (nm)	D (m^2/s)	R_h (nm)	D (m^2/s)	R_h (nm)
6.9e-11	1.95	7.1e-11	1.9	1.2e-9	0.1

The length of YD molecule, based on the simulation data discussed later, is around 1.44 nm. The value of R_h, shown in Table 4.4, is a complicated average based on the measured diffusion coefficient, which is weight-averaged over monomers and aggregates. Using a simplified model of monodisperse compact spheres, for which the hydrodynamic radius is the same as the radius of the sphere and assuming a density of 1 g/cm^3, R_h= 1.9 nm can be converted to an aggregation number of 37. By using another model of loose spheres, the estimated aggregation number is 22. Both models can be considered as limiting cases, thus the real aggregation number is between 22 and 37.

The measured value of the water diffusion coefficient is in good agreement with the literature data[103] (at 25°C D_{water}= $1.872x10^{-9}$ m^2/s and at 5°C D_{water}= $1.015x10^{-9}$ m^2/s). In case of dye solution the diffusion of the water is a bit slower based on the obstruction.

It is important to recall that the Stokes-Einstein equation is valid for spherical particles of colloidal dimension (much larger size than the solvent molecules), which move with uniform velocity in a fluid continuum.

In case of dye aggregation only the average dimension of monomer and aggregates can be estimated because there is no individual peak of the monomer and the aggregates based on the fast chemical exchange. Moreover the aggregates might have ellipsoidal, elongated or wormlike shape.

Using the above discussed steps of the diffusion NMR data analysis the average hydrodynamic radius of the aggregating dye system was estimated at various concentrations and temperatures, under conditions similar to those of the ^{1}H chemical shift measurements (Chapter 4.2.2). Before discussing the results, some difficulties of the diffusion measurements and the data analysis are described, such as convection artifacts and fitting problems of the decay curve.

Temperature gradient and convection

Convection within a sample of low viscosity is a serious problem affecting diffusion measurements especially at higher temperature. Convection currents are caused by small temperature gradients in the sample. It causes additional signal attenuation leading to erroneous diffusion coefficients. This artifact can be compensated by using the double stimulated echo experiment, described in Chapter 2.2.3.

A comparison of the results obtained with the double stimulated (DSTE) echo and the simple stimulated echo (STE) pulse sequence at various temperatures (T= 10, 30 and 50 °C) is presented in Fig. 4.34, Fig. 4.35 and Fig. 4.36. At each temperature the DSTE and STE measurement conditions (diffusion time and gradient) were exactly the same.

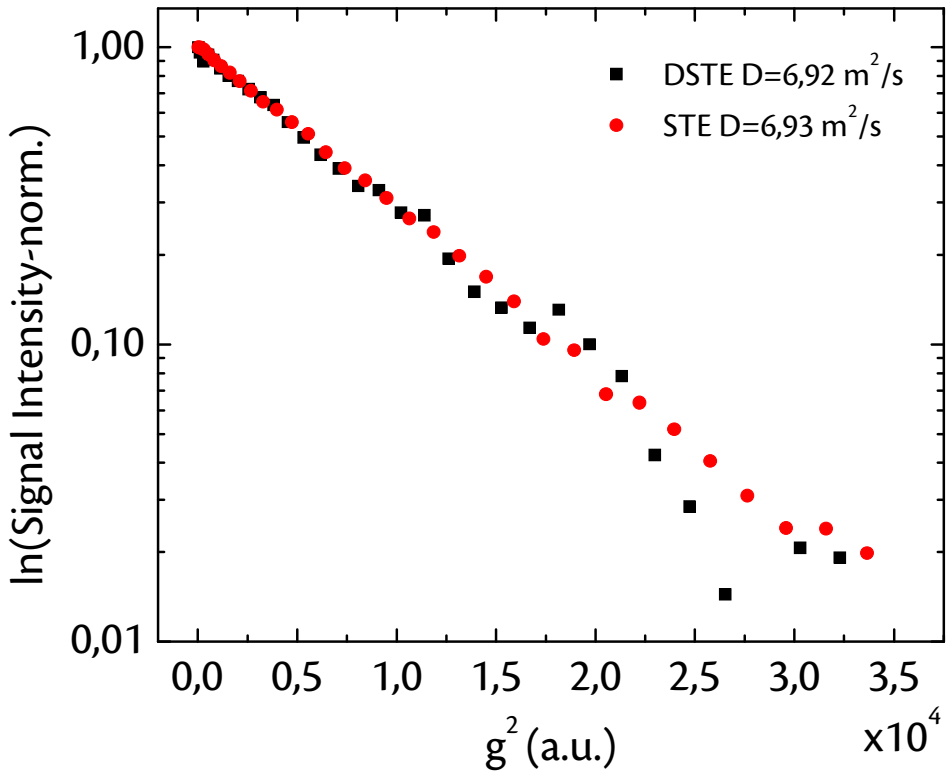

FIGURE 4.34: Comparison of double stimulated echo (DSTE) and stimulated echo (STE) pulse sequence at T=10°C in case of YD in aqueous solution. ([YD]= 30 mM, T= 10 °C, Δ= 100 ms, δ= 500 µs, g_{max}= 568 G/cm, $n_{spectrum}$= 64, ns= 128).

At low temperatures the DSTE and STE signal decays are the same (Fig. 4.34), indicating that no convection occurs. A higher accuracy of the measurement can be achieved by increasing the number of scans or by decreasing diffusion time and/or gradient strength.

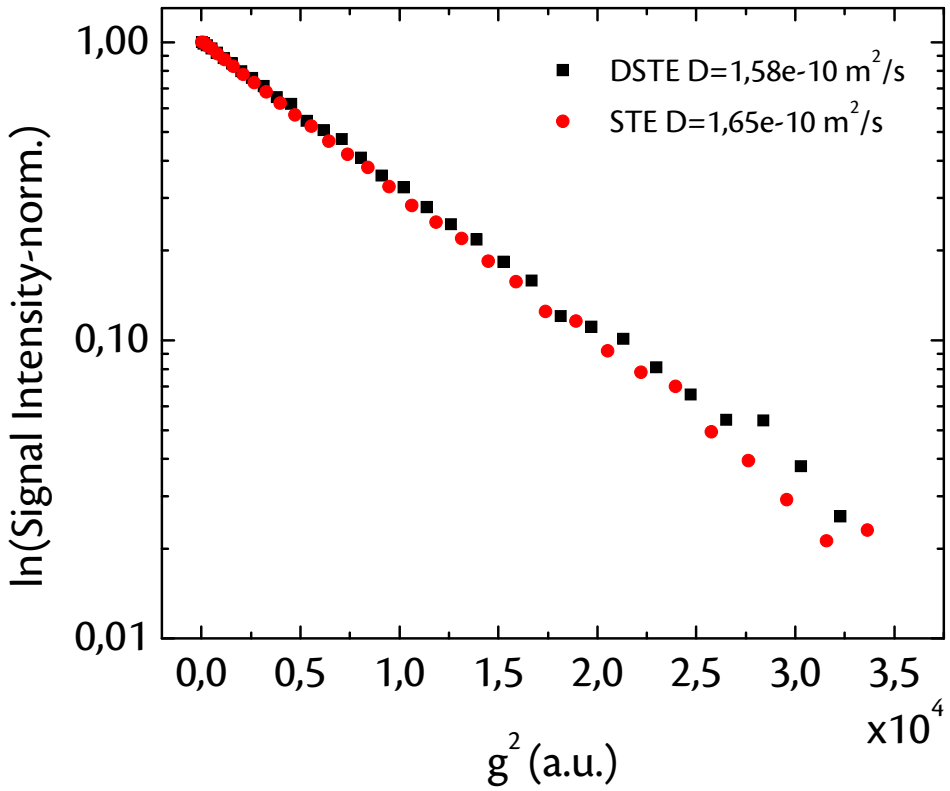

FIGURE 4.35: Comparison of double stimulated echo (DSTE) and stimulated echo (STE) pulse sequence at T= 30°C in case of YD in aqueous solution. ([YD]= 30 mM, T= 30 °C, Δ=100 ms, δ= 500 µs, g_{max}= 568 G/cm, $n_{spectrum}$=64 (not all shown), ns= 128).

At somewhat elevated temperature (30 °C) DSTE and STE experiments are still comparable. The signal decay in case of STE is only slightly faster compared to the DSTE experiment. Close to room temperature no convection occurs.

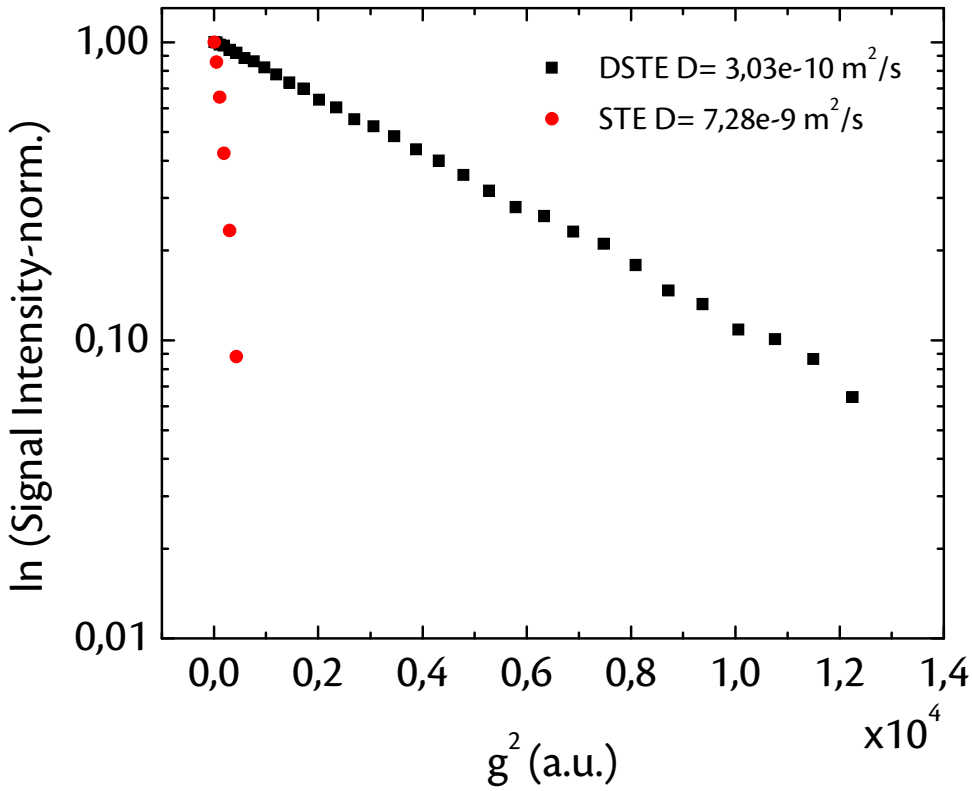

FIGURE 4.36: Comparison of double stimulated echo (DSTE) and stimulated echo (STE) pulse sequence at T= 50 °C in case of YD in aqueous solution. ([YD]= 30 mM T= 50 °C Δ= 100 ms δ= 500 μs g_{max}= 568 G/cm $n_{spectrum}$=64 ns= 128). In case of STE the attenuation of the signal is very fast because convection occurs.

The convection artifact at low temperature (up to 30 °C) is negligible, but at higher temperature (Fig. 4.36) convection occurs in the sample, leading to false values for D. Therefore the double stimulated echo pulse sequence must be used in the diffusion NMR experiments.

On the basis of these results the diffusion NMR experiments were carried out at low temperature (up to 30 °C) with STE pulse sequence and at higher temperature DSTE was applied.

In principle the DSTE pulse sequence can be used at low temperature as well but it is not recommended because of the bigger signal loss due to the longer sequence.

Reproducibility and fitting problem of the diffusion experiment

In this part the reproducibility of the diffusion measurement is investigated and guidelines for the optimum choice of experimental parameters, such as diffusion time and gradient strength are given.

The first experiment of verification was carried out at T= 60 °C using the DSTE pulse sequence which was repeated twice using exactly the same settings on the same day and the same sample. The data analysis was carried out using exactly the same frequency range for integration. The good reproducibility of the diffusion NMR experiment can be recognized in Fig. 4.37.

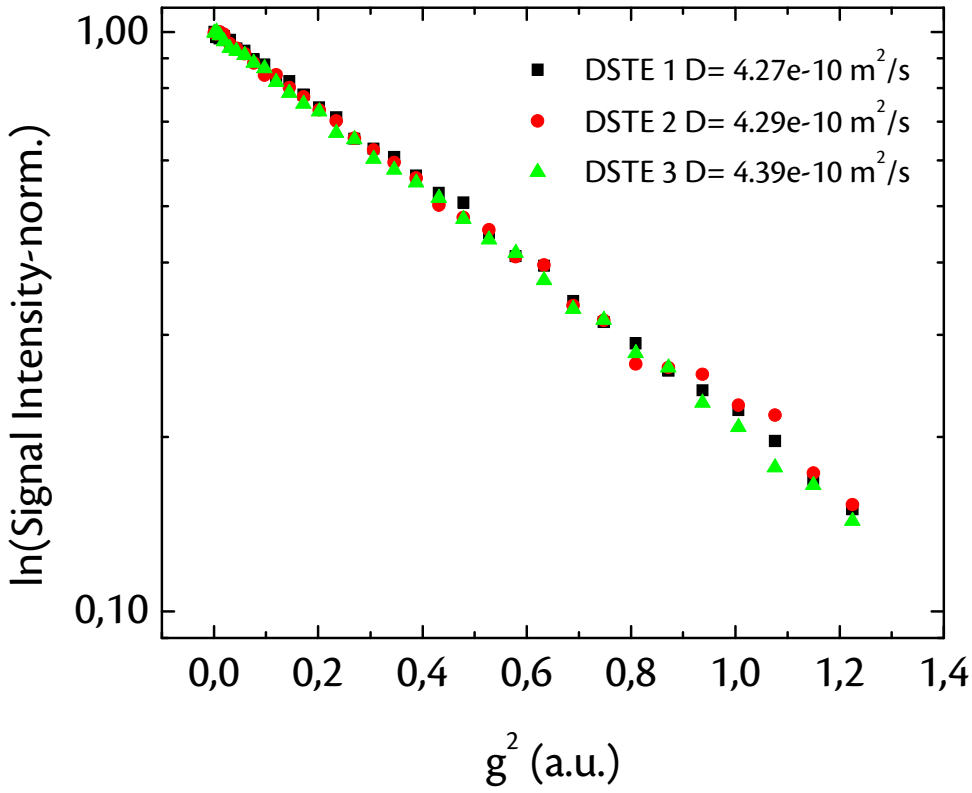

FIGURE 4.37: Reproducibility of the diffusion NMR experiment [YD]=15 mM, T= 60 °C, Δ= 20 ms, δ= 500 µs, g_{max}= 3,5 T/m).

The diffusion measurement is a fairly time-consuming experiment. Therefore it is not possible to use high numbers of scans, diffusion times, and gradient strengths. So it is very important to find the optimal parameters of the diffusion NMR experiment. For example when too long diffusion time and strong gradient are used there are only few accurate points within the entire curve and a lot of points, with almost zero intensity, leading to big errors. On the other hand, with short diffusion times and weak gradients, all measured points are in the first part of the decay curve and deviations from Gaussian diffusion may not be detected. Fig. 4.38 shows the calculated diffusion coefficient values versus the number of points fitted to determine the required number of points.

The whole curve contains 64 points. The first diffusion coefficient of the diagram comes from the fitting of the first 3 points and the rest was neglected. The fitting was done from 3 up to 64 points of the decay curve and the diffusion coefficients were calculated for each case.

The calculated diffusion coefficient is not accurate enough if only the first few decay points are considered. At least 30-35 points are required, which corresponds to the full range of data shown in Fig. 4.35. Of course it also plays a role how the given numbers of points is distributed over the whole decay curve, which is not further analyzed here.

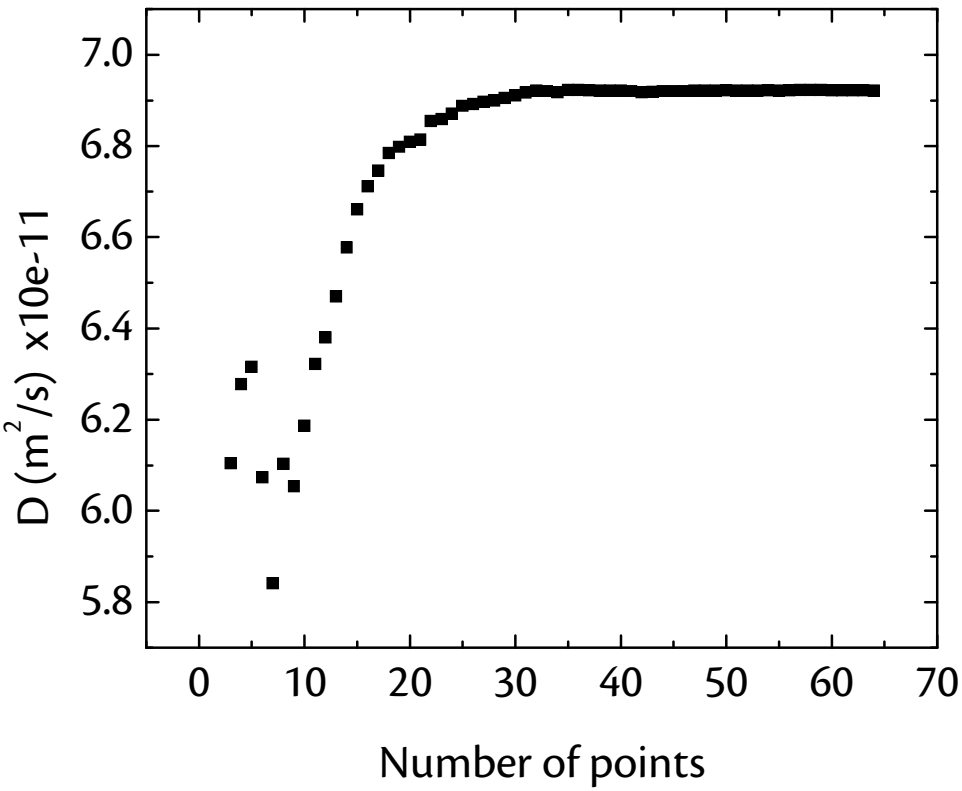

FIGURE 4.38: The calculated diffusion coefficient versus the number of point in the decay curve of Fig. 4.34 ([YD]= 30 mM T= 10 °C Δ= 100 ms δ= 500 μs g_{max}= 650 G/cm).

Dye Diffusion

The diffusion coefficients were calculated at various solutions, dye concentrations and temperatures and the dimensions of the aggregates were estimated by using the Stokes-Einstein equation.

A simple stimulated echo pulse sequence was used up to 30 °C to obtain a better signal to noise ratio while at higher temperatures the double stimulated echo sequence was used to compensate the convection in the sample.

Because of the fast chemical exchange between the monomer and the aggregates every signal attenuation curve shows monoexponential decay independently of the solvent, temperature or dye concentration. The average diffusion coefficient of the system contains the diffusion of the fast/small monomer molecules and the

slow/big aggregates which are still in solution and detectable by NMR spectroscopy.

Diffusion of dye in DMSO

As shown in Chapter 4.2.1 and 4.2.2 the ^{1}H NMR chemical shifts and line widths of YD in DMSO solution are independent of the concentration and the temperature. To get information about the dimensional properties under the same concentrations and temperatures diffusion NMR measurement were carried out.
In Fig. 4.39 is shown the diffusion coefficient of YD in DMSO versus the temperature. The dye diffusion gets faster with increasing temperature because the viscosity of the solvent decreases.

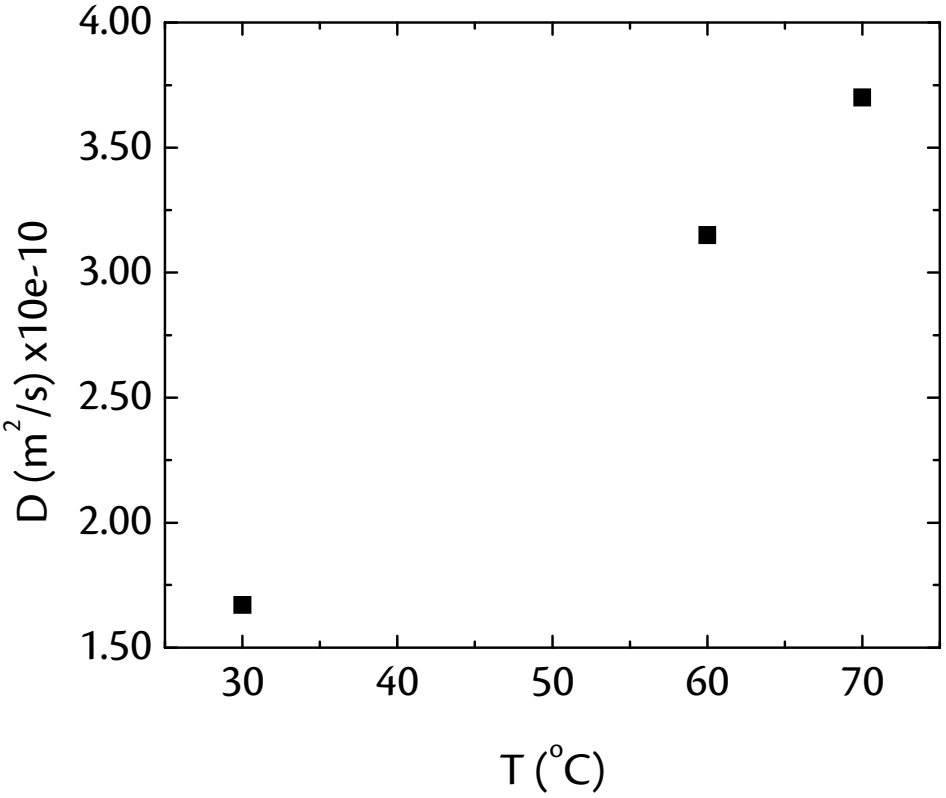

FIGURE 4.39: Average diffusion coefficient of YD in DMSO as a function of temperature. ([YD]= 20 mM Δ= 20-60 ms δ= 500 μs g_{max}= 150- 650 G/cm).

Fig. 4.40 shows the size of YD particles estimated on the basis of the Stokes-Einstein equation as a function of temperature in DMSO. The temperature independence of YD dimension is well observable.

The estimated hydrodynamic radii of YD solution and the one calculated by DFT simulations, presented in section 4.3, are in very good agreement. Based on DFT simulation the molecular length of a planar YD molecule is about 1.4 nm and the estimated hydrodynamic radius is about one half of it, 0.7 nm.

The diffusion measurements clearly show that in DMSO there are only individual YD molecules and no aggregation occurs. This corresponds in an excellent way to the result of the chemical shift and linewidth analysis of the ^{1}H NMR experiments.

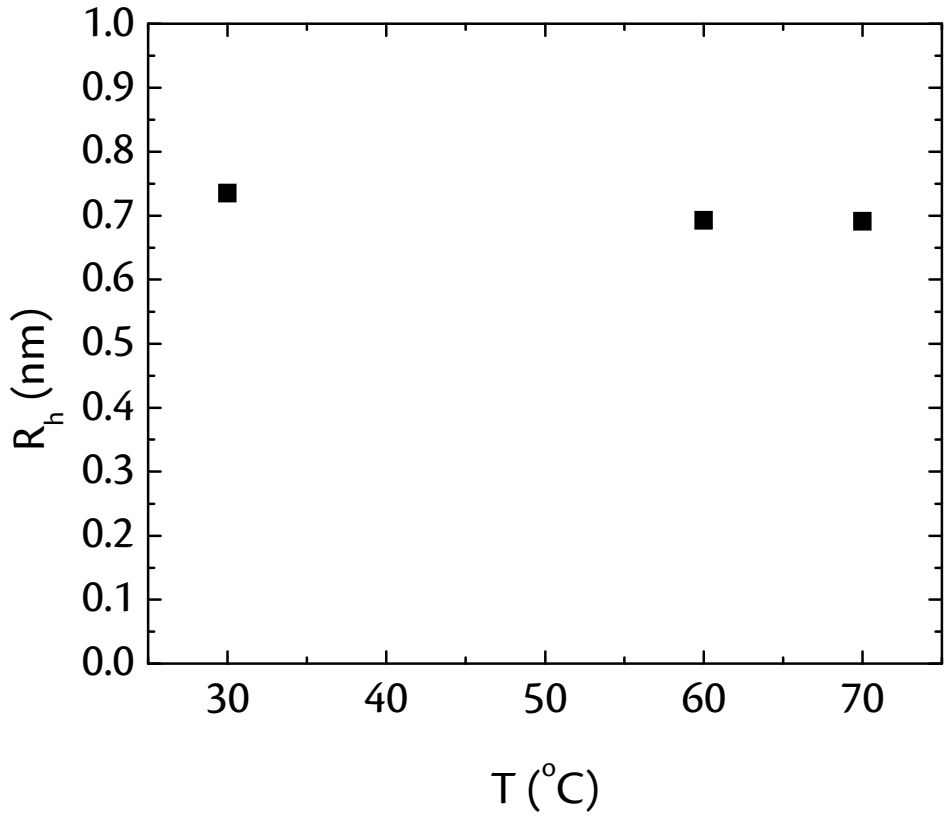

FIGURE 4.40: Estimated hydrodynamic radius of YD as a function of temperature.

Dye diffusion in aqueous solution

YD forms aggregates in aqueous solution as mentioned in Chapter 4.2.2. In D_2O diffusion measurements were carried out under various conditions, such as various diffusion times and gradient strengths. The measured diffusion coefficient is independent of the diffusion time, there is free diffusion. The results of the diffusion coefficient at various diffusion times and for repeated experiments were averaged and used for later analysis.

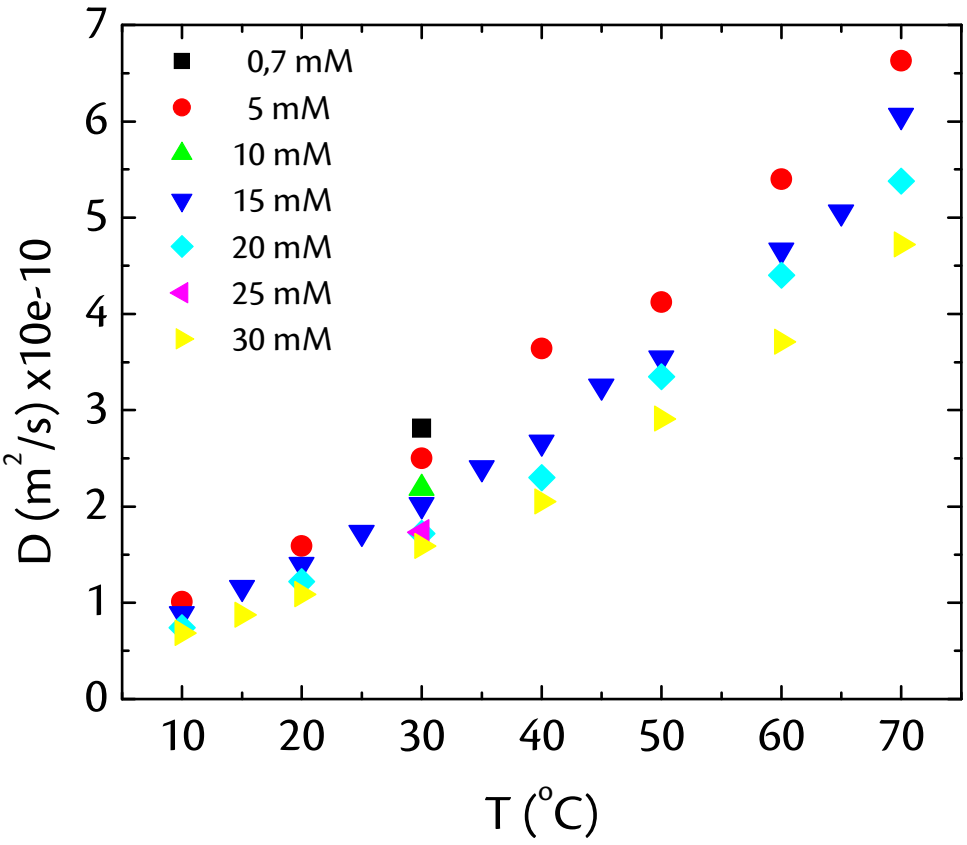

Figure 4.41: Diffusion coefficient of YD versus temperature at various dye-concentrations in aqueous solution ([YD]= 0.7 – 30 mM).

Fig. 4.41 shows the diffusion coefficient versus temperature at various dye concentrations (0.7 mM to 30 mM). The diffusion of the system becomes faster upon increasing temperature and decreasing concentration of the dye.

There is equilibrium between the monomers and the aggregates. At higher dye concentration the possibility of the aggregate formation is higher due to the large number of accidental collisions. Based on the equilibrium $n[M] \leftrightarrow [M]^n$ increasing the dye concentration an exponential growth of the aggregate dimension can occur. The temperature-dependent diffusion measurements show that at higher temperature the equilibrium is shifted to the formation of the monomer.

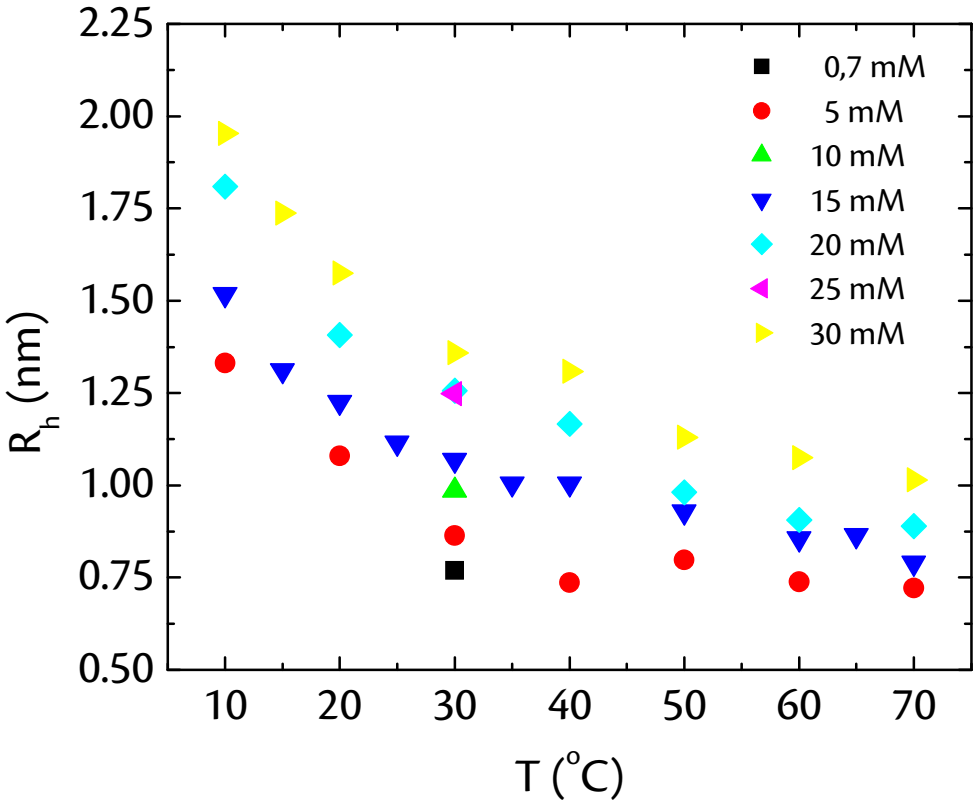

FIGURE 4.42: Estimated hydrodynamic radii of YD versus temperature at various dye-concentrations in aqueous solution in case of sphere shape aggregate. ([YD]= 0.7 – 30 mM).

The estimated hydrodynamic radius as a function of temperature is shown in Fig. 4.42. At low dye concentration and high temperature the estimated hydrodynamic radii are in the range of 0.75 nm, which is comparable with the monomer dimension. Under these conditions the individual dye molecules do not show an inclination to form aggregates. At higher dye concentration and lower temperature

the estimated average radius of the dye system increases up to 2 nm. The reason of this small average size is that the really big aggregates do not contribute to the NMR signal.

In order to understand how many units constitute the aggregate it is important to know the hydrodynamic volume of the single dye molecule (in case of a sphere: V_{h0}=1.437 nm^3). This was calculated from the diffusion data in DMSO solution where no aggregation was observed (R_h= 0.7 nm)

The aggregation number (N) is a parameter which quantifies the degree of aggregation and in case of non compact spheres can be estimated from

$$N = \frac{V_h}{V_{h_o}} \qquad [4.1]$$

N represents the average number of monomers constituting the aggregate.

In Fig. 4.43a the aggregation number is plotted as a function of temperature at various dye concentrations. The number of the monomers in the aggregate depends on the dye concentration and the temperature. At low concentrations and high temperatures only individual monomer exist in aqueous solution. With increasing concentration and decreasing temperature the aggregation number increases up to 22. This estimation is very rough because it assumes spherical monomers and does not take into account the shape of the aggregates.

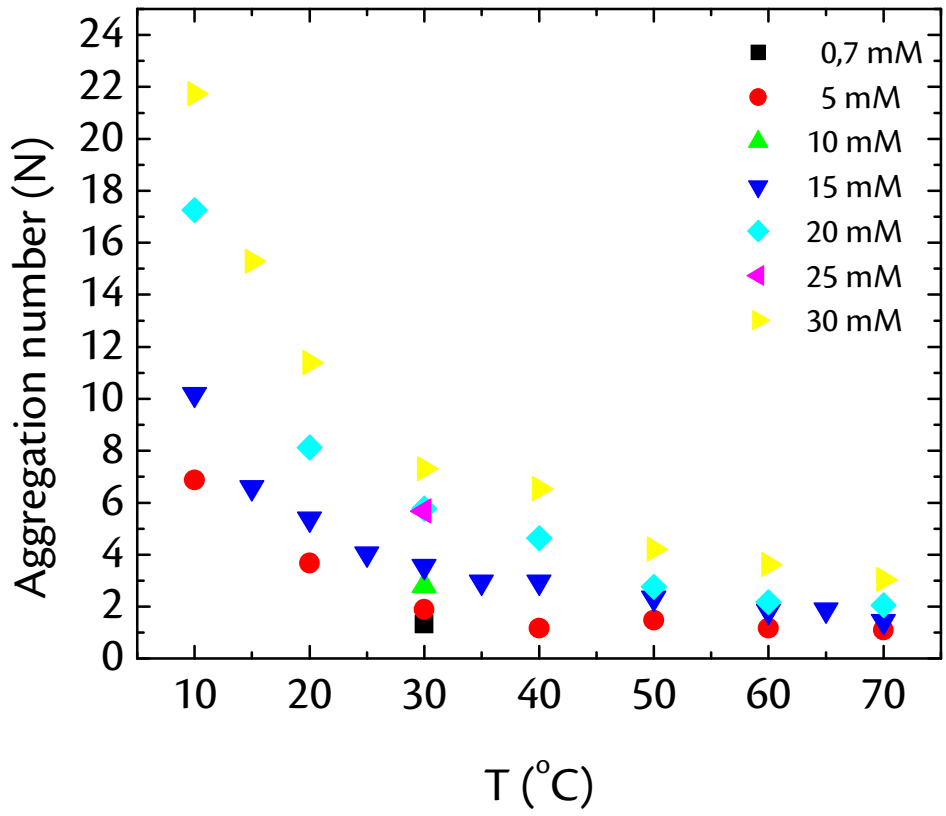

FIGURE 4.43a: Estimated aggregation number of YD versus temperature at various dye-concentrations in aqueous solution in case of spherical aggregates. ([YD]= 0.7 – 30 mM).

In case of compact spheres the aggregation number can be calculated according to equation [4.2]

$$N = \frac{\frac{4}{3}\pi R_h^3}{V_{molecule}} = \frac{4}{3}\pi R_h^3 \frac{\varphi N_A}{M_{molecule}} \qquad [4.2]$$

Based on equation [4.2] and the estimated R_h values from the diffusion data the aggregation number N as a function of temperature is shown in Fig. 4.43b.

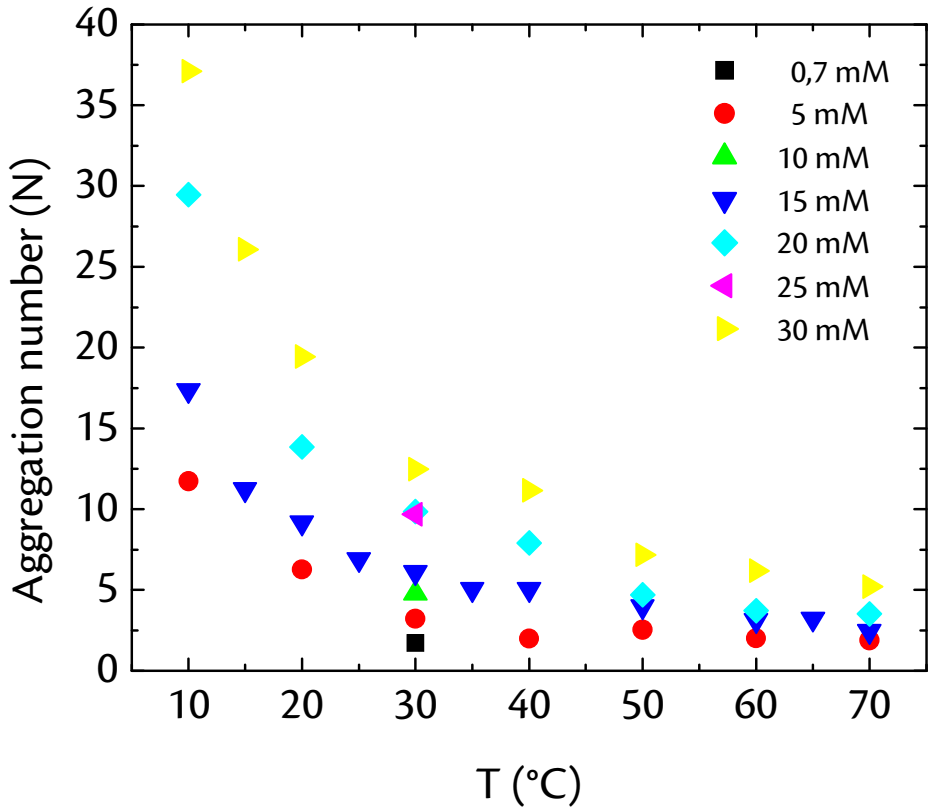

FIGURE 4.43b: Estimated aggregation number of YD versus temperature at various dye-concentrations in aqueous solution in case of compact spheres. ([YD]= 0.7 – 30 mM).

4.3 *COMPUTER SIMULATION*

In order to get more information about the dye system a high accuracy density functional theory (DFT) method was used to obtain an optimized structure of the yellow dye (YD) monomer in the gas phase and subsequently its NMR and UV spectra were calculated.

4.3.1 DFT STRUCTURE OPTIMIZATION OF THE MONOMER

The first input structure was drawn by GaussView. A planar structure was chosen and converted to a NWChem input file. For the optimization of yellow dye (YD) the 6-311g(p,d) basis set was used along with a DFT-based method with b3lyp exchange correlation implemented into the computational chemistry software package of NWChem.

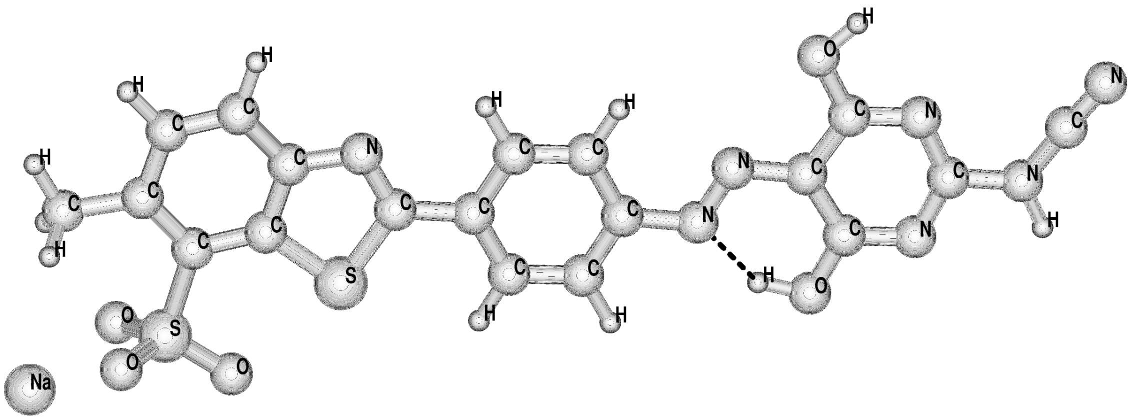

FIGURE 4.44: DFT optimized structure of YD (b3lyp/6-311g(d,p)).

An energy minimum was found by this very time consuming optimization, corresponding to the structure shown in Fig. 4.44, which was used for the simulations discussed later. The optimized yellow dye has a planar structure, where the carbonyl oxygen atoms are in the enol form and the hydrogen atoms are

building strong H-bonds with the neighboring nitrogen atoms. To validate this structure the NMR and UV spectra were computed.

4.3.2 DFT SIMULATION OF NMR SPECTRA OF THE MONOMER

For the calculation of the NMR spectra of YD its DFT optimized structure was applied as starting geometry using the same 6-311g(p,d) basis set of the Gaussian 03' program package. After the structure optimization the isotropic shielding values of the proton were calculated by using GIAO (Gauge-Including Atomic Orbital) method. The calculated shielding values were extracted from the Gaussian output, the value of shielding tensors of equivalent hydrogen atoms are averaged. The isotropic shielding value of the hydrogen atom was then subtracted from the value of the shielding value of TMS.

Table 4.5 shows the comparison of the calculated and measured ^{1}H chemical shifts and Fig. 4.45 represents the calculated NMR spectra.

As shown in Table 4.5 the calculated and measured chemical shifts are in good agreement, suggesting that the geometry obtained by the quantum-chemical optimization is a possible structure and can be used for later calculations.

TABLE S 4.5

Measured and calculated ^{1}H NMR chemical shift of YD

H atom number	Measured ^{1}H chemical shift (ppm)	Calculated ^{1}H chemical shift (ppm)	Deviation (pmm)
1	2.69	2.32	0.37
3	7.35	6.87	0.48
4	7.86	7.57	0.29
10,11	8.13	8.13	0.00
12,13	7.61	7.63	0.02

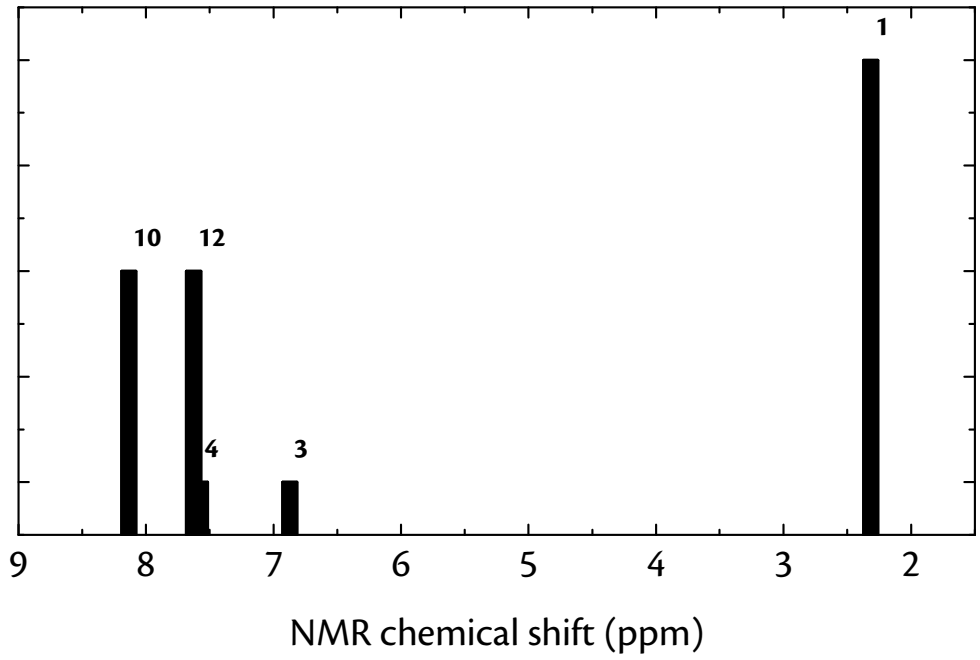

FIGURE 4.45: Calculated ^{1}H NMR spectrum of YD in gas phase (b3lyp/6-311g(d,p)).

4.2.4 DFT SIMULATION OF UV SPECTRA OF THE MONOMER

Another verification of our computational model is the calculation of the UV spectra. The input structure was the optimized structure of YD obtained by using the Gaussian program package. In Fig. 4.46 the simulated and measured UV spectra are shown.

The measured and the calculated spectra are in very good agreement. However, there is additional absorbance in the measured spectra (410 - 360 nm), which can be an effect of the aggregate formation. One other reason can be additional absorption at lower wavelength by the glass of the home made sample holders.

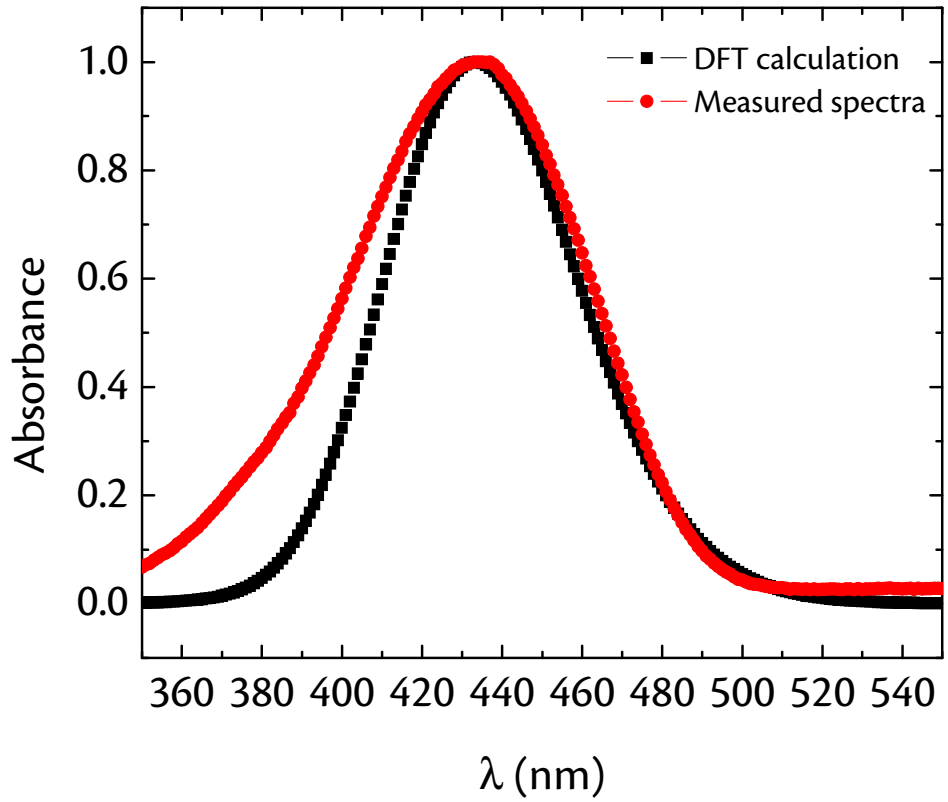

FIGURE 4.46: Measured and calculated UV spectrum of YD in gas phase (td b3lyp/6-311g(d,p).

4.2.5 DFT STRUCTURE OPTIMIZATION OF THE DIMER

The input for the dimer structure simulation was a stack of two monomers. The central rings were placed exactly upon each other and one molecule was rotated 180° with respect to the other, such that the methyl groups and the SO_3^- groups are most distant. There are several possibilities to put the molecules upon each other but due to the big amount of computer time consumed by just this one calculation, only one variation was optimized. The starting distance of the two planar molecules was determined by energy calculation; a value of 2.5 Å was obtained. Starting from this stack of two planar molecules, all constrains on

dihedral angles were relieved in the further optimization. The optimized structure is shown in Fig. 4.47.

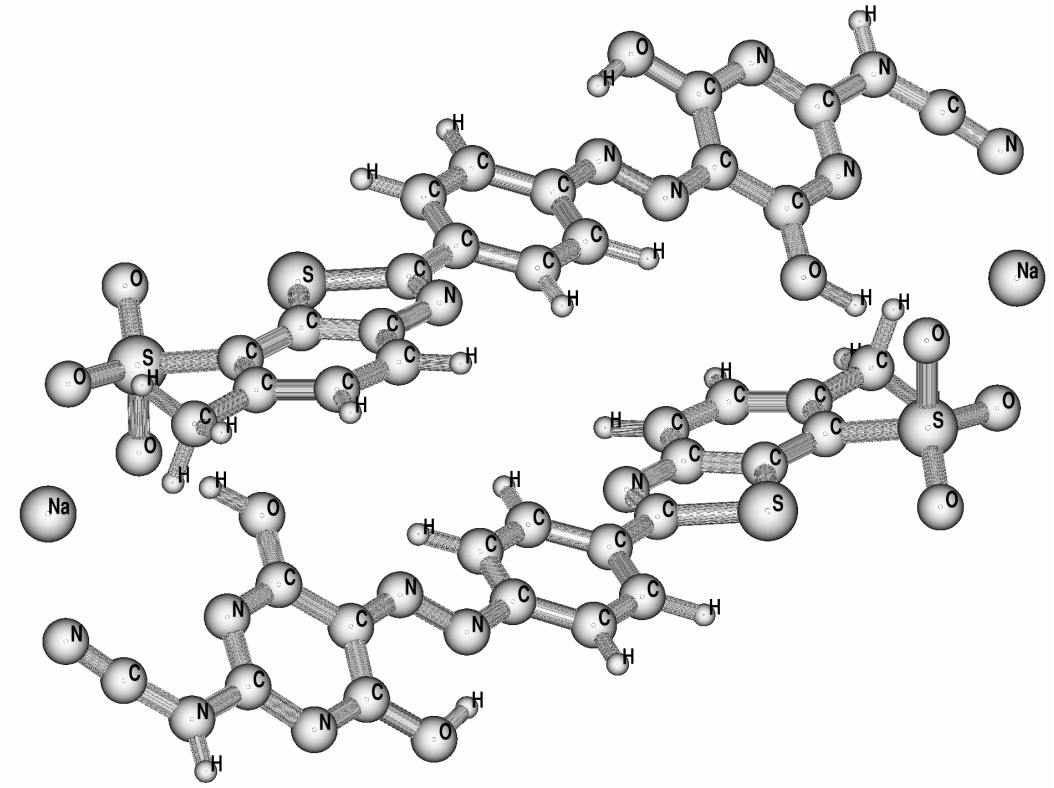

FIGURE 4.47: DFT optimized structure of a stack of two YD (b3lyp/6-311g(d,p)).

The initially planar structure has changed. A twist of the molecular structure can be observed and the dimer tends to form H bonds. This conformational change of the structure may result from the deficiency of the chosen simulation method, which is not very accurate for π-π interactions.

4.2.5 DFT NMR SPECTRUM SIMULATION OF THE DIMER

After the structure optimization the NMR spectra of the dimer was calculated by the same method as before (b3lyp/6-311g(d,p)). The ^{1}H NMR chemical shifts are shown in Table 4.6 and Fig. 4.48 shows a schematic representation of the calculated ^{1}H NMR spectrum.

TABLE 4.6

Structure optimation of the dimer

H atom number	Calculated ^{1}H chemical shift of the dimer (ppm)	Difference of calculated ^{1}H chemical shift of the monomer and the dimer (ppm)	Maximum shift observed in experiment
1	2.54	0.23	2.46
3	6.78	-0.09	6.96
4	7.45	-0.12	7.36
10,11	7.69	-0.44	7.26
12,13	7.35	-0.28	6.8

The NMR chemical shifts of the aromatic protons are shifted to the low ppm values while the methyl peak is shifted to the higher ppm values.

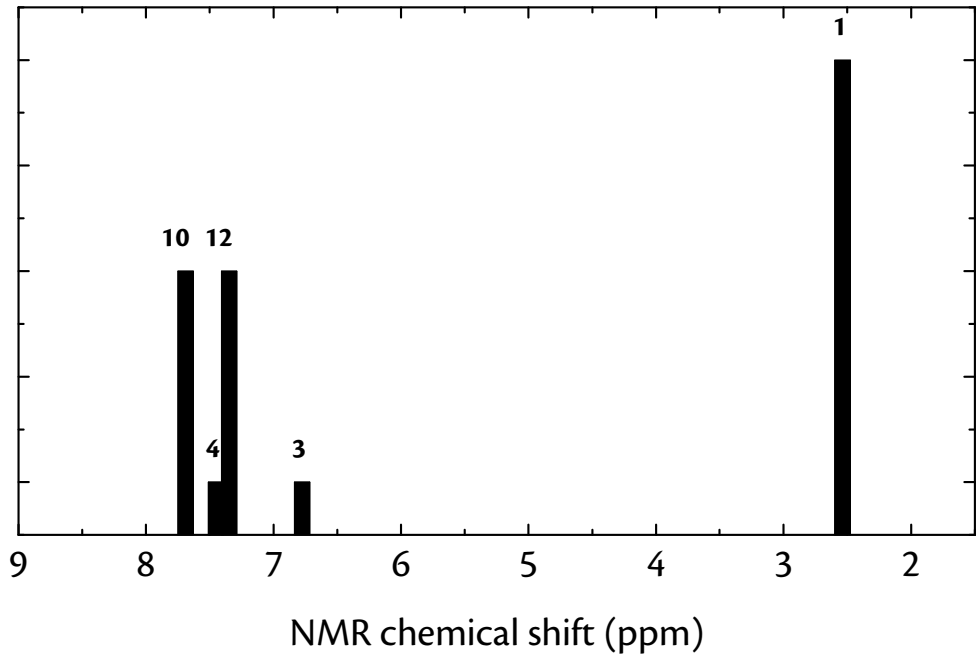

FIGURE 4.48: The calculated ^{1}H NMR spectrum of YD dimer model in the gas phase (b3lyp/6-311g(d,p)).

The calculated upfield shift of the aromatic protons in the dimer agrees well with the experimental observations for the aggregates. This shift can be explained by additional shielding of π electron system, which is above or below the adjacent ring. In case of the methyl peak the calculation show a downfield shift whereas the measurements show a small upfield chemical shift change at various dye concentrations and temperatures (Fig.4.19). The reason can be the insufficient accuracy of the calculated dimer structure. Another possible explanation for the difference of calculated and observed changes in chemical shift upon dimer formation may be that the relative orientation of the monomer assumed in the model does not agree with the aggregate structure.

During the structure optimization the planar structure is changed to the twisted structure, thus the position and the chemical environment of the methyl protons are also changed resulting in chemical shift changes, which do not agree with experimental observation. In the central part of the molecules there is almost no

twist (hydrogen atoms 10-13) and calculated and measured chemical shift changes have the same direction.

To extract more information about the structures of the aggregates more calculations for different models are needed.

CHAPTER 5 SUMMARY

The formation of aggregates from single molecules is a well-known phenomenon, which can be observed, for example, in case of dye molecules or peptides. Previous studies by light scattering had shown that mixtures of anionic direct dyes, namely "Rot 2G" (RD) and "Gelb GA" (YD) form very large aggregates in the presence of Mg^{2+} ions. This was confirmed in this study by light microscopy, which showed that even the pure YD formed aggregates in aqueous solutions containing Mg^{2+} ions. However, no visible aggregates were found for the RD. Therefore YD was chosen as a typical model molecule for the investigation of the aggregation process in aqueous solution. Different NMR techniques, such as chemical shift analysis, relaxometry, pulsed-field gradient diffusion NMR in combination with UV spectroscopy and quantum chemical calculation were used to obtain information about the structure and the size of the aggregates.

The peaks in ^{1}H and ^{13}C NMR spectra of YD in DMSO solution, where no aggregates occurs, were assigned using two-dimensional methods, such as COSY, HMQC and HMBC. Good agreement is found between the measured chemical shifts and the ones obtained from quantum chemical calculation for the monomer. In aqueous solutions broad NMR peaks are observed due to aggregation. Compared to the monomer spectra in DMSO, the peaks are shifted but no additional peaks are found, indicating that there is fast exchange between monomers and aggregates. ^{1}H spectra in aqueous solution were measured for concentrations from 0.7 mM to 30 mM and in the temperature range 10-70° C. A growth of the aggregates with increasing dye concentration and decreasing temperature is found, which can be seen from the corresponding broadening of the NMR peaks. In particular at low temperature and high concentrations the measured peak intensities are up to 40 % lower than theoretically (based on the concentration) expected. This shows that there are aggregates which are too big to be detected by the NMR method used. From the line widths an average hydrodynamic radius, corresponding to the NMR-visible fraction of the aggregates,

can be estimated. The values obtained are between 0.7 nm at a dye concentration of 0.7 mM and a temperature of 70° C and up to 1.9 nm for the 30 mM solution at T= 10° C. As the aggregates increase with increasing dye concentration and decreasing temperature an upfield shift (towards lower ppm) of the ^{1}H NMR peaks is found, which is more pronounced for the aromatic protons in the central region of the molecules than for the methyl protons of the outer part of the molecules. This shift occurs as a result of the shielding property of the π-electrons of neighboring molecules. Since the molecules are stacked upon each other, the effect is more significant for the middle section. The model of stacked molecules is in good agreement with UV spectroscopy data, which show a blue shift of the absorption maximum from 434 nm at a dye concentration 0.07 mM to 418 nm at 5 mM.

Diffusion NMR measurements of YD in aqueous solutions (0.7 – 30 mM) yield a monoexponential decay, confirming that there is fast exchange between monomers and aggregates. The diffusion coefficients were analyzed in terms of the Stokes-Einstein model, yielding values of the hydrodynamic radius between 0.7 and 1.9 nm in very good agreement with the estimates obtained from the line width, where from 0.2 nm up to 2 nm were found. The hydrodynamic radius of 1.9 nm corresponds to an aggregation number between 22 and 37, depending on whether a model of loosely aggregated molecules or a model of compact spherical aggregates is used.

APPENDIX

A1 DIFFUSION OF THE MIXTURE

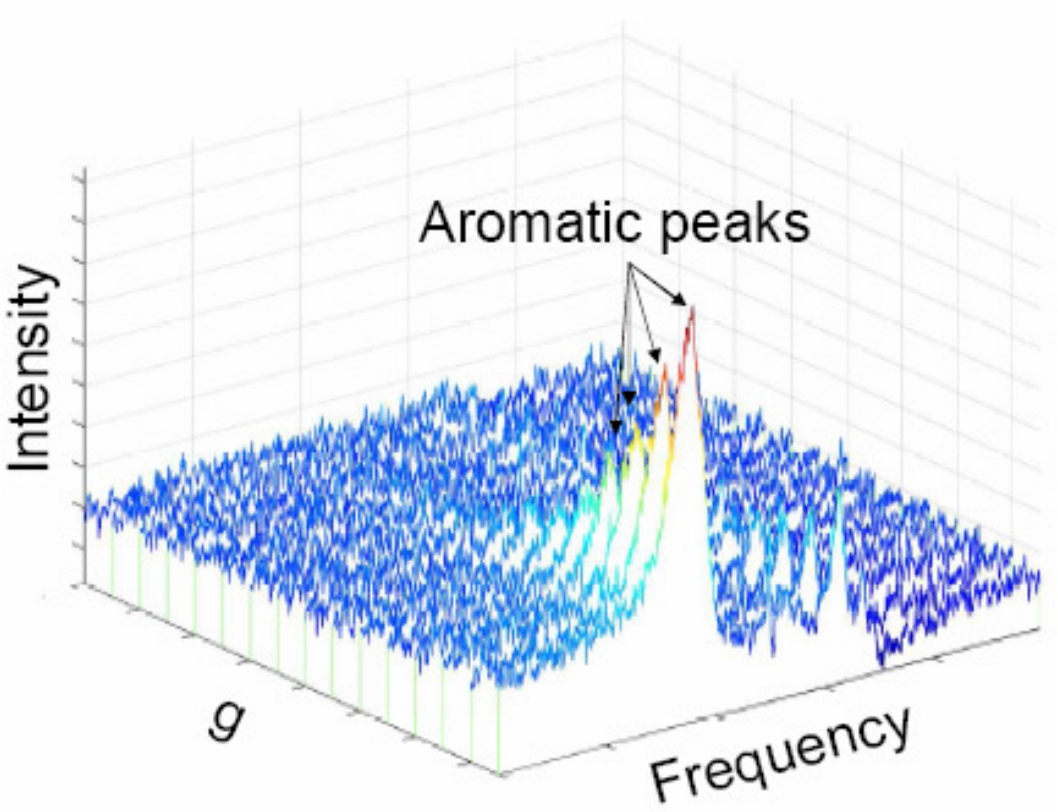

Figure A1.1: 1:1 mixture of RD and YD in aqueous solution [dye] = 45 mM [Mg^{2+}] = 0.68 mM STE sequence (G = 0 – 9.63 T/m, = 0.5 ms, Δ = 100 ms).

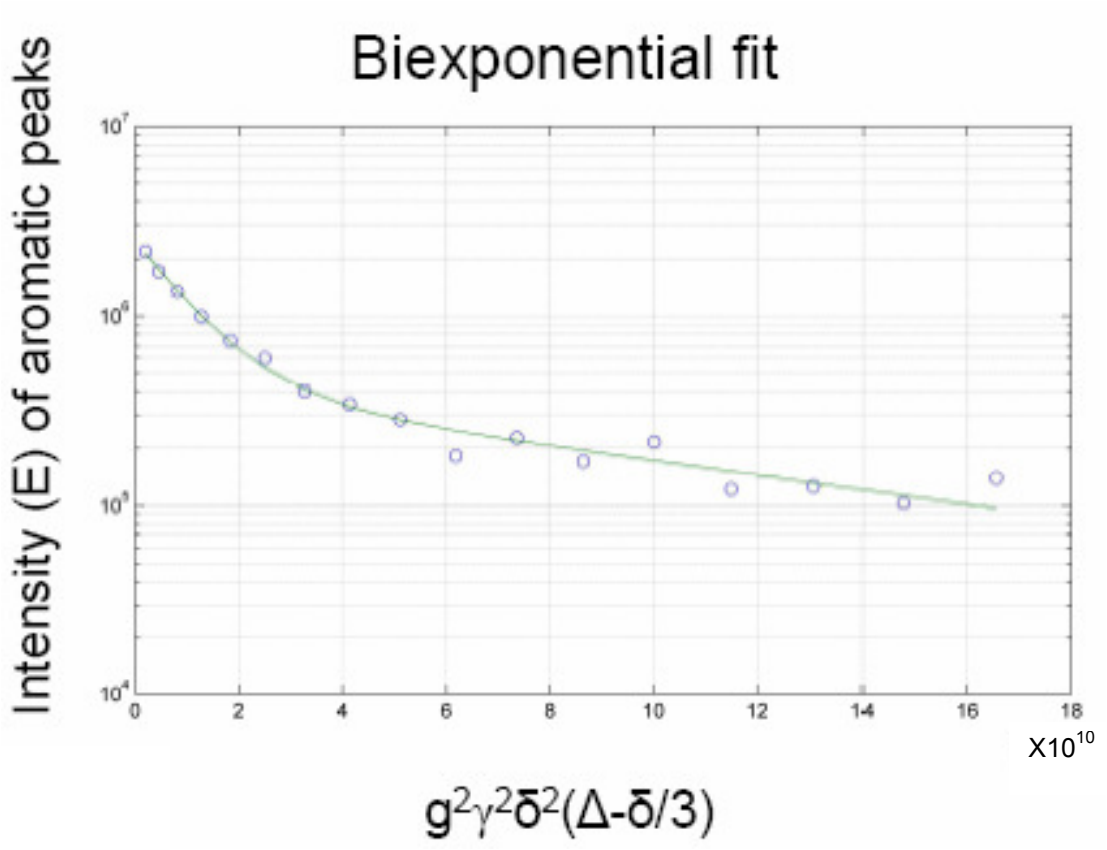

Figure A1.2: $D_{(fast)} = 9.58 \cdot 10^{-11}$ m^2/s $D_{(slow)} = 9.06 \cdot 10^{-12}$ m^2/s Fast component = 83 % $R_{h\,(small)}$ = 2 nm $R_{h\,(big)}$ = 20 nm. The aromatic region of the dyes was analyzed. A non-exponential decay is observed, which can be fitted by two exponentials, meaning that there are two species, slow/big aggregates and fast/small molecules in the solution.

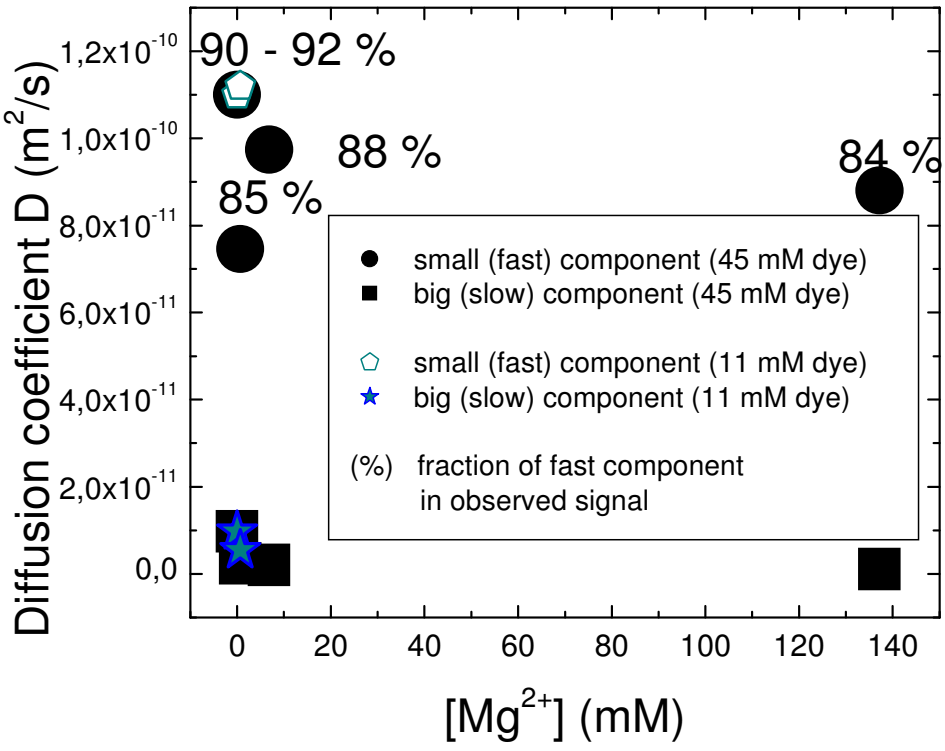

Figure A1.3: Diffusion coefficients of the dyes as a function of $[Mg^{2+}]$ at two different dye concentrations. From the biexponential fit two diffusion coefficients were extracted, showing that there are fast/small and slow/big aggregates.

Table A1.1

Diffusion coefficient as a function of $[Mg^{2+}]$ at two different dye concentrations

$[Mg^{2+}]$	[dye] = 45 mM		[dye] = 11 mM	
(mM)	R_h (small) (nm)	R_h (big) (nm)	R_h (small) (nm)	R_h (big) (nm)
0.00	2.5	40	1.8	20
0.69	2.1	95	1.7	35
6.87	2.0	96		
137.18	2.2	181		

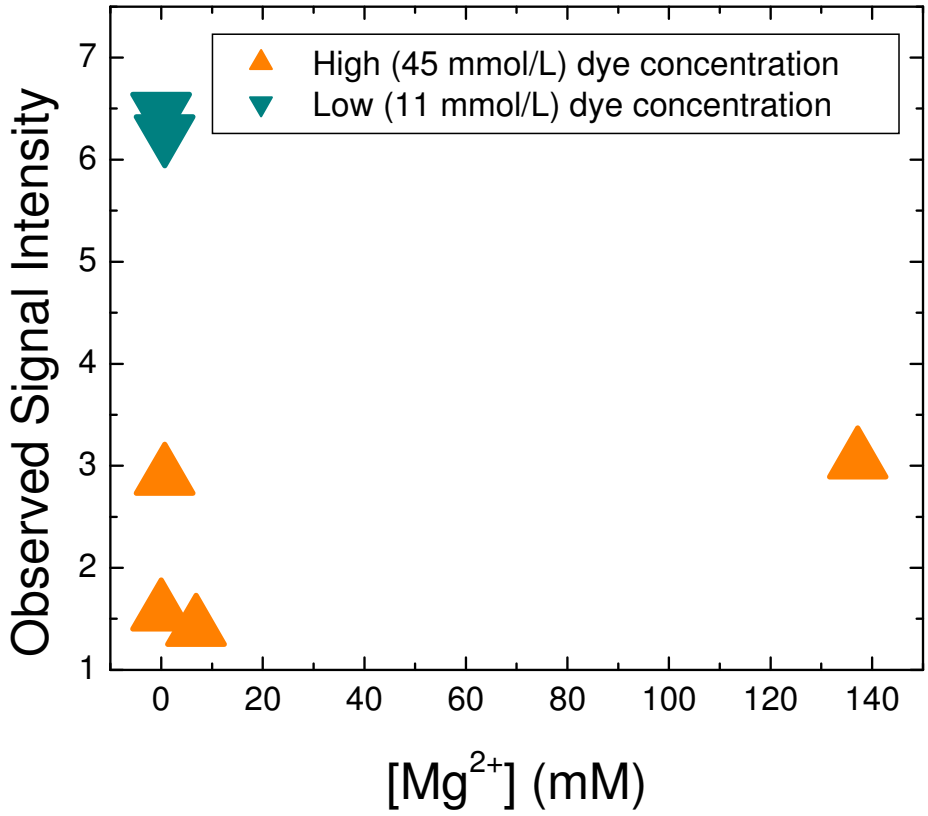

FIGURE A1.4: Observed signal intensity at various [Mg^{2+}] at two dye concentrations. The lower dye concentration show higher signal intensity. The reason of these observations is that the big aggregates do not give signal (too big, rigid or precipitated).

A2 DIFFUSION DATA OF YD

Table A2.1 Diffusion Data in aqueous solution – Aromatic region

[YD] (mM)	T (°C)	D (m^2/s)	G_{max} (T/m)	Δ (s)	All points	Used Points	Pulse
0,7	30	2,81E-10	3,8058	0,01982	24	22	STE
10	30	2,19E-10	5,6875	0,01998	24	22	STE
15	10	7,89E-11	5,6875	0,01999	32	30	DSTE
15	10	8,57E-11	5,6875	0,03999	32	30	DSTE
15	10	9,13E-11	5,6875	0,09999	32	13	DSTE
15	10	9,35E-11	7,5075	0,02004	16	14	STE
15	10	9,36E-11	5,5055	0,03992	16	13	STE
15	15	1,15E-10	9,0098	0,02037	16	14	STE
15	15	1,16E-10	7,0078	0,02013	24	22	STE
15	20	1,34E-10	5,6875	0,02999	32	28	DSTE
15	20	1,42E-10	5,6875	0,09999	32	17	DSTE
15	20	1,41E-10	6,507	0,01981	16	14	STE
15	20	1,42E-10	6,0062	0,0399	16	14	STE
15	25	1,75E-10	6,0062	0,01978	16	14	STE
15	25	1,70E-10	5,0057	0,03992	16	14	STE
15	30	1,78E-10	5,6875	0,01999	32	30	DSTE
15	30	2,15E-10	5,6875	0,09999	32	16	DSTE
15	30	2,04E-10	5,5055	0,01984	16	14	STE
15	30	2,04E-10	4,0042	0,03984	16	14	STE
15	35	2,46E-10	5,0057	0,01982	16	14	STE
15	35	2,64E-10	3,5034	0,03986	16	14	STE
15	35	2,10E-10	5,6856	0,02006	16	14	DSTE
15	40	2,51E-10	5,6875	0,01999	32	28	DSTE
15	40	2,75E-10	5,6875	0,09999	32	12	DSTE
15	40	2,55E-10	5,6875	0,01999	32	30	DSTE
15	40	2,86E-10	3,5034	0,0811	32	19	DSTE
15	45	3,39E-10	4,5049	0,04133	16	10	DSTE
15	45	3,11E-10	2,0021	0,03971	16	14	DSTE
15	50	3,36E-10	5,6875	0,01999	32	30	DSTE
15	50	3,71E-10	3,5034	0,03936	32	30	DSTE
15	60	4,34E-10	3,5034	0,01936	32	30	DSTE
15	60	4,49E-10	3,5034	0,01936	32	30	DSTE
15	60	4,47E-10	3,5034	0,01936	32	30	DSTE
15	60	4,73E-10	3,5034	0,03936	32	23	DSTE

[YD] (mM)	T (°C)	D (m^2/s)	Gmax (T/m)	Δ (s)	All points	Used Points	Pulse
15	60	4,38E-10	5,6875	0,01999	32	23	DSTE
15	60	5,52E-10	3,0036	0,03922	16	14	DSTE
15	65	4,96E-10	3,5034	0,01936	32	30	DSTE
15	65	5,16E-10	2,5028	0,03863	16	14	DSTE
15	70	5,96E-10	3,0036	0,01922	32	30	DSTE
15	70	6,16E-10	2,0021	0,03908	16	14	DSTE
15	30	3,79E-10	5,6875	0,00911	16	9	STE
15	30	4,07E-10	3,5034	0,01884	16	14	STE
15	30	2,83E-10	3,5034	0,03936	16	14	DSTE
15	30	2,06E-10	3,5034	0,03989	24	22	STE
15	30	2,06E-10	5,6875	0,01998	24	22	STE
20	10	7,16E-11	3,5034	0,01936	32	30	DSTE
20	10	7,40E-11	5,6875	0,01999	32	30	DSTE
20	10	7,73E-11	5,6875	0,03999	32	30	DSTE
20	20	1,22E-10	5,6875	0,02999	32	29	DSTE
20	30	1,62E-10	5,6875	0,01999	32	30	DSTE
20	40	2,30E-10	5,6875	0,01999	32	30	DSTE
20	50	3,35E-10	3,5034	0,03936	32	30	DSTE
20	60	4,40E-10	3,5034	0,02936	32	30	DSTE
20	70	5,38E-10	3,5034	0,01936	32	28	DSTE
20	30	1,82E-10	5,6875	0,01998	24	22	STE
25	30	1,73E-10	5,6875	0,01998	24	22	STE
30	10	6,92E-11	5,6875	0,09999	32	26	DSTE
30	10	6,93E-11	5,8059	0,09998	32	26	STE
30	10	6,67E-11	5,6875	0,09999	32	23	DSTE
30	10	6,87E-11	9,63	0,09998	32	18	STE
30	10	6,95E-11	6,507	0,10006	16	14	STE
30	10	6,91E-11	6,507	0,10001	64	62	STE
30	15	8,76E-11	9,0098	0,02011	16	14	STE
30	15	8,75E-11	7,0078	0,03998	24	22	STE
30	20	1,09E-10	8,5091	0,02005	16	14	STE
30	20	1,09E-10	6,507	0,03992	24	22	STE
30	30	1,58E-10	5,6875	0,03999	32	30	DSTE
30	30	1,65E-10	5,8059	0,03998	32	30	STE
30	30	1,53E-10	5,6875	0,03999	32	23	DSTE
30	30	1,46E-10	5,6875	0,01999	32	30	DSTE
30	40	2,05E-10	5,6875	0,01999	32	30	DSTE
30	50	3,05E-10	3,5034	0,03936	32	30	DSTE
30	50	1,67E-08	3,5034	0,0398	32	30	STE
30	50	2,76E-10	5,6875	0,01999	32	30	DSTE
30	60	3,71E-10	5,6875	0,01999	32	24	DSTE
30	70	4,72E-10	3,5034	0,01936	32	30	DSTE
30	30	1,65E-10	9,63	0,04082	19	13	STE
30	30	1,66E-10	5,6875	0,01968	24	22	STE

[YD] (mM)	T (°C)	D (m^2/s)	G_{max} (T/m)	Δ (s)	All points	Used Points	Pulse
5	10	9,20E-11	3,5034	0,01936	32	30	DSTE
5	10	1,09E-10	5,6875	0,01999	32	30	DSTE
5	20	1,59E-10	5,6875	0,01999	32	30	DSTE
5	30	2,44E-10	3,5034	0,03936	32	30	DSTE
5	40	3,64E-10	3,5034	0,03936	32	26	DSTE
5	50	4,12E-10	3,5034	0,01936	32	30	DSTE
5	60	5,40E-10	3,5034	0,01936	32	30	DSTE
5	70	6,63E-10	3,5034	0,01936	32	26	DSTE
5	30	2,56E-10	5,6875	0,01998	24	22	STE

Table A2.2 Diffusion Data in DMSO solution – Aromatic region

[YD] (mM)	T (°C)	D (m^2/s)	G_{max} (T/m)	Δ (s)	All points	Used Points	Pulse
20	30	1,64E-10	3,5034	0,01936	32	30	DSTE
20	30	1,65E-10	5,6875	0,01999	32	30	DSTE
20	70	3,52E-10	1,5013	0,01908	16	14	DSTE
20	70	3,87E-10	2,5028	0,03908	16	14	DSTE
20	60	3,22E-10	5,6875	0,01999	32	30	DSTE
20	60	3,07E-10	5,6875	0,01999	32	30	DSTE
20	30	1,62E-10	6,0062	0,02006	24	21	DSTE
20	30	2,31E-10	3,5034	0,03971	16	14	STE
20	30	1,75E-10	3,0036	0,06013	16	13	DSTE
20	30	1,99E-10	5,6875	0,01998	24	22	STE

Table A2.3 Diffusion Data in aqueous solution – Methyl peak

[YD] (mM)	T (°C)	D (m^2/s)	G_{max} (T/m)	Δ (s)	All points	Used Points	Pulse
0,7	30	2,92E-10	3,8058	0,01982	24	22	STE
10	30	2,22E-10	5,6875	0,01998	24	22	STE
15	10	8,58E-11	5,6875	0,01999	32	30	DSTE
15	10	8,96E-11	5,6875	0,03999	32	30	DSTE
15	10	1,02E-10	5,6875	0,09999	32	13	DSTE
15	10	9,43E-11	7,5075	0,02004	16	14	STE
15	10	9,40E-11	5,5055	0,03992	16	13	STE
15	15	1,17E-10	9,0098	0,02037	16	14	STE
15	15	1,16E-10	7,0078	0,02013	24	22	STE
15	20	1,38E-10	5,6875	0,02999	32	28	DSTE
15	20	1,48E-10	5,6875	0,09999	32	17	DSTE
15	20	1,43E-10	6,507	0,01981	16	14	STE
15	20	1,44E-10	6,0062	0,0399	16	14	STE
15	25	1,69E-10	6,0062	0,01978	16	14	STE
15	25	1,71E-10	5,0057	0,03992	16	14	STE
15	30	1,87E-10	5,6875	0,01999	32	30	DSTE
15	30	2,16E-10	5,6875	0,09999	32	16	DSTE
15	30	2,05E-10	5,5055	0,01984	16	14	STE
15	30	2,07E-10	4,0042	0,03984	16	14	STE
15	35	2,48E-10	5,0057	0,01982	16	14	STE
15	35	2,65E-10	3,5034	0,03986	16	14	STE
15	35	2,13E-10	5,6856	0,02006	16	14	DSTE
15	40	2,60E-10	5,6875	0,01999	32	28	DSTE
15	40	2,81E-10	5,6875	0,09999	32	12	DSTE
15	40	2,56E-10	5,6875	0,01999	32	30	DSTE
15	40	2,71E-10	3,5034	0,0811	32	19	DSTE
15	45	3,33E-10	4,5049	0,04133	16	10	DSTE
15	45	3,27E-10	2,0021	0,03971	16	14	DSTE
15	50	3,39E-10	5,6875	0,01999	32	30	DSTE
15	50	3,70E-10	3,5034	0,03936	32	30	DSTE
15	60	4,69E-10	3,5034	0,01936	32	30	DSTE
15	60	4,77E-10	3,5034	0,01936	32	30	DSTE
15	60	4,73E-10	3,5034	0,01936	32	30	DSTE
15	60	4,93E-10	3,5034	0,03936	32	23	DSTE

[YD] (mM)	T (°C)	D (m^2/s)	G_{max} (T/m)	Δ (s)	All points	Used Points	Pulse
15	60	4,31E-10	5,6875	0,01999	32	23	DSTE
15	60	5,51E-10	3,0036	0,03922	16	14	DSTE
15	65	5,03E-10	3,5034	0,01936	32	30	DSTE
15	65	5,34E-10	2,5028	0,03863	16	14	DSTE
15	70	5,88E-10	3,0036	0,01922	32	30	DSTE
15	70	6,83E-10	2,0021	0,03908	16	14	DSTE
15	30	3,58E-10	5,6875	0,00911	16	9	STE
15	30	4,46E-10	3,5034	0,01884	16	14	STE
15	30	3,01E-10	3,5034	0,03936	16	14	DSTE
15	30	2,07E-10	3,5034	0,03989	24	22	STE
15	30	2,04E-10	5,6875	0,01998	24	22	STE
20	10	7,50E-11	3,5034	0,01936	32	30	DSTE
20	10	7,54E-11	5,6875	0,01999	32	30	DSTE
20	10	7,85E-11	5,6875	0,03999	32	30	DSTE
20	20	1,21E-10	5,6875	0,02999	32	29	DSTE
20	30	1,67E-10	5,6875	0,01999	32	30	DSTE
20	40	2,32E-10	5,6875	0,01999	32	30	DSTE
20	50	3,42E-10	3,5034	0,03936	32	30	DSTE
20	60	4,43E-10	3,5034	0,02936	32	30	DSTE
20	70	5,41E-10	3,5034	0,01936	32	28	DSTE
20	30	1,83E-10	5,6875	0,01998	24	22	STE
25	30	1,74E-10	5,6875	0,01998	24	22	STE
30	10	7,02E-11	5,6875	0,09999	32	26	DSTE
30	10	6,94E-11	5,8059	0,09998	32	26	STE
30	10	6,92E-11	5,6875	0,09999	32	23	DSTE
30	10	6,96E-11	9,63	0,09998	32	18	STE
30	10	6,97E-11	6,507	0,10006	16	14	STE
30	10	6,97E-11	6,507	0,10001	64	62	STE
30	15	8,81E-11	9,0098	0,02011	16	14	STE
30	15	8,93E-11	7,0078	0,03998	24	22	STE
30	20	1,10E-10	8,5091	0,02005	16	14	STE
30	20	1,10E-10	6,507	0,03992	24	22	STE
30	30	1,60E-10	5,6875	0,03999	32	30	DSTE
30	30	1,66E-10	5,8059	0,03998	32	30	STE
30	30	1,52E-10	5,6875	0,03999	32	23	DSTE
30	30	1,47E-10	5,6875	0,01999	32	30	DSTE
30	40	2,10E-10	5,6875	0,01999	32	30	DSTE
30	50	3,03E-10	3,5034	0,03936	32	30	DSTE
30	50	1,57E-08	3,5034	0,0398	32	30	STE
30	50	2,79E-10	5,6875	0,01999	32	30	DSTE
30	60	3,72E-10	5,6875	0,01999	32	24	DSTE
30	70	4,86E-10	3,5034	0,01936	32	30	DSTE
30	30	1,62E-10	9,63	0,04082	19	13	STE
30	30	1,63E-10	5,6875	0,01968	24	22	STE

[YD] (mM)	T (°C)	D (m^2/s)	G_{max} (T/m)	Δ (s)	All points	Used Points	Pulse
5	10	1,23E-10	3,5034	0,01936	32	30	DSTE
5	10	1,12E-10	5,6875	0,01999	32	30	DSTE
5	20	1,63E-10	5,6875	0,01999	32	30	DSTE
5	30	2,43E-10	3,5034	0,03936	32	30	DSTE
5	40	3,70E-10	3,5034	0,03936	32	26	DSTE
5	50	4,06E-10	3,5034	0,01936	32	30	DSTE
5	60	5,60E-10	3,5034	0,01936	32	30	DSTE
5	70	6,60E-10	3,5034	0,01936	32	26	DSTE
5	30	2,57E-10	5,6875	0,01998	24	22	STE

Table A2.4 Diffusion Data in DMSO solution – Methyl peak

[YD] (mM)	T (°C)	D (m^2/s)	G_{max} (T/m)	(s)	All points	Used Points	Pulse
20	30	1,78E-10	3,5034	0,01936	32	30	DSTE
20	30	1,83E-10	5,6875	0,01999	32	30	DSTE
20	70	4,67E-10	1,5013	0,01908	16	14	DSTE
20	70	4,60E-10	2,5028	0,03908	16	14	DSTE
20	60	3,52E-10	5,6875	0,01999	32	30	DSTE
20	60	3,34E-10	5,6875	0,01999	32	30	DSTE
20	30	1,82E-10	6,0062	0,02006	24	21	DSTE
20	30	2,40E-10	3,5034	0,03971	16	14	STE
20	30	1,97E-10	3,0036	0,06013	16	13	DSTE
20	30	2,06E-10	5,6875	0,01998	24	22	STE

A3 PULSE PROGRAM FOR DIFFUSION EXPERIMENTS

STE

```
;diffSte
;2D stimulated echo sequence
;new version including decoupling 13.05.04 KLZ
;comments updated 24.06.04 KLZ
;decoupling corrected 02.07.04 KLZ
;CLASS, DIM, TYPE, define list<gradient>, acqt0 added 24.05.06 KLZ
;blanking syntax updated 20.02.2007 KLZ

;$CLASS=diff
;$DIM=2D
;$TYPE=exp
;$OWNER=Bruker

#include <Grad.incl>
#include <Avance.incl>

define list<gradient> diff_ramp=<diff_ramp>

"acqt0=0"

ze
10u
5m pl1:f1               ;set rf power level

start,     1u
if (l14) {                      ; if decoupling in use
        1u do:f2                ; decoupler off during d1
} else  {
        1u
}
 if (l12) {                     ; if lock in use
                        d1 LOCKH_OFF            ; lock on during d1
                                d11 UNBLKGRAD               ; unblank gradient amplifier, lock hold during
experiment
} else {                        ; if locnuc off
```

```
                d1
                        d11 UNBLKGRAMP          ; unblank gradient amplifier
}
;------------------------ Start of dummy gradient loop -------------------------
if (l3) {                       ; dummy gradient pulses in use
                        dummy,  p17:gp1*diff_ramp           ; trapezoidal gradient pulse
                                p18:gp2*diff_ramp                   ; trapezoidal gradient pulse
                                p17:gp3*diff_ramp                   ; trapezoidal gradient pulse
                                d2                                      ; gradient stabilisation time
                                d9 BLKGRAMP                         ; tau
   if (l11) {                       ; if spoiler in use
          d11 UNBLKGRAMP                            ; unblank gradient amplifier
                                p17:gp4                             ; trapezoidal gradient pulse
                                p19:gp5                             ; trapezoidal gradient pulse
                                p17:gp6                             ; trapezoidal gradient pulse
                                d2              ; gradient stabilisation time
          }
          if (l12) {                ; if lock in use
                                d5 BLKGRAD              ; blank gradient amp., lock on during long
tau
                                d11 UNBLKGRAD           ; unblank gradient amplifier
          } else {                  ; if locnuc off
                                d5 BLKGRAMP                         ; long tau
                                d11 UNBLKGRAMP                          ;    unblank    gradient
amplifier
          }
                        lo to dummy times l13     ; l13 number of dummy gradient pulses
}
;------------------------ Start of experiment ----------------------------------
                        p1:f1 ph1                       ; 90 degree pulse
                        p17:gp1*diff_ramp                   ; trapezoidal gradient pulse
                        p18:gp2*diff_ramp                   ; trapezoidal gradient pulse
                        p17:gp3*diff_ramp                   ; trapezoidal gradient pulse
                        d2                                      ; gradient stabilisation time
                        d9 BLKGRAMP                         ; tau
                        p1:f1 ph2                       ; 90 degree pulse
if (l11) {                      ; if spoiler in use
       d11 UNBLKGRAMP                       ; unblank gradient amplifier
                        p17:gp4                             ; trapezoidal gradient pulse
                        p19:gp5                             ; trapezoidal gradient pulse
```

```
                    p17:gp6                         ; trapezoidal gradient pulse
                    d2                              ; gradient stabilisation time
}
if (l12) {          ; if lock in use
                    d5 BLKGRAD                      ; blank gradient amp., lock on during long
tau
                    d11 UNBLKGRAD       ; unblank gradient amplifier
} else {            ; if locnuc off
                    d5 BLKGRAMP                     ; long tau
                    d11 UNBLKGRAMP                  ; unblank gradient amplifier
}
                    p1:f1 ph3                ; 90 degree pulse
                    p17:gp1*diff_ramp               ; trapezoidal gradient pulse
                    p18:gp2*diff_ramp               ; trapezoidal gradient pulse
                    p17:gp3*diff_ramp               ; trapezoidal gradient pulse
                    d2                              ; gradient stabilisation time
                    d10 ph0 BLKGRAMP                ; tau
if (l14) {          ; if f2 on
                go=start ph31 cpd2:f2   ; start acquisition with decoupling
} else {            ; if f2 off
                go=start ph31           ; start acquisition
}
                100u wr #0 if #0 zd igrad diff_ramp    ; store data, increment gradient ramp
        lo to start times td1                   ; td1 = number of gradientsteps
if (l14) {          ; if decoupling in use
    100m do:f2          ; wait for data storage, decoupler off
} else  {
    100m                ; wait for data storage
}
if (l12) {          ; if lock in use
        100m rf #0 LOCKH_OFF            ; reset file pointer, lock on
} else {            ; if locnuc off
        100m rf #0                              ; reset file pointer
}
        lo to start times l1                    ; l1 = Number of repetitions
exit

ph0=0
ph1= 0 0 0 0 2 2 2 2  1 1 1 1 3 3 3 3
ph2= 1 3 0 2
```

ph3= 1 3 0 2

ph31=0 0 2 2 2 2 0 0 3 3 1 1 1 1 3 3

;pl1: f1 channel - power level for pulse (default)

;p1: f1 channel - 90 degree pulse

;p17: gradient ramp time

;p18: gradient duration - p17

;p19: spoil gradient duration - 2*p17

;d1: relaxation delay; 1-5 * T1

;d2: gradient stabilisation time

;d5: DELTA remainder

;d9: tau remainder

;d10: tau remainder, used to shift trigger position

;d11: gradient amplifier unblank delay 200 us

;gpnam1: ramp up of trapezoidal

;gpnam2: plateau of trapezoidal

;gpnam3: ramp down of trapezoidal

;gpnam4: ramp up of trapezoidal

;gpnam5: plateau of trapezoidal

;gpnam6: ramp down of trapezoidal

;gpx1: x-diffusion gradient amplitude

;gpx2: x-diffusion gradient amplitude

;gpx3: x-diffusion gradient amplitude

;gpx4: x-spoiler gradient amplitude

;gpx5: x-spoiler gradient amplitude

;gpx6: x-spoiler gradient amplitude

;gpy1: y-diffusion gradient amplitude

;gpy2: y-diffusion gradient amplitude

;gpy3: y-diffusion gradient amplitude

;gpy4: y-spoiler gradient amplitude

;gpy5: y-spoiler gradient amplitude

;gpy6: y-spoiler gradient amplitude

;gpz1: z-diffusion gradient amplitude

;gpz2: z-diffusion gradient amplitude

;gpz3: z-diffusion gradient amplitude

;gpz4: z-spoiler gradient amplitude

;gpz5: z-spoiler gradient amplitude

;gpz6: z-spoiler gradient amplitude

;NS: 16 * n

;td1: number of experiments

;l1: Repetitions of the whole experiment

;l3: dummy gradient pulses off/on 0/1

;l11: spoil gradient off/on 0/1

;l12: lock off/on 0/1

;l13: number of dummy gradient pulses

;l14: decoupling off/on 0/1

;l21: diffusion gradient list type

;l27: use taumin off/on 0/1

;l28: use default parameters off/on 0/1

;l29: use userdefined pulse program off/on 0/1

DSTE

```
;diffDste
;2D double stimulated echo sequence
;new version including decoupling 09.06.04 KLZ
;comments updated 24.06.04 KLZ
;decoupling corrected 02.07.04 KLZ
;CLASS, DIM, TYPE, define list<gradient>, acqt0 added 24.05.06 KLZ
;blanking syntax updated 20.02.2007 KLZ

;$CLASS=diff
;$DIM=2D
;$TYPE=exp

;$OWNER=Bruker
#include <Grad.incl>
#include <Avance.incl>
3m ; do not remove this delay

define list<gradient> diff_ramp=<diff_ramp>

ze
10u
5m pl1:f1               ;set rf power level

start,     1u
if (l14) {                      ; if decoupling in use
        1u do:f2                ; decoupler off during d1
} else  {
        1u
}
if (l12) {                      ; if lock in use
                        d1 LOCKH_OFF            ; lock on during d1
                                d11 UNBLKGRAD                   ; unblank gradient amplifier, lock hold during
experiment
} else {                        ; if locnuc off
                        d1
                                d11 UNBLKGRAMP          ; unblank gradient amplifier
}
;------------------------- Start of dummy gradient loop --------------------------
```

```
if (l3) {                    ; dummy gradient pulses in use
                    dummy,  p17:gp1*diff_ramp          ; trapezoidal gradient pulse
                            p18:gp2*diff_ramp                  ; trapezoidal gradient pulse
                            p17:gp3*diff_ramp                  ; trapezoidal gradient pulse
                            d2                                      ; gradient stabilisation time
                            d9 BLKGRAMP                        ; tau
  if (l11) {                 ; if spoiler in use
       d11 UNBLKGRAMP                        ; unblank gradient amplifier
                            p17:gp4                            ; trapezoidal gradient pulse
                            p19:gp5                            ; trapezoidal gradient pulse
                            p17:gp6                            ; trapezoidal gradient pulse
                            d2            ; gradient stabilisation time
       }
       if (l12) {            ; if lock in use
                            d5 BLKGRAD                 ; blank gradient amp., lock on during
long tau
                            d11 UNBLKGRAD          ; unblank gradient amplifier
       } else {              ; if locnuc off
                            d5 BLKGRAMP                    ; long tau
                            d11 UNBLKGRAMP                 ;  unblank  gradient
amplifier
       }
                    lo to dummy times l13    ; l13 number of dummy gradient pulses
}
;------------------------ Start of experiment ----------------------------------
                    p1:f1 ph1                  ; 90 degree pulse
                    p17:gp1*diff_ramp                  ; trapezoidal gradient pulse
                    p18:gp2*diff_ramp                  ; trapezoidal gradient pulse
                    p17:gp3*diff_ramp                  ; trapezoidal gradient pulse
                    d2                                      ; gradient stabilisation time
                    d9 BLKGRAMP                        ; tau
                    p1:f1 ph2                  ; 90 degree pulse
if (l11) {                  ; if spoiler in use
     d11 UNBLKGRAMP                    ; unblank gradient amplifier
                    p17:gp4                            ; trapezoidal gradient pulse
                    p19:gp5                            ; trapezoidal gradient pulse
                    p17:gp6                            ; trapezoidal gradient pulse
                    d2                                      ; gradient stabilisation time
}
if (l12) {                  ; if lock in use
```

```
                d5 BLKGRAD                  ; blank gradient amp., lock on during long
tau
                d11 UNBLKGRAD       ; unblank gradient amplifier
} else {            ; if locnuc off
                d5 BLKGRAMP                 ; long tau
                d11 UNBLKGRAMP                  ; unblank gradient amplifier
}
                p1:f1 ph3               ; 90 degree pulse
                p17:gp1*diff_ramp           ; trapezoidal gradient pulse
                p18:gp2*diff_ramp           ; trapezoidal gradient pulse
                p17:gp3*diff_ramp           ; trapezoidal gradient pulse
                d2                          ; gradient stabilisation time
                d9 ph0              ; tau
                p17:gp1*diff_ramp           ; trapezoidal gradient pulse
                p18:gp2*diff_ramp           ; trapezoidal gradient pulse
                p17:gp3*diff_ramp           ; trapezoidal gradient pulse
                d2                          ; gradient stabilisation time
                d9 BLKGRAMP                 ; tau
                p1:f1 ph4               ; 90 degree pulse
if (l11) {          ; if spoiler in use
        d11 UNBLKGRAMP              ; unblank gradient amplifier
                p17:gp4*1.13                ; trapezoidal gradient pulse
                p19:gp5*1.13                ; trapezoidal gradient pulse
                p17:gp6*1.13                ; trapezoidal gradient pulse
                d2
}
if (l12) {          ; if lock in use
                d5 BLKGRAD                  ; blank gradient amp., lock on during long
tau
                d11 UNBLKGRAD       ; unblank gradient amplifier
} else {            ; if locnuc off
                d5 BLKGRAMP                 ; long tau
                d11 UNBLKGRAMP                  ; unblank gradient amplifier
}
                p1:f1 ph5               ; 90 degree pulse
                p17:gp1*diff_ramp           ; trapezoidal gradient pulse
                p18:gp2*diff_ramp           ; trapezoidal gradient pulse
                p17:gp3*diff_ramp           ; trapezoidal gradient pulse
                d2                          ; gradient stabilisation time
                d10 ph0 BLKGRAMP            ; tau
```

```
if (l14) {                      ; if f2 on
                        go=start ph31 cpd2:f2       ; start acquisition with decoupling
} else {                        ; if f2 off
                        go=start ph31               ; start acquisition
}
                        100u wr #0 if #0 zd igrad diff_ramp    ; store data, increment gradient ramp
            lo to start times td1                       ; td1 = number of gradientsteps
if (l14) {                      ; if decoupling in use
      100m do:f2                ; wait for data storage, decoupler off
} else  {
      100m                      ; wait for data storage
}
if (l12) {                      ; if lock in use
            100m rf #0 LOCKH_OFF                ; reset file pointer, lock on
} else {                        ; if locnuc off
            100m rf #0                                      ; reset file pointer
}
            lo to start times l1                        ; l1 = Number of repetitions
exit

ph0=0
ph1= 0 1 2 3
ph2= 0
ph3= 2 3
ph4= 2 2 2 2 0 0 0 0
ph5= 0
ph6= 0
ph7= 0
ph31=0 0 2 2 2 2 0 0

;pl1: f1 channel - power level for pulse (default)
;p1: f1 channel -  90 degree pulse
;p17: gradient ramp time
;p18: gradient duration - p17
;p19: spoil gradient duration - 2*p17
;d1: relaxation delay; 1-5 * T1
;d2: gradient stabilisation time
;d5: DELTA/2 remainder
;d9: tau remainder
;d10: tau remainder, used to shift trigger position
```

;d11: gradient amplifier unblank delay 200 us

;gpnam1: ramp up of trapezoidal
;gpnam2: plateau of trapezoidal
;gpnam3: ramp down of trapezoidal
;gpnam4: ramp up of trapezoidal
;gpnam5: plateau of trapezoidal
;gpnam6: ramp down of trapezoidal
;gpx1: x-diffusion gradient amplitude
;gpx2: x-diffusion gradient amplitude
;gpx3: x-diffusion gradient amplitude
;gpx4: x-spoiler gradient amplitude
;gpx5: x-spoiler gradient amplitude
;gpx6: x-spoiler gradient amplitude
;gpy1: y-diffusion gradient amplitude
;gpy2: y-diffusion gradient amplitude
;gpy3: y-diffusion gradient amplitude
;gpy4: y-spoiler gradient amplitude
;gpy5: y-spoiler gradient amplitude
;gpy6: y-spoiler gradient amplitude
;gpz1: z-diffusion gradient amplitude
;gpz2: z-diffusion gradient amplitude
;gpz3: z-diffusion gradient amplitude
;gpz4: z-spoiler gradient amplitude
;gpz5: z-spoiler gradient amplitude
;gpz6: z-spoiler gradient amplitude

;NS: 8 * n
;td1: number of experiments
;l1: Repetitions of the whole experiment
;l3: dummy gradient pulses off/on 0/1
;l11: spoil gradient off/on 0/1
;l12: lock off/on 0/1
;l13: number of dummy gradient pulses
;l14: decoupling off/on 0/1
;l21: diffusion gradient list type
;l27: use taumin off/on 0/1
;l28: use default parameters off/on 0/1
;l29: use userdefined pulse program off/on 0/1

LIST OF SYMBOLS

^{13}C NMR	Carbon NMR
1D	One Dimensional
^{1}H NMR	Proton NMR
2D	Two Dimensional
α	Shearing angle
B_0	External magnetic field
COSY	Correlation Spectroscopy
δ	Gradient duration
Δ	Diffusion time
D_2O	Deuterated water
DFT	Density functional theory
DMSO	Dimethyl sulfoxide
[dye]	Dye concentration (mM)
$\Delta\nu$	Line width
DSS	Sodium 4,4-dimethyl-4-silapentane-1-sulfonate
DST	Double stimulated echo
ε	Molar extinction coefficient
f	Friction coefficient
γ	Gyromagnetic ratio
g	Gradient strength
GIAO	Gauge invariant atomic orbitals
G_s	Spoil gradient
h	Planck constant
η	Viscosity
HMBC	Heteronuclear multiple bond correlation
HMQC	Heteronuclear multiple quantum coherence
I	Spin quantum number
k_B	Boltzmann constant

λ	Wavelength (nm)
μ	Transition dipole vector
M	Magnetization vector
$[MgSO_4]$	Magnesium sulfate concentration
M_{RD}	Molar mass of the RD anions
M_{YD}	Molar mass of YD anions
ν	Frequency
N	Aggregation number
NMR	Nuclear Magnetic Resonance
PFG	Pulsed field gradient
r	Coordinate vector of the nuclei
RD	Red dye
rf	Radio frequency
R_h	Hydrodynamic radius
S	Signal attenuation
STE	Stimulated echo
T	Temperature
τ	Delay between pulses
T_1	Spin-lattice relaxation time
T_2	Spin-spin relaxation time
τ_c	Rotational correlation time
TMS	Tetra methyl silane
UV	Ultra violet (λ= 190-400 nm)
v	Flow velocity
V_h	Hydrodynamic volume
$V_{i,j}$	Interaction energy
ω_0	Larmor frequency
YD	Yellow dye
Θ	Dihedral angle

REFERENCES

1. Tiddy, G. J. T.; Mateer, D. L.; Ormerod, A. P.; Harrison, W. J.; Edwards, D. J. *Langmuir* **1995,** *11*, 390-393.
2. Yamazaki, T.; Chang, T. Y.; Haass, C.; Ihara, Y. *Journal of Biological Chemistry* **2001,** *276*, 4454-4460.
3. Bayer, T. A.; Breyhan, H.; Duan, K.; Rettig, J.; Wirths, O. *European Neuropsychopharmacology* **2007,** *17*, S205-S206.
4. Tanford, C. *The hydrophobic effect: formation of micelles and biological membranes*, 2d ed.; Wiley: New York, 1980.
5. Evans, D. F.; Wennerström, H. *The colloidal domain: where physics, chemistry, biology, and technology meet*; VCH Publishers: New York, NY, 1994.
6. Kannan, N.; Vishveshwara, S. *Protein Engineering* **2000,** *13*, 753-761.
7. Gazit, E. *Faseb Journal* **2002,** *16*, 77-83.
8. McGaughey, G. B.; Gagne, M.; Rappe, A. K. *Journal of Biological Chemistry* **1998,** *273*, 15458-15463.
9. Cockroft, S. L.; Perkins, J.; Zonta, C.; Adams, H.; Spey, S. E.; Low, C. M. R.; Vinter, J. G.; Lawson, K. R.; Urch, C. J.; Hunter, C. A. *Organic & Biomolecular Chemistry* **2007,** *5*, 1062-1080.
10. Hunter, C. A.; Lawson, K. R.; Perkins, J.; Urch, C. J. *Journal of the Chemical Society-Perkin Transactions 2* **2001**, 651-669.
11. Waters, M. L. *Biopolymers* **2004,** *76*, 435-445.
12. Waters, M. L. *Current Opinion in Chemical Biology* **2002,** *6*, 736-741.
13. Scheibe, G. *Angewante Chemie* **1936,** *49*, 563.
14. Jelley, E. E. *Nature* **1936,** *138*, 1009.
15. Rohatgi, K. K.; Singhal, G. S. *Journal of Physical Chemistry* **1966,** *70*, 1695-&.
16. Hida, M.; Yabe, A.; Murayama, H.; Hayashi, M. *Bulletin of the Chemical Society of Japan* **1968,** *41*, 1776-&.
17. Mukerjee, P.; Ghosh, A. K. *Journal of the American Chemical Society* **1970,** *92*, 6419-&.
18. Mukerjee, P. *Journal of Pharmaceutical Sciences* **1972,** *61*, 478-&.
19. Pugh, D.; Giles, C. H.; Duff, D. G. *Transactions of the Faraday Society* **1971,** *67*, 563-&.
20. Monahan, A. R.; Germano, N. J.; Blossey, D. F. *Journal of Physical Chemistry* **1971,** *75*, 1227-&.
21. Monahan, A. R.; Deluca, A. F.; Ward, A. T. *Abstracts of Papers of the American Chemical Society* **1971**, 24-&.
22. Monahan, A. R.; Blossey, D. F. *Abstracts of Papers of the American Chemical Society* **1970**, 141-&.
23. Monahan, A. R.; Blossey, D. F. *Journal of Physical Chemistry* **1970,** *74*, 4014-&.
24. Reeves, R. L.; Maggio, M. S.; Harkaway, S. A. *Journal of Physical Chemistry* **1979,** *83*, 2359-2368.
25. Roda, A.; Hofmann, A. F.; Mysels, K. J. *Journal of Biological Chemistry* **1983,** *258*, 6362-6370.
26. Hamada, K.; Yamada, K.; Mitsuishi, M.; Ohira, M.; Mesuda, K. *Journal of the Chemical Society-Faraday Transactions* **1995,** *91*, 1601-1605.
27. Hamada, K.; Take, S.; Iijima, T.; Amiya, S. *Journal of the Chemical Society-Faraday Transactions I* **1986,** *82*, 3141-3148.

28. Sanna, C.; La Mesa, C.; Mannina, L.; Stano, P.; Viel, S.; Segre, A. *Langmuir* **2006,** *22*, 6031-6041.
29. Katsuyama, I.; Khalil, A. A.; Dunbar, C.; Zjawiony, J. K. *Spectroscopy Letters* **2003,** *36*, 477-485.
30. Neumann, B. *Langmuir* **2001,** *17*, 2675-2682.
31. Mitra, A.; Seaton, J.; Capitani, J. F.; Assarpour, A. *Abstracts of Papers of the American Chemical Society* **1999,** *217*, U169-U169.
32. Mitra, A.; Seaton, P. J. *Abstracts of Papers of the American Chemical Society* **2000,** *219*, U185-U185.
33. Mitra, A.; Seaton, P. J.; Assarpour, R. A.; Williamson, T. *Tetrahedron* **1998,** *54*, 15489-15498.
34. Mitra, A.; Seaton, P. J.; Capitani, J. F.; Assarpour, A. *Journal of the Indian Chemical Society* **1998,** *75*, 823-830.
35. Rodriguez-Ropero, F.; Casanovas, J.; Aleman, C. *Journal of Computational Chemistry* **2008,** *29*, 69-78.
36. Silverstein, R. M.; Bassler, G. C.; Morrill, T. C. *Spectrometric identification of organic compounds*, 5th ed.; Wiley: New York, 1991.
37. Sehnert, J., Universität Bayreuth, 2007.
38. Cramer, C. J. *Essentials of computational chemistry: theories and models*, 2nd ed.; Wiley: Chichester, West Sussex, England; Hoboken, NJ, 2004.
39. Young, D. C. *Computational chemistry: a practical guide for applying techniques to real-world problems*; Wiley-Interscience: New York, 2001.
40. Hahn, E. L. *Physical Review* **1950,** *77*, 746-746.
41. Hahn, E. L. *Physical Review* **1950,** *80*, 580-594.
42. Stejskal, E. O.; Tanner, J. E. *Journal of Chemical Physics* **1965,** *42*, 288-&.
43. Stejskal, E. O. *Journal of Chemical Physics* **1965,** *43*, 3597-&.
44. Stejskal, E. O. *Advances in Molecular Relaxation Processes* **1972,** *3*, 27-&.
45. Beck, S.; Geyer, A.; Brintzinger, H. H. *Chemical Communications* **1999**, 2477-2478.
46. Cohen, Y.; Avram, L.; Frish, L. *Angewandte Chemie-International Edition* **2005,** *44*, 520-554.
47. Dehner, A.; Kessler, H. *Chembiochem* **2005,** *6*, 1550-1565.
48. Adalsteinsson, T.; Dong, W. F.; Schonhoff, M. *Journal of Physical Chemistry B* **2004,** *108*, 20056-20063.
49. Adalsteinsson, T.; Schoenhoff, M. *Abstracts of Papers of the American Chemical Society* **2005,** *229*, U725-U725.
50. Johnson, C. S. *Progress in Nuclear Magnetic Resonance Spectroscopy* **1999,** *34*, 203-256.
51. Lauterbu.Pc. *Nature* **1973,** *242*, 190-191.
52. Price, W. S.; Nara, M.; Arata, Y. *Biophysical Chemistry* **1997,** *65*, 179-187.
53. Price, W. S. *Concepts in Magnetic Resonance* **1998,** *10*, 197-237.
54. Price, W. S. *Concepts in Magnetic Resonance* **1997,** *9*, 299-336.
55. Katzenstein, A.; Huber, K. *Langmuir* **2002,** *18*, 7049-7056.
56. Ingles, S. E.; Katzenstein, A.; Schlenker, W.; Huber, K. *Langmuir* **2000,** *16*, 3010-3018.
57. Sinemus, T., Master Thesis, Universität Paderborn, 2006.
58. Aksnes, D. W.; Gjerdaker, L. *Journal of Molecular Structure* **1999,** *475*, 27-34.
59. Aksnes, D. W.; Kimtys, L. *Journal of Molecular Structure* **1998,** *440*, 25-33.
60. Bain, A. D. *Progress in Nuclear Magnetic Resonance Spectroscopy* **2003,** *43*, 63-103.
61. Chen, A. D.; Johnson, C. S.; Lin, M.; Shapiro, M. J. *Journal of the American Chemical Society* **1998,** *120*, 9094-9095.

62. Moren, A. K.; Nyden, M.; Soderman, O.; Khan, A. *Langmuir* **1999,** *15*, 5480-5488.
63. Cotts, R. M.; Hoch, M. J. R.; Sun, T.; Markert, J. T. *Journal of Magnetic Resonance* **1989,** *83*, 252-266.
64. Geil, B. *Concepts in Magnetic Resonance* **1998,** *10*, 299-321.
65. Macchioni, A.; Ciancaleoni, G.; Zuccaccia, C.; Zuccaccia, D. *Chemical Society Reviews* **2008,** *37*, 479-489.
66. Martin, N. H.; Allen, N. W.; Moore, J. C. *Journal of Molecular Graphics & Modelling* **2000,** *18*, 242-+.
67. Martin, N. H.; Allen, N. W.; Moore, K. D.; Vo, L. *Journal of Molecular Structure-Theochem* **1998,** *454*, 161-166.
68. Davydov, A. S. *Theory of Molecular Excitons*; Plenum Press: New York, London, 1971.
69. Kasha, M. *Radiation Research* **1963,** *20*, 55-&.
70. Korger, M., Heinrich-Heine-Universität Düsseldorf, 2005.
71. Kasha, M.; Rawls, H. R.; El-Bayoumi, M. A. *Pure Appl. Chem.* **1965,** *11*, 371-392.
72. Abbott, L. C.; Batchelor, S. N.; Oakes, J.; Gilbert, B. C.; Whitwood, A. C.; Smith, J. R. L.; Moore, J. N. *Journal of Physical Chemistry A* **2005,** *109*, 2894-2905.
73. Abbott, L. C.; Batchelor, S. N.; Oakes, J.; Smith, J. R. L.; Moore, J. N. *Journal of Physical Chemistry B* **2004,** *108*, 13726-13735.
74. Harrison, W. J.; Mateer, D. L.; Tiddy, G. J. T. *Faraday Discussions* **1996**, 139-154.
75. Harrison, W. J.; Mateer, D. L.; Tiddy, G. J. T. *Journal of Physical Chemistry* **1996,** *100*, 2310-2321.
76. Herzog, B.; Huber, K.; Stegemeyer, H. *Langmuir* **2003,** *19*, 5223-5232.
77. Zhang, Y. Z.; Xiang, J. F.; Tang, Y. L.; Xu, G. Z.; Yan, W. P. *Dyes and Pigments* **2008,** *76*, 88-93.
78. Hore, P. J. *Nuclear magnetic resonance*; Oxford University Press: Oxford [England] ; New York, 1995.
79. Keeler, J. *Understanding NMR spectroscopy*; Wiley: Chichester, England ; Hoboken, NJ, 2005.
80. Cavanagh, J. *Protein NMR spectroscopy: principles and practice*; Academic Press: San Diego, 1996.
81. Macomber, R. S. *A complete introduction to modern NMR spectroscopy*; Wiley: New York, 1998.
82. Aksnes, D. W.; Kimtys, L. L. *Magnetic Resonance in Chemistry* **1991,** *29*, 698-705.
83. Breitmaier, E. *Structure elucidation by NMR in organic chemistry: a practical guide*, 3rd rev. ed.; Wiley: Chichester, West Sussex, England, 2002.
84. Gogoll, A.; Tanner, D. *Magnetic Resonance in Chemistry* **1989,** *27*, 863-871.
85. Hassanzadeh, A.; Zeini-Isfahani, A.; Habibi, M. H.; Heravi, M. R. A. P.; Abdollahi-Alibeik, M. *Spectrochimica Acta Part a-Molecular and Biomolecular Spectroscopy* **2006,** *63*, 247-254.
86. Kleinschmidt, F., Albert-Ludwigs-Universität, 2005.
87. Levitt, M. H. *Spin dynamics: basics of nuclear magnetic resonance*; John Wiley & Sons: Chichester ; New York, 2001.
88. Imran, M.; Ahmed, E.; Malik, A. *Magnetic Resonance in Chemistry* **2007,** *45*, 785-788.
89. Pettirossi, S.; Bellachioma, G.; Ciancaleoni, G.; Zuccaccia, C.; Zuccaccia, D.; Macchioni, A. *Chemistry-a European Journal* **2009,** *15*, 5337-5347.
90. Inglesby, M. K.; Zeronian, S. H. *Dyes and Pigments* **2001,** *50*, 3-11.
91. Viel, S.; Capitani, D.; Mannina, L.; Segre, A. *Biomacromolecules* **2003,** *4*, 1843-1847.

92. Saveyn, P.; Topgaard, D.; Ghent University, Lund University: Lund, 2006.
93. Lounila, J.; Oikarinen, K.; Ingman, P.; Jokisaari, J. *Journal of Magnetic Resonance Series A* **1996,** *118*, 50-54.
94. Jerschow, A.; Muller, N. *Journal of Magnetic Resonance* **1997,** *125*, 372-375.
95. Tait, K. M.; Parkinson, J. A.; Jones, A. C.; Ebenezer, W. J.; Bates, S. P. *Chemical Physics Letters* **2003,** *374*, 372-380.
96. Baldridge, K. K.; Siegel, J. S. *Journal of Physical Chemistry A* **1999,** *103*, 4038-4042.
97. Truflandier, L.; Paris, M.; Boucher, F. *Physical Review B* **2007,** *76*, -.
98. Kim, D. H.; Eun, H. M.; Choi, H. S. *Bulletin of the Korean Chemical Society* **2000,** *21*, 148-150.
99. Gottlieb, H. E.; Kotlyar, V.; Nudelman, A. *Journal of Organic Chemistry* **1997,** *62*, 7512-7515.
100. Neumann, B. *Dyes and Pigments* **2002,** *52*, 47-53.
101. Neumann, B.; Huber, K.; Pollmann, P. *Physical Chemistry Chemical Physics* **2000,** *2*, 3687-3695.
102. Neumann, B.; Pollmann, P. *Physical Chemistry Chemical Physics* **2001,** *3*, 4508-4514.
103. Mills, R. *J. Phys. Chem.* **1973,** *77*, 685.